School of Medicine
Oregon Health & Science University

CERTIFICATE OF APPROVAL

This is to certify that the Ph.D. Thesis of

Andrew Bruening-Wright

has been approved

[redacted]

John Adelman, PhD., Mentor

[redacted]

Edwin McCleskey, Ph.D., Member

[redacted]

James Maylie, Ph.D., Member

[redacted]

David Farrens, Ph.D., Member

[redacted]

H. Peter Larsson, Ph.D., Member

THE LOCATION OF THE ACTIVATION GATE IN SMALL CONDUCTANCE CALCIUM-ACTIVATED POTASSIUM CHANNELS

by

Andrew H. Bruening-Wright

A DISSERTATION

Presented to the Neuroscience Graduate Program

and the Oregon Health and Science University

School of Medicine

in partial fulfillment of

the requirements for the degree of

Doctor of Philosophy

June 2003

TABLE OF CONTENTS

I. CHAPTER 1 ..... **1**

INTRODUCTION 1

A. OVERVIEW *1*

B. SK CHANNEL PHSYIOLOGY *2*

C. K^+ PORE STRUCTURE AND GATING: CLASSIC STUDIES *6*

a. Squid Giant Axon Delayed Rectifier 6

b. Ion Trapping: Delayed Rectifier and BK Channels 7

D. K^+ PORE STRUCTURE AND GATING: CLONING AND CRYSTALS *8*

a. Subunit Composition 9

b. Selectivity and Permeation 11

c. The Inner Vestibule 12

d. Locating the Activation Gate 13

i. *Shaker* channels: the TM6 bundle crossing makes a gate 13

ii. Crystallized bacterial channels 16

iii. A possible exception: CNG channels 19

iv. Evidence for selectivity filter involvement in gating 21

v. C-type inactivation: gating at the channel pore 22

E. SK CHANNELS *23*

a. Cloning 23

b. Pore Structure 25

c. Gating 26

i. Identification of Calmodulin (CaM) 26

ii. Functional confirmation of CaM as the gating molecule 27

iii. Crystal structure of CaM interaction with SK C-terminus 30

iv. Missing pieces: coupling and location of the gate 33

II. CHAPTER 2 ..... **34**

LOCALIZATION OF THE ACTIVATION GATE FOR SMALL CONDUCTANCE Ca^{2+}-ACTIVATED K^+ CHANNELS 34

A. ABSTRACT *35*

B. INTRODUCTION *36*

C. MATERIALS AND METHODS *38*

a. Molecular Biology 38

b. Electrophysiology 38

c. Data Analysis 39

D. RESULTS *41*

a. A Conserved Inner Vestibule Topology Between SK and K_v Channels 41

b. State-Dependent Conformational Changes in the TM6 Helix 42

c. Localization of the SK2 Activation Gate 51

E. DISCUSSION *56*

III. CHAPTER 3 ..... **63**

EVIDENCE FOR A DEEP PORE ACTIVATION GATE IN SMALL CONDUCTANCE Ca^{2+}-ACTIVATED K^+ CHANNELS 63

A. ABSTRACT *64*

C. MATERIALS AND METHODS *68*

a. Molecular Biology 68

b. Electrophysiology 68

c. Data Analysis 69

D. RESULTS *70*

a. Ba^{2+} Block: Dependence on Voltage and External K^+ 70

b. Ba^{2+} Trap 72

c. State-Dependence of Ba^{2+} Binding in the Pore 75

E. DISCUSSION *84*

V. DISCUSSION **89**

A. SK CHANNELS SHARE FEATURES WITH OTHER K^+ CHANNELS *89*
B. LOCATION OF THE SK CHANNEL ACTIVATION GATE *90*
C. FUTURE EXPERIMENTS *91*
a. Structure-Function Studies 91
b. Crystal Structures 92

VI. SUMMARY AND CONCLUSIONS **96**

VII. REFERENCES **97**

VIII. APPENDIX A **110**

SUPPLEMENTARY DATA 110

IX. APPENDIX B **114**

BICUCULLINE BLOCK OF SMALL CONDUCTANCE CALCIUM-ACTIVATED POTASSIUM CHANNELS 114
A. ABSTRACT *115*
B. INTRODUCTION *116*
C. MATERIALS AND METHODS *118*
D. RESULTS *119*
a. Bicuculline Blocks SK channels 119
b. Residues Influencing Rundown and Reduced Bicuculline Sensitivity 125
c. Voltage-Dependence of Bicuculline-m Block 128
E. DISCUSSION *134*
F. REFERENCES *137*

LIST OF FIGURES

Figure i1: SK Channels make an afterhyperpolarization (AHP)

Figure i2: K Channel Anatomy — KcsA and MthK crystal structures

Figure i3: Calmodulin schematic

Figure i4: Calmodulin-SK crystal structure

Figure 1: Possible SK channel gating mechanisms

Figure 2: MTSET reactivity in WT and cysteine substituted channels

Figure 3: Determination of MTSET modification rates

Figure 4: Summary of MTSET reactivity

Figure 5: MTSEA reactivity

Figure 6: TBuA protection of T387C

Figure 7: SK2 reactivity mapped onto KcsA structure

Figure 8: Barium block of SK2, dependence on voltage and external K^+

Figure 9: Barium trap, open state

Figure 10: Barium application, closed state

Figure 11: Barium is an open state blocker

Figure 12: Po-dependence of barium block, steady state

Figure 13: Po-dependence of barium block, kinetics

Figure 14: Sequence alignment and cartoon of SK channel gating

Figure Aa-1: TEA derivative block of SK2 is dependent on side-chain length

Figure Aa-2: Voltage and Po-dependence of TBuA block

Figure Aa-3: Mutation T387C increases TBuA block potency

Figure Aa-4: Residue 391C can be modified by cadmium in the open and closed states

Figure Ab-1: Concentration response of bicuculline-m block of SK2

Figure Ab-2: Bicuculline-m block of SK1 decreases with time following patch excision

Figure Ab-3: Mutations E330D, H357N in the outer vestibule of SK1 reduce the time dependent shift of bicuculline-m block of SK1

Figure Ab-4: Voltage-dependence of bicuculline-m block of SK2 and SK1

Figure Ab-5: Voltage-dependence of bicuculline-m block of SK2 in asymmetrical K^+

Figure Ab-6: Concentration response of block of SK2 and SK1 by the free base of bicuculline A

LIST OF ABBREVIATIONS

Afterhyperpolarization (AHP)

Barium (Ba^{2+})

Cadmium (Cd^{2+})

Calcium (Ca^{2+})

Calcium-activated potassium channel (K_{ca})

Calmodulin (CaM)

Calmodulin binding domain (CaMBD)

Charybdotoxin (CTX)

Cyclic nucleotide-gated channels (CNG channels)

Decyltriethylammonium (C_{10})

Electron paramagnetic resonance (EPR)

Ethylene glycol-bis (aminoethylether) N,N,N ,N -tetraacetic acid (EGTA)

Inward rectifer potassium channel (K_{ir})

Large-conductance calcium-activated potassium channel (BK channel)

Magnesium (Mg^{2+})

Methanethiosulfonate (MTS)

2-(aminoethyl) methanethiosulfonate (MTSEA)

[2-(trimethylammonium)] methanethiosulfonate (MTSET)

Nickel (Ni^{+})

Nonyltriethylammonium (C_9)

Potassium (K^{+})

Quaternary ammonium (QA)

Silver (Ag^{+})

Small-conductance calcium-activated potassium channel (SK channel)

Substituted cysteine scanning mutagenesis (SCAM)

Tetraethylammonium (TEA)

Tetrabutylammonium (TBuA)

Transmembrane domain (TM)

Voltage-gated potassium channel (K_v channel)

Wild-type (WT)

ACKNOWLEDGMENTS

First and foremost, I thank my wife, Marie, for unconditional support in every aspect of my life, and for providing hugely necessary perspective and balance. I thank my family, particularly my parents, who never stop encouraging and supporting higher education. And finally, to my mentors John Adelman and James Maylie, who have invested so much of their time and energy supporting my advancement through graduate school, I express heartfelt gratitude.

ABSTRACT

Ion channels are responsible for transmission of electrical signals throughout the nervous system. Essential for normal physiology in all excitable tissue, the malfunctioning of even one class of ion channel can have drastic consequences at the clinical level, leading to problems such as cardiac arrythmia, ataxia, or even death. Efforts to develop therapies to rectify channel dysfunction require a basic understanding of normal ion channel function at the molecular level. This thesis focuses on elucidating the molecular mechanism by which small conductance calcium-activated potassium channels (SK channels) regulate ion flux through their pores. This opening and closing in response to appropriate stimuli, or gating , is the primary movement required of all ion channels; deficits in channel gating often underlie the clinical abnormalities caused by mutant ion channels.

SK channels, like their voltage-gated relatives, consist of four subunits, each with six transmembrane domains (TM) and a pore loop that contains a selectivity filter that allows only potassium (K^+) to readily permeate the channel. The subunits are arranged with four-fold symmetry such that a hole through which potassium flows is formed down the central axis. The selectivity filter resides at the extracellular end of the channel, and, at least for certain K+ channels, hydrophobic residues contributed by the sixth TM (TM6) of each subunit line the inner surface of the channel pore. For many K^+ channels permeation of ions is regulated by a gate at the intracellular end of the pore. The specific aim of this thesis is to elucidate the location of the gate in SK channels.

Heterologously expressed wild-type (WT) SK2 channels or SK2 channels with a cysteine residue introduced at a specific location are examined electrophysiologically by excising inside-out membrane patches from CosM6 cells or Xenopus oocytes. The composition of the intracellular solution is altered to open and close the channels, or to apply chemicals to probe the channel pore from the cytoplasmic face. Several molecules that block conduction are identified and used in combination with cysteine-specific modifying reagents to search for an activation gate in the channel pore. Cysteine residues introduced in TM6 are shown to be modified by cysteine-reactive methanethiosulfonate (MTS) compounds that covalently bind to the introduced cysteine and block conduction. These data demonstrate that residues in TM6 line the SK channel pore. Different from channels that possess a gate at the intracellular end of the pore, however, MTS access to a residue relatively deep in the pore is not restricted when channels are closed, and the quaternary ammonium (QA) ion tetrabutylammonium (TBuA) can protect this site even in the closed state, suggesting that it has access to its pore binding site in closed channels. These data suggest that SK channels do not have an activation gate at the distal end of the channel pore.

In contrast to the MTS reagent and TBuA, the divalent ion barium (Ba^{2+}), which is known to bind deep in the pore near the selectivity filter, shows strong state-dependent access to its binding site; it binds in the open state with high affinity, but doesn t bind in the closed state. Further, Ba^{2+} can be trapped in the channel pore if it is applied to open channels and the channels are subsequently closed. Taken together, the data suggest that SK channels possess an activation gate between the Ba^{2+}-binding site near the selectivity filter, and the TM6 position to which the MTS compound and TBuA have unrestricted

access. It is proposed that channels in the calcium-activated class (SK and intermediate-conductance or IK channels) are distinct from other K^+ channels that they regulate ion flux using a gate that resides not at the cytoplasmic end of the conduction pathway, but deep in the channel pore.

I. CHAPTER 1

Introduction

A. OVERVIEW

Over 70 years ago a series of experiments was begun with the central goal of understanding how an electrical signal, the action potential, could be conducted along the length of a neuron. Highly successful, many of the results of these efforts were published from 1930's through the 1950's from the labs of Curtis and Cole and Hodgkin and Huxley [1]. These experiments, together with later work primarily by Clay Armstrong on the Squid Giant Axon [2], defined the fundamental characteristics of the molecules that underlie action potential propagation: the molecules were pores (not carriers) that were selective for one ion over all others, and they utilized changes in the voltage across a cell membrane as a cue to open and conduct ions, or to close. We now know that the molecules they were describing belong to a subset of voltage-gated sodium (Na^+) and potassium (K_v) channels. The evolution of increasingly advanced electrophysiological techniques in combination with molecular cloning has allowed us to conclude that ion channels underlie the majority of electrical signaling in every excitable tissue. A critical question, then, is how do ion channels sense an appropriate cue such as voltage and translate it into the molecular rearrangements that underlie channel gating? While much effort has been applied to this question and considerable progress made, the details of channel gating for even the most well studied channels remain unresolved. This thesis focuses on elucidating the gating mechanism of a recently cloned class of ion channel, calcium-activated K^+ channels.

B. SK CHANNEL PHSYIOLOGY

Different from their voltage-sensitive cousins, SK channels gate in response to changes in intracellular calcium (Ca^{2+}) and are entirely voltage-independent. Nonetheless, SK channels play a fundamental role in shaping the action potential and are critical in regulating neural excitation. In this regard, it is useful to examine the action potential. Figure i1A shows the voltage response of a neuron following a short injection of current. The upstroke of the action potential begins when voltage-activated Na^+ channels open in response to the current injection, generate inward Na^+ current, and depolarize the cell. These channels quickly inactivate and stop conducting Na^+. Concomitantly, voltage-sensitive K^+channels activate, pass outward current, and drive the membrane potential back past the resting potential (approximately –80 mV), causing a hyperpolarization or "overshoot". These three basic elements of the action potential – depolarization, repolarization, and overshoot – are very fast compared to the amount of time it takes the cell to return to its resting potential after the spike. The prolonged recovery phase, or slow afterhyperpolarization (AHP), is dictated primarily by SK channel activity.

A

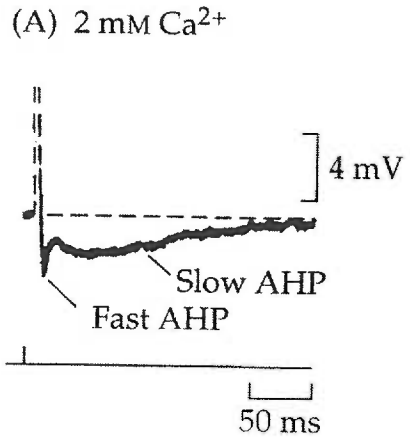

B

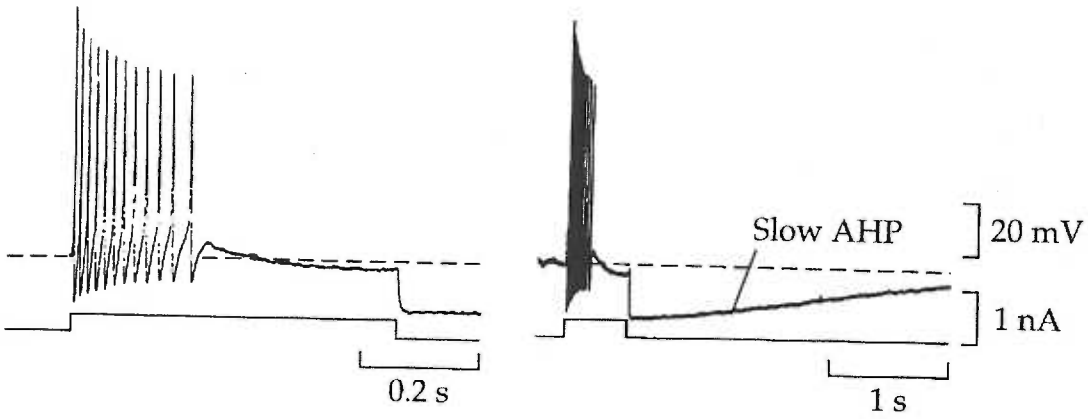

Figure i1. AHP's in motoneurons. A, Following an action potential, a Ca^{2+}-dependent K^+ conductance maintains the cell at a hyperpolarized potential, generating a slow AHP. B, In the presence of a continuous stimulus (current injection), spike frequency adaptation occurs leading to a cessation of action potential firing (left panel). Removing the stimulus reveals the presence of a slow AHP (right panel). Adapted from Hille [1], original sources [3, 4].

During the action potential, intracellular Ca^{2+} rises due to influx through voltage-activated Ca^{2+} channels and release from intracellular stores. SK channels activate in response to this rise in Ca^{2+}, pass outward current, and hyperpolarize the cell. The AHP can last for several seconds and have dramatic effects on short-term excitability. Figure i1B shows the response of a frog motoneuron to an injection of current that is sufficiently long to elicit multiple action potentials. Repeated action potential firing causes a progressive accumulation of intracellular Ca^{2+}, leading to an AHP of increasing amplitude and duration. This AHP noticeably increases the interspike interval such that the cell becomes less and less responsive to the stimulus. In certain cells, the AHP can become so dominant that severe spike frequency adaptation occurs, eventually leading to cessation of firing even in the continued presence of stimulus (Fig i1B) [1].

Several studies indicate that the ion channels underlying the AHP are Ca^{2+}-activated K^+-selective ion channels [5-10]. Madison and Nicoll, using an intracellular recording technique on hippocampal CA1 pyramidal cells, demonstrated that an accommodation –inducing AHP was diminished by the Ca^{2+} chelator ethylene glycol-bis (aminoethylether) N,N,N',N'-tetraacetic acid (EGTA) and the Ca^{2+} channel blocker cadmium (Cd^{2+}) [5]. In addition, Lancaster et al. recorded Ca^{2+}-activated conductances in inside-out patches excised from cultured CA1 neurons that were primarily K^+ permeant [6], and Hirschberg et al., using a similar technique, recorded channels that were small conductance (10 pS) and half-activated by 600 nM Ca^{2+} [10]. Perhaps most significantly, application of the specific SK channel blocker apamin to CA1 neurons selectively eliminates a significant component of the AHP and attenuates spike frequency adaptation [9]. This may explain the apparent role of SK channels in learning and

memory. In rat hippocampal slices, blockade of SK channels with apamin appears to facilitate synaptic enhancement, an electrophysiological phenomenon correlated with learning and memory [11, 12]. Further, apamin may enhance learning and memory in certain behavioral tasks. The most convincing evidence of this comes from studies of medial septal-lesioned animals, where application of apamin improves spatial navigation as assessed using the water maze test [13]. Thus, the importance of SK channel-generated AHP's is evident not only at the cellular level, but also at the level of whole animal behavior.

The physiological role of SK channels is not limited to the hippocampal region of the brain or even to the nervous system. In dopaminergic cells in the midbrain, a region believed to be important for "reward" behavior, metabotropic glutamate receptors initiate a response which triggers SK channels to generate an inhibitory post-synaptic potential [14]. In this way an excitatory signal, glutamate, is counter-acted at the cellular level by activation of an inhibitory K^+ current through SK channels. Thus, the Ca^{2+}-sensing properties of SK channels may be employed in the nervous system by various feedback systems that require inhibitory activity that is not directly triggered by voltage. A role for SK channels has been proposed, for example, in the tonic membrane voltage oscillations experienced by rat subthalamic neurons [15]. In these cells, oscillations can be accounted for by apamin-sensitive AHP's acting to counter a persistently active Na^+ current. SK channels also are important in muscle tissue pathologies. For example, denervation of rat skeletal muscle leads to hyperexcitability and upregulation of an apamin-sensitive K^+-selective current as recorded electromyographically and electrophysiologically [16-18]. A role for SK channels in disease is suggested by an experiment that showed that

injection of apamin to the thenar muscle of patients with myotonic dystrophy could suppress the hyperexcitablility of the muscle [19]. Finally, recent experiments using a genetically modified mouse in which an SK channel subtype (SK3) can be conditionally overexpressed or "knocked-out" dramatically demonstrate the importance of SK channels to normal physiology [20]. Overexpression of the channel induces an abnormal breathing response to oxygen deprivation (hypoxia) and disrupts parturition. Chemical "silencing" of the SK3 gene corrects both responses.

C. K^+ PORE STRUCTURE AND GATING: CLASSIC STUDIES

a. Squid Giant Axon Delayed Rectifier

While it is clear that SK channels play key physiological roles in excitable tissue, the fundamental mechanism by which they gate is not known. To this end, it is instructive to understand what is known about the gating of other K^+ channels. Elegant studies during the past seven decades have provided insight into the architecture of the pore and inner vestibule, as well as the gating mechanism, of voltage-gated K^+ channels. Using native voltage-dependent K^+ channels in the Squid Giant Axon, Clay Armstrong demonstrated that tetraethylammonium (TEA) and its derivatives (quaternary ammoniumium or QA ions) not only blocked conduction through K^+ channels when applied cytoplasmically, they could inhibit channel closure [2, 21, 22]. Further, TEA could only enter K^+ channels with open activation gates, and the potency of block was decreased by either decreasing voltage or by increasing external K^+. It was proposed that TEA acts like a K^+ ion that can't conduct through the channel pore. Instead, TEA behaves like a hydrated K^+ ion; it can bind to a site in the conduction pathway of an open channel, but can't permeate the channel. Inhibition of channel closure could be explained if TEA derivatives bound to

this intracellular site and prevented movement of an intracellular gate. QA ions with long hydrophobic side chains such as pentyltriethylammonium bound more tightly to the QA receptor than did TEA, and it was presumed this was because the QA binding site resides in a hydrophobic region of the channel, in or near the channel "mouth" [22, 23]. Thus, by the early 1970's, the K^+ channel pore was envisioned as containing three main parts: a region that selects K^+ over other ions (a selectivity filter), an intracellular vestibule large enough to accommodate hydrophobic QA ions, and an intracellular gate that moves in response to an environmental stimulus such as voltage.

b. Ion Trapping: Delayed Rectifier and BK Channels

Support for this structural model of K^+ channels was derived from Armstrong's experiments on the Squid Giant Axon and from an elegant set of experiments using native large-conductance Ca^{2+}-activated K^+ (BK) channels from skeletal muscle incorporated into lipid bilayers. One of the observations that Armstrong made was that squid axon K^+ channels closed more slowly in the presence of nonyltriethylammonium (C9) as if channels could not close until C9 was cleared from a binding site in the pore [22]. Inconsistent with this idea, however, he also observed a slow component of recovery from blockade that became more pronounced and slower at very negative voltages. This slowed recovery could be explained if in a fraction of the channels, C9 was "trapped" in the inner vestibule of closed channels by a cytoplasmic gate [22].

Chris Miller reasoned that if an intracellular gate exists in K^+ channels, impermeant ions should be "trapped" in the lumen between the selectivity filter and the intracellular gate if the ion is applied to an open channel and the channel subsequently closed. Measuring

single BK channels, he found that a single Ba^{2+} ion could in fact be trapped in a single channel, and could not escape to the cytoplasm until the channel opened [24]. Further analysis of this trapping effect allowed characterization of at least three Ba^{2+} binding sites in the pore of BK channels, and suggested that Ba^{2+} can occupy sites immediately internal and external to the selectivity filter, as well as at least one site in the selectivity filter itself [25, 26]. These data provided good evidence that for BK channels, as for the delayed rectifier of Squid Giant Axon, the cytoplasmic end of the channel pore is obstructed by a gate in the closed state.

D. K^+ PORE STRUCTURE AND GATING: CLONING AND CRYSTALS

The availability of cloned K_v channels, particularly *Shaker* channels from *Drosophila*, together with heterologous expression systems, have permitted detailed studies of the K^+ channel pore and gating mechanism. The *Shaker* phenotype, a persistent twitching or shaking, was originally observed when certain fruit flies were placed under ether anesthesia. Subsequent voltage-clamp experiments revealed that one of the K^+currents in the flight wing muscle isolated from *Shaker* mutant flies exhibited altered electrical characteristics compared with wild-type (WT) flies [27, 28]. Depending on the particular mutation, an early inactivating K^+ current (Ia) was either absent or had shifted activation or inactivation kinetics. Cloning of the *Shaker* locus identified a K^+ channel-encoding gene that could reproduce Ia-like currents when heterologously expressed in *Xenopus* oocytes [29-31]. These studies spurred an exciting new era in K^+ channel research in which the ramifications of manipulating protein structure at the genetic level could be assayed at the level of channel function using heterologous expression and voltage-clamp methodologies.

a. Subunit Composition

The earliest indication that channel gating required cooperation of four independent "particles" came from pioneering work in the labs of Hodgkin and Huxley. They observed that upon depolarization, a K^+ conductance (gK) in Squid Giant Axon activated sigmoidally, but when the axon was repolarized, gK decayed exponentially [32, 33]. This behavior could be explained quantitatively by supposing that for the K^+ conductance, there are four independent voltage-sensitive "particles", each with "n" probability of being in the permissive state that allows conduction of K^+. The probability that all four particles are in the permissive state is n^4, and thus the K^+ current (I_k) was represented mathematically in the Hodgkin-Huxley model as:

$I_k = (n^4)(gK)(E-E_k)$

where E and E_k are the membrane potential and the K^+ reversal potential, respectively. This simple representation could explain both the sigmoidal rise and exponential decay of gK in the Squid Giant Axon, and, though it was not interpreted as such, provided the first evidence for cooperative action of four independent voltage-sensing domains in K^+ channel activation and deactivation [34].

These early Hodgkin and Huxley experiments on native channels, and later, Armstrong's experiments with QA ions, provided remarkably accurate predictions about the overall structure and function of voltage-gated ion channels. It wasn't until the *Shaker* channel was cloned and examined in detail in heterologous systems, however, that the number of subunits was clearly determined. The first clues from sequence analysis came from comparison of *Shaker* sequence with that of a cloned voltage gated Na^+ chanel [35].

Whereas analysis of hydropathy plots of the Na^+ channel predicted four subunits, each with 6 hydrophobic TM's, the *Shaker* gene encoded the equivalent of only one 6 TM subunit. Despite the shortened sequence, expression of the cDNA yielded functional channels in oocytes with properties similar to native Ia currents. This suggested that four identical subunits might come together as a tetramer to form functional *Shaker* channels.

Clever experiments from several labs provided nice evidence in support of this notion. Channel subunits that, when expressed alone as homomultimers, differed in their kinetics or drug-binding properties were co-expressed in oocytes and their properties recorded. If the different channel subunits came together as multimers, it was reasoned, then the heteromultimers formed should have kinetic or binding properties intermediate to either homomultimer expressed on its own. This was exactly what was observed, and the evidence for multimerization was convincing [36-39]. Determination of the actual number of subunits that comprised the channel required analysis of charybdotoxin (CTX) binding to WT and mutant *Shaker* channels, and ultimately crystallization of a set of K^+ channels. In 1991, kinetic analysis of CTX binding to WT *Shaker* channels, *Shaker* channels with a mutation that alters CTX binding, or both WT and mutant channels expressed together, strongly suggested that four subunits come together to form a functional tetrameric *Shaker* channel [39]. Finally, the recent crystallization of several bacterial K^+ channels by Mackinnon's group has verified almost beyond doubt that a variety of K^+ channels do indeed assemble as tetramers [40-43].

b. Selectivity and Permeation

One of the key functional characteristics of K^+ channels is their extraordinary ability to select for K^+ over other monovalent ions. For example in most K^+ channels, K^+ permeates greater than 10,000 times better than Na^+ [1]. Examination of sequence alignments of a large number of K^+ channels reveals that between TM5 and TM6 there is a highly conserved region that contains a consensus glycine-tyrosine-glycine (GYG) sequence. Mutations in this region alter selectivity of the channel, lending support to the notion that the GYG motif is critical for K^+ selectivity [44]. It is now widely accepted that this GYG motif is the "signature sequence" of K^+ channels as almost all known K^+ channels contain the sequence (a few contain GFG instead). The GYG sequence is contained in what is called the "pore loop" of the channel, and forms the core of the region that selects K^+ over other ions, the selectivity filter. Electrophysiological experiments designed to test the relative location of the selectivity filter indicate that it resides near the extracellular end of the pore [45, 46].

Crystallization of the first K^+ channel pores confirmed many of the ideas derived from years of functional experiments and modeling aimed at determining not just the overall structure of K^+ channels, but also K^+ permeation at the molecular level [1, 41, 47, 48]. As proposed based on functional studies, the crystal structures showed that K^+ must dehydrate in order to pass through the narrow selectivity filter. K^+ ions in the selectivity filter are uniformly dehydrated, whereas a K^+ ion resolved in the wide inner vestibule of the channel is clearly surrounded by 8 water molecules arranged in a square antiprism [48]. The energetically unfavorable process of dehydrating K^+ is compensated for by the architecture of the selectivity filter; the backbone carbonyl oxygens of the GYG motif act

as "surrogate" water molecules. Very similar to the 8-water hydration shell surrounding K^+ in the inner vestibule, there are 8 oxygen atoms stabilizing K^+ in the selectivity filter. This tight interaction of selectivity filter residues with K^+ can explain why ions smaller than K^+, such as Na^+, can't permeate the selectivity filter. Simply put, they are too small to tightly interact with the oxygen atoms, and so are not readily stabilized in the filter. Impermeability of ions with diameters larger than the diameter of the selectivity filter, such as Ca^{2+}, can be explained by assuming that while the selectivity filter may be flexible, it can't expand enough to accommodate the larger ions.

c. The Inner Vestibule

The K^+ channel crystal structures discussed above provided elegant structural explanations of selectivity and permeation that agree nicely with theories derived from modeling and functional studies. These crystal structures, however, were of a 2 TM K^+ channel with an unknown gating mechanism. More recently, the solution of a 6 TM functional K_v channel (K_vAP) has provided structural information about the overall architecture of K^+ channel pores [43]. Though the details of TM domain arrangement in this structure are certain to be controversial (see discussion), the general structure agrees in several ways with functional studies of other voltage-gated ion channels. In the K_vAP structure, the N- and C-terminus of each of the four subunits resides at the opposite side of the protein from the selectivity filter (therefore intracellularly), and each subunit contributes a GYG-containing pore loop to the central axis of the channel. Further, as in the *Shaker* channel, TM4 is highly positively charged, and functional analysis suggests that it undergoes large outward movement during channel opening [49]. For *Shaker*, extensive studies implicate TM4 as the primary "voltage-sensor" for the channel; it

moves in response to changes in membrane potential and this movement is somehow coupled to the operation of the channel gate [50-53]. Mutational analysis of *Shaker* channels has demonstrated that specific residues in the pore and TM6 are crucial structural determinants of block, providing good evidence that TM6 forms at least part of the inner vestibule of K_v [54-56]. These data localized the binding site of long-chain TEA derivatives to a position in TM6 deep in the channel pore, and showed that mutations near the selectivity filter region could affect binding of TEA. Thus, for *Shaker* channels, TM6 is believed to line the inner vestibule and to form a binding site for QA ions. This structure is probably conserved in the K^+ channel family, since functional data derived from mutant cycle analysis of $K_v1.4$ channels also demonstrate that TBuA interacts with specific residues in TM6 [57]. In support of this, co-crystallization of the KcsA bacterial channel with a heavy-labelled TBuA derivative, tetrabutylantimony (TBSb), show a TM6-formed binding site deep in the channel pore [57].

d. Locating the Activation Gate

i. *Shaker* channels: the TM6 bundle crossing makes a gate

Similar to the Ba^{2+} trapping that Chris Miller observed in reconstituted BK channels, it was discovered that TEA and decyltriethylammonium (C_{10}) could be effectively trapped in heterologously expressed *Shaker* channels that contained a mutation in the internal vestibule [58]. Further, Holmgren et al. demonstrated that C_{10} escape from the trap site was correlated with the open probability (Po) of the channel; as the likelihood the channels were open (the Po) was increased by depolarization, the rate of C_{10} escape from its' binding site was also increased. Thus, it appeared that a TM6-based gate could close behind C_{10}, trapping it between the gate and the selectivity filter.

Applying the substituted cysteine scanning mutagenesis (SCAM) [59] method to *Shaker* channels allowed more precise localization of the cytoplasmic gate [60]. Briefly, cysteines were introduced one at a time to a contiguous series of amino acids in TM6 of *Shaker*. Each position was then assayed for availability to cysteine-specific modifying reagents (MTS compounds) in both the open and closed state of the channel. It was observed that positions that were internal to a region close to the predicted cytoplasmic membrane boundary exhibited strong state-dependence; they were rapidly modified by MTS compounds in the open state of the channel but not in the closed state. In contrast, residues that were cytoplasmic to this region were modified quickly in both the open and closed states of the channel. These data suggested that a cytoplasmic gate was formed by the few amino acids that defined the boundary between residues exhibiting strong state-dependent access and those exhibiting no state-dependence. These data were further supported by examining Cd^{2+} reactivity at a cysteine introduced internal to the cytoplasmic gate (474C) [60]. It was found that Cd^{2+} could block current conduction when applied at depolarized potentials, but not when applied at hyperpolarized potentials, presumably by coordinating several cysteines from different subunits. The current could be recovered only if the di-thiol compound 2,3-dimercapto-1-propanesulfonate (DMPS) was applied, and the rate of recovery from Cd^{2+} block correlated well with the voltage dependence of channel conductance, suggesting that DMPS, like MTS compounds and Cd^{2+}, demonstrates state-dependent access to the inner vestibule.

The observation that Cd^{2+} access to the inner vestibule was state-dependent prompted a follow-up study examining in detail reactivity of Cd^{2+} and silver (Ag^{+}) ions at this same

474C residue [61]. It was found that access of these ions, whose chemical properties are much more similar to a K^+ ion than are the properties of MTS compounds, was strongly state-dependent; the blocking rate was slowed by several orders of magnitude when the channel was closed compared to when it was open. These experiments provided good evidence that in *Shaker* channels, closed state access to positions deep in the inner vestibule is occluded by a gate localized to the region cytoplasmic to position 474C. To understand the physical nature of the gate, channels with the 474C mutation were probed with MTS compounds of positive, neutral, or negative charge. It was found that all three modified 474C with strong state-dependence, suggesting that the activation gate did not operate by excluding only positively charged compounds – it was not a "field effect" gate [60].

To further examine the topography of the *Shaker* pore near the activation gate, cysteine-reactive compounds of various sizes, shapes and charges were applied to channels harboring the 478C mutation. This residue, just cytoplasmic to the region that forms a gate, did not show strong state-dependent modification by one MTS compound in the SCAM study [60]. Moreover, it had been observed that TEA, TBuA, and a "ball" peptide (a synthetic molecule that can plug the channel pore just as the channel N-terminus does during a type of gating known as N-type inactivation) all could protect 478C from open-state MTS modification [62]. This suggested to the authors that the cytoplasmic end of the channel below the gate was wide open since even large molecules could enter the open channel pore. To accommodate this data a structural hypothesis was advanced that suggested a bend occurred at a proline-x-proline motif that is conserved in TM6 of all K_v channels. It appeared that this "bent-TM6" model applied even to closed

channels, as access to 478C was not restricted in the closed state compared with the open state as measured by modification rate, even for very large thiol-reactive compounds [61]. This model is very different from the model derived from crystallization studies of bacterial K^+ channels, for which it is proposed channel closure occurs when TM6 α-helices move from a bent conformation to a straight conformation (see below) [40].

Taken together, the model that has emerged for *Shaker* channels is one in which the TM6 helices are bent near the activation gate which is a tight steric closure formed by the cytoplasmic end of TM6. Thus, studies on both native (Squid Giant Axon and BK) and cloned (K_v) channels strongly suggest that the intracellular end of TM6 forms an internal gate that, in the closed state, prevents K^+ flux through the channel.

ii. Crystallized bacterial channels

The crystal structures of K^+ channel pores have provided not only a structural picture of K^+ channel permeation and selectivity, but may also provide insight into K^+ channel gating [40-43, 49]. One of these, the KcsA pore, contains the K^+-selective pore and two TM s analogous to TM5 and TM6 of K_v channels [41]. The KcsA protein crystallizes as a teepee-like structure; its wide extracellular domains form the teepee base and the TM6 helices cross each other at their intracellular ends creating a small smokehole at the region called the bundle crossing. As predicted from functional studies, the narrow selectivity filter is formed by the consensus K^+ selectivity motif, GYG, near the extracellular side of the channel. Immediately intracellular to the selectivity filter resides a wide lumen, the internal vestibule, which acts to stabilize charged K^+ ions in the otherwise energetically unfavorable environment of the cell membrane.

Aided by spectroscopic techniques, it was originally proposed that the opening and closing of the KcsA pore occurs by a rotation and translation of the four identical TM6 α-helices (one from each subunit) relative to one another [41, 63]. Later, comparison of a crystallized channel presumably in the closed state (KcsA) with that of a different K^+ channel presumably in the open state (MthK) [40, 42] suggested specific molecular rearrangements that may take place during gating (Fig. i2A, B). The primary difference between the closed channel (Fig. i2A) and the open channel (Fig. i2B) is that each vestibule-lining TM of the open channel contains a kink that bends the α-helix approximately 30°; in contrast, the closed channel α-helix is almost completely straight. The result of this kink is readily apparent at the intracellular end of the channel – in the open channel the helices splay apart whereas in the closed channel they are so close together that they would occlude K^+ ions from entering the pore. This, it is proposed, is the fundamental rearrangement that underlies channel gating. The kink in the helix occurs at a glycine residue that is highly conserved across a wide range of ion channels [40]. The basic mechanism in which an intracellular gate is created by straightening of a pore-lining helix at its "glycine hinge" has been proposed to underlie the gating of a large range of channels, including the SK family [40]. Thus, while the details of TM6 bending may vary (as discussed, it is believed *Shaker* channels are bent at the proline-x-proline motif even in the closed state), the functional data from *Shaker* and BK channels is generally consistent with data obtained from the crystallization studies, providing further evidence that the activation gate of these channels resides at the cytoplasmic end of the last TM.

A

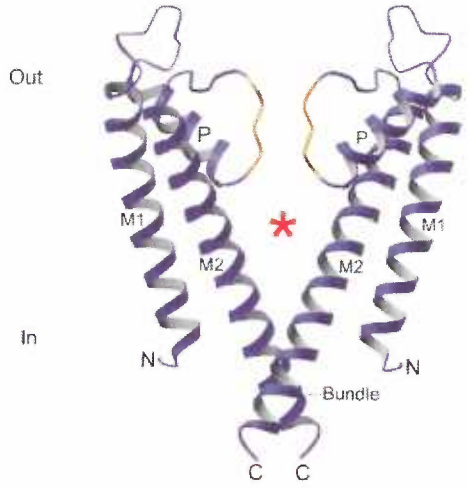

B

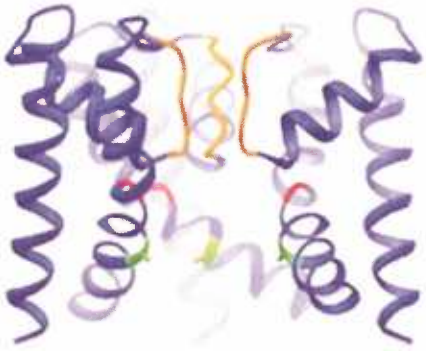

Figure i2. Crystal structures of K^+ channel pores in the presumed closed (A, KcsA) and open (B, MthK) states. Helices corresponding to TM5 and TM6 are shown in blue and the selectivity filter of the P-loop in orange. In A, the inner vestibule is marked with a red asterisk and the bundle crossing that is believed to form the activation gate is labelled bundle . Note that the gate is formed at the cytoplasmic end of the pore. For MthK, the inner helices are splayed open at the glycine hinge residue shown in red, and the alanine residue at the narrowest portion of the entryway to the pore is shaded green. Reproduced from Jiang et al. [40].

iii. A possible exception: CNG channels

Studies of native and cloned K^+ channels using chemical probes, structure-function methodologies, and crystallography all support the notion that an internal gate plays a critical role in K^+ channel activation gating. It has been proposed, however, that the activation gate of cyclic nucleotide-gated (CNG) channels lies not intracellularly, but in the selectivity filter of the channel [64-67]. Like K_v channels, CNG channels are tetrameric complexes of 6 TM domain subunits. Different from K_v channels, the pore of the channels is not selective for K^+; it lacks the consensus K^+-selectivity sequence GYG . Moreover, CNG channels are primarily gated by cyclic nucleotides, not by voltage, although voltage does modulate CNG gating to varying degrees depending on channel subtype [68]. Interestingly, as for SK channels, calmodulin (CaM) interacts with the intracellular domain of CNG channels and modulates their gating behavior. In the case of CNG channels, however, Ca^{2+}-CaM inhibits channel activity and does not activate the channels [69, 70].

Some of the first data suggesting that CNG channels may not possess an intracellular gate was provided by Jeffrey Karpen s lab. They showed that the blocking rate of nickel (Ni^+), a pore-blocking cation, was not Po-dependent when applied to the cytoplasmic face of excised inside-out patches, suggesting that access to the pore is not restricted by a cytoplasmic gate [71]. Later it was shown that CNG channel block by the anesthetic tetracaine was state-dependent, and that in contrast to blockers of the *Shaker* channel, this molecule blocked better in the closed state than in the open state [72, 73].

The first SCAM experiments designed to examine state-dependent reactivity of specific positions in CNG channels were performed in the pore loop (P-loop), not in TM6 [66, 67]. Though the emphasis of the experiments was to understand the role of the P-loop in gating, they also provide evidence against the existence of an intracellular gate. These experiments demonstrated state-independent access of internally applied MTS compounds to at least two P-loop positions, demonstrating that there is not all-or-none access to the pore from the intracellular side [66, 67]. Perhaps more impressive, even Ag^+ ions could bind at one P-loop position with very rapid kinetics ($>10^6$ $M^{-1}s^{-1}$) in both the open and closed states of the channel, though exact rates were not determined [67]. Based on reactivity of certain P-loop positions to MTS compounds applied either to the inside or to the outside of the channel, a model was proposed in which the activation gate was formed by the selectivity filter acting as a thin, iris-like structure that could dilate or constrict to allow or prevent ion flux [67] but see [66]. Later work demonstrated state-dependent modification of four positions in the P-loop by externally applied MTS compounds, suggesting that the P-loop re-orients during gating [65].

More recent experiments have applied the SCAM technique to the TM6 region of a CNG channel to determine if CNG channels do or do not possess an intracellular gate [64]. Different from the results obtained in the *Shaker* studies, it was found that both the MTS compound 2-(aminoethyl) methanethiosulfonate (MTSEA) and Ag^+ could modify a cysteine residue introduced to a position internal to the smokehole equally well whether the channel was open or closed. In fact, this residue was analogous to *Shaker* residue 474C that showed strong state-dependent accessibility when exposed to Cd^{2+} or Ag^+ [61]. This data, taken together with data obtained from Ni^+ and tetracaine block and from

cysteine-scanning of the P-loop, strongly suggest that the primary gate of CNG channels does not reside at the cytoplasmic end of TM6, but may instead be in the selectivity filter of the channel. Thus for CNG channels, it is believed that the selectivity filter has two functions; it defines the permeation characteristics of the channel, and it forms the channel gate.

iv. Evidence for selectivity filter involvement in gating

The hypothesis that the selectivity filter may also function in channel gating is clearly supported by data from the CNG channel family, but also by experiments performed on K^+ channels. In the KcsA channel, electron paramagnetic resonance (EPR) studies suggest that in addition to large movements at the cytoplasmic end of the pore, the intracellular end of the selectivity filter moves during gating [63]. Moreover, altering the K^+ concentration in the KcsA crystal structure to simulate high and low conductance states of the channel demonstrates that the selectivity filter can undergo significant conformational changes [48]. These changes alone would be sufficient to dictate whether the channel was open (conducting) or closed (non-conducting). In a very different type of K^+ channel that contains 2 TM's and is modulated by ATP (K_{ATP}), altering the electronegativity of the backbone amino acids in the selectivity filter also alters the gating properties of the channel [74]. Finally, *Shaker* channels are known to enter sub-conductance states that are dependent on the identity of the permeating ion, as if the ion itself affects the gate [75, 76]. Thus, even for channels for which it is believed that the intracellular gate is the primary activation gate, the selectivity filter most likely also undergoes conformational changes that contribute to the conduction state of the channel.

v. C-type inactivation: gating at the channel pore

Activation gating is a complicated process that, depending on the ion channel, can involve movement of a cytoplasmic gate, a selectivity filter gate, or both. The mechanism underlying one type of gating known as C-type inactivation, however, clearly involves re-orientation of the external pore very near the selectivity filter. Inactivation is the process by which ion channels stop conducting even in the presence of a maintained opening stimulus. For K_v channels, inactivation may occur by at least two separate mechanisms, called N- and C-type inactivation. N-type inactivation occurs when an N-terminal portion of the channel [77], or a portion of an attached β-subunit of the channel [78], enters and plugs the conduction pathway of open channels. This type of inactivation, sometimes called ball-and-chain gating since it involves insertion of a tethered ball into the mouth of the channel, is generally very rapid; as soon as the TM6 gate opens, the ball plugs the pore leading to the transient current that scientists observe physiologically as a transient K^+ current, or Ia. C-type inactivation is a slower and completely separate process (it persists even if the N-terminal ball is deleted) [79] that involves re-orientation of the α-subunits of the channel at the external end of the pore. C-type inactivation is strongly influenced by external K^+ concentration [80], and can be prevented if the pore is plugged with TEA [81]. Further, specific mutations in the outer pore specifically alter C-type inactivation [80], and introduction of a cysteine at a particular position allows the inactivation gate to be locked shut in the presence of metal ion [82, 83]. Thus C-type inactivation is distinct from both N-type inactivation and activation gating in that it clearly involves gross re-arrangement of the outer mouth of the pore. It seems likely that this re-arrangement is reflected in crystal structures of the selectivity filter in the presence of low and high K^+; in high K^+, the carbonyl oxygens of

the filter embrace K^+, acting as a perfect surrogate for water thus allowing both high throughput and high selectivity [48]. In low K^+, the carbonyl oxygens twist out and the selectivity filter deforms and collapses slightly — clearly a non-conducting conformation [48]. The notion that this may represent a C-type inactivated state is intriguing, if circumstantial - certain K_v channels as they enter the C-type inactivated state do not allow conduction of K^+, but do allow conduction of Na^+ [84]. Since the selectivity filter in the low K^+ crystal is smaller, one could imagine that it would more readily accommodate the smaller Na^+ ion, and allow it but not the larger K^+, to permeate [48].

E. SK CHANNELS

a. Cloning

SK channels were first described by the Lazdunski lab in 1984 [85]. Studying the action potential of cultured rat skeletal muscle cells, they noticed a persistent AHP in the presence of TEA, a blocker of the large conductance Ca^{2+}-activated K^+ (BK) channels that were believed responsible for repolarization and generation of the AHP in excitable tissues. The persistent AHP channels were, however, sensitive to a component of honeybee venom, apamin. A subsequent study of inside-out patches excised from CA1 hippocampal neurons identified two populations of Ca^{2+}-activated K^+ (K_{ca}) channels [6]. The first had BK-like properties including high external TEA sensitivity, large conductance (220 pS), K^+ selectivity, and activation by voltage and by Ca^{2+}. The second was not voltage-dependent, but was activated by low levels of Ca^{2+}. Further, the outward current was blocked by internal magnesium (Mg^{2+}) (the current rectified inwardly) and the channel had a small conductance (19pS) [6]. Though not tested in these experiments, this second channel was presumed to underlie the AHP in CA1 neurons. Such an AHP

had seven years earlier been shown to cause severe accommodation in voltage clamp studies of CA1 pyramidal neurones [5].

Motivated by this data, the Adelman lab set out to clone the channel that was responsible for generating the AHP in excitable tissue. Armed with knowledge derived from the cloning of other K^+ channels, an expressed sequence tag (EST) database was screened for GYG-motif-containing fragments. Once identified, a rat cDNA library was screened with radio-labelled nucleotide fragments corresponding to the novel EST, and hybridizing candidates cloned into appropriate vectors and sequenced. The result of this effort was that three highly homologous SK channels (SK1, SK2 and SK3) were cloned and functionally characterized by heterologous expression in Xenopus oocytes [86]. As for the AHP currents described in native tissue, SK channels were shown to be voltage-independent, Ca^{2+}-activated (EC_{50} ~ 600 nM), K^+-selective, inwardly rectifying, and low conductance (approximately 10 pS). Analysis of inside-out patches excised from CA1 pyramidal neurons showed that native channels, like the cloned channel, were about half-activated by 600 nM Ca^{2+}, and had a chord conductance of 10 pS [10]. Further analysis of the cloned channels demonstrated that at least two of the three channels, SK2 and SK3, had high sensitivity to extracellularly applied apamin (IC50 ~ 10 and 100 nM, respectively), but were relatively insensitive to external TEA [87]. Close correlation between the properties of cloned SK channels and native conductances provide evidence that the cloned SK channel family underlies AHP's in excitable tissue. Direct proof of this will be obtained by genetic knock-out of SK channels in mice combined with detailed recording of AHP's from a range of excitable tissue.

b. Pore Structure

Like K_v channels, sequence alignment and functional expression suggest that SK channels are tetrameric assemblies of α subunits, each consisting of six TMs with their N- and C- termini residing in the cytoplasm. The pore of SK channels shares homology with other K^+ channels, as well as a high selectivity for K^+ over other ions. Interestingly, similar to inwardly rectifying K^+ channels, SK channels are blocked by divalent ions of the alkaline earth metal family, including Ca^{2+} and Mg^{2+}. Block is strongly voltage-dependent and influenced by external K^+ and direction of ion flow, suggesting that these ions interact deep in the pore within the membrane field [88]. A somewhat quantitative technique for examining channel interaction with other proteins or compounds, mutant cycle analysis, has been applied to the pore region of the SK2 channel to further localize the divalent ion binding site [89]. These experiments indicated that the ions interact most strongly with reside 359, a serine just below the selectivity filter. When this serine is mutated to alanine, blocking potency of Ba^{2+}, for example, is decreased approximately 50-fold [89]. This result is nicely consistent with data obtained from KcsA; when Ba^{2+} is added to the crystal it clearly localizes to the region just below the selectivity filter [90]. Further, Ba^{2+} blocks BK and *Shaker* channels in a voltage-dependent manner, and at least one of its binding sites is believed to lie just internal to the selectivity filter [26, 91-94]. These data, coupled with the strong K^+ selectivity of SK channels and sequence conservation across K^+ channel families, suggest that the inner vestibule and deep pore of SK channels likely share a common architecture with other K^+ channels.

c. Gating

i. Identification of Calmodulin (CaM)

While the overall structure of SK channels might be similar to the structure of voltage-gated channels, it is clear that the SK gating mechanism is drastically different since SK channels open in response to increases in Ca^{2+}, not voltage. After cloning the SK family, it was clearly important to understand how Ca^{2+} was sensed by the channels. It was reasoned that Ca^{2+}-sensitivity was most likely conferred in one of two ways; either directly, by Ca^{2+} binding to the channel, or indirectly, by Ca^{2+} binding to a β-subunit that could then effect gating. It seemed unlikely to be a second-messenger based mechanism since gating was very fast. Initial experiments on the cloned channels seeking to identify an intracellular Ca^{2+}-binding site were straightforward, but wholly unsuccessful [95]. Each negative charge, and in some cases multiple negative charges, in the cytoplasmic domains of rSK2 were individually mutated to a neutral amino acid, and the Ca^{2+} sensitivity of the mutant channel assayed electrophysiologically. The logic was that if Ca^{2+} directly bound the channel, it would necessarily bind to negatively charged amino acids, and charge neutralization should be sufficient to disrupt Ca^{2+} binding and thus gating. The result of the experiments was clear; none of the mutant channels had significantly altered Ca^{2+} sensitivity [95].

The results from yeast two-hybrid and GST pulldown experiments were more informative. It was found that a portion of the channel C-terminus (termed the ABC region since it contained 3 putative α-helical domains, A, B, and C), could directly bind the ubiquitous Ca^{2+}-sensing molecule CaM. Further biochemical characterization of the interaction provided the first clues that CaM could change conformation when bound to

the SK C-terminus. In the presence of Ca^{2+}, a 65 amino acid stretch of the C-terminus was sufficient to bind CaM, but in the absence of Ca^{2+}, the entire ABC region was required. Thus it appeared that CaM binding to the C-terminus of SK channels could confer Ca^{2+} sensitivity to the channel by altering its conformation in response to changes in intracellular Ca^{2+} levels [95].

ii. Functional confirmation of CaM as the gating molecule

To test the idea that CaM interacts with the ABC region in a dynamic Ca^{2+}-dependent manner, an *in vitro* experiment that exploited the environment-sensitive fluorescent properties of the sole tryptophan in the ABC domain was performed [96]. The peptide was solubilized and its fluorescence profile determined by exciting the sample at 295 nm and sampling in 1 nm intervals from 310 to 410 nm. CaM was then added to the sample, causing a left-shift in the fluorescence profile, consistent with the residue getting buried in a more hydrophobic environment. Upon addition of Ca^{2+} (100 μM free Ca^{2+}), the fluorescence was significantly quenched, and a further left-shift was observed, suggesting that Ca^{2+} induced further conformational change around the tryptophan residue. This was the first real-time observation of CaM interacting with the ABC fragment, and it suggested that the tryptophan residue on SK2 interacts with CaM in a dynamic Ca^{2+}-dependent fashion.

Functional evidence that CaM acts as the Ca^{2+}-sensor for SK channels was obtained by mutating the Ca^{2+}-sensing EF hands of CaM, heterologously overexpressing these mutant CaM's with WT SK channels, and looking for changes in the SK gating properties as measured electrophysiologically. Thus, a dominant negative strategy was employed in

which the four Ca^{2+}-sensing EF hand motifs of CaM were mutated in all possible combinations, and the mutant CaM molecules overexpressed in oocytes together with the channels [95, 96]. It was found that if the first amino acid of all four EF hands contained a D to A mutation (Figure i3) and this CaM was expressed with the channel, the channel did not express currents. If, however, just EF hands 3 and 4 were mutated, the channel functioned normally as assayed by Ca^{2+} sensitivity. Mutation of EF hand 1 or 2 alone rendered the channels approximately 2-fold less sensitive to Ca^{2+}, and lowered the Hill coefficient. Taken together with further yeast two hybrid and mutational studies of the CaM-SK interaction, a model was proposed in which the N-lobe of CaM (which contains EF hands 1 and 2) was responsible for sensing Ca^{2+}, whereas the C-lobe (containing EF hands 3 and4) and the linker region between the two lobes was responsible for constitutive interaction with the channel [95, 96].

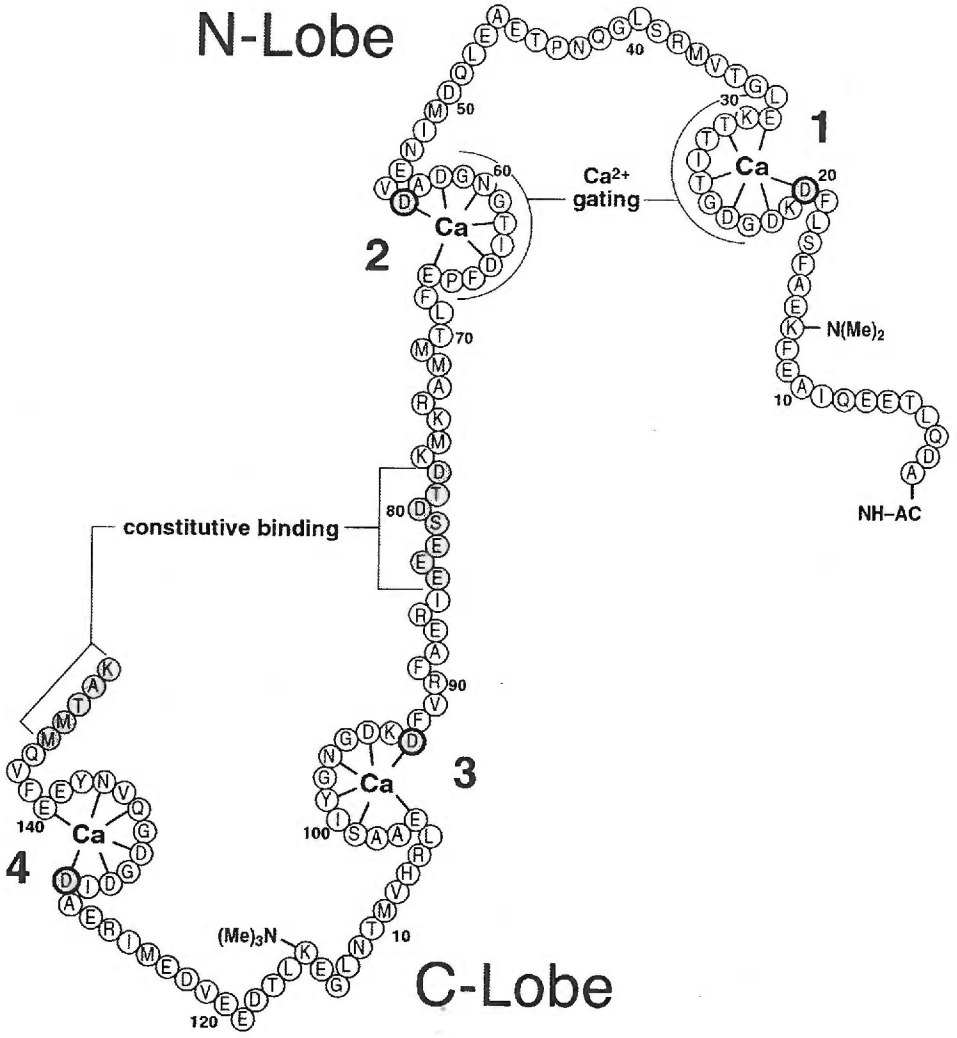

Figure i3. Schematic of CaM. EF hands 1-4 are shown coordinating Ca^{2+}, and aspartate residues at the first position of each EF hand are circled. Note that for SK channels, EF hands 1 and 2 in the N-lobe of CaM bind Ca^{2+}, whereas a portion of the linker region and the C-lobe are responsible for constitutive binding to the SK C-terminus. Adapted from Keen et al. [96].

iii. Crystal structure of CaM interaction with SK C-terminus

The fundamental characteristics of this model were affirmed when the crystal structure of Ca^{2+}-CaM interacting with the CaMBD of SK2 (the A, B, C and D helices of the C-terminus) was resolved at 1.98 Å [97]. In the structure, the EF hands 1 and 2 are occupied by Ca^{2+} ions, whereas EF hands 3 and 4 are so distorted that they can't bind Ca^{2+} (Figure i4). Further, the tryptophan in the SK channel that was assayed fluorescently is completely buried in a hydrophobic pocket provided by the C-lobe of CaM, suggesting that CaM re-arrangement during gating would, as observed *in vitro,* alter the fluorescent properties of the tryptophan residue. Finally, two SK residues (464 and 467) that were shown biochemically and functionally to be critical for tight association of CaM with the CaMBD, are seen in the crystal structure forming salt bridges to two oppositely charged residues in CaM (84 and87) [95-97]. It was subsequently demonstrated by cell surface expression, biochemistry, and electrophysiology that altering either pair of residues (in SK or CaM) inhibits the CaM-CaMBD interaction [98].

Interestingly, the crystal structure shows a dimer of CaMBDs, with each CaMBD complexed to two CaMs. Thus each CaM interacts with two of the four SK subunits. This suggests that although the pore of the channel most likely retains the C4 symmetry common to all known K^+ channels, the C-terminal gating domain exists as a "dimer-of dimers". Determining how this dimer -of-dimers acts to gate the channel will most likely require crystallization of the Ca^{2+}-free CaM-CaMBD structure together with complimentary functional and biochemical assays. Understanding this gating mechanism may have broad implications since gating domains of both an inwardly rectifying K+

channel (K_{ir}) and a glutamate receptor crystallize in this same dimer-of-dimers configuration [99, 100].

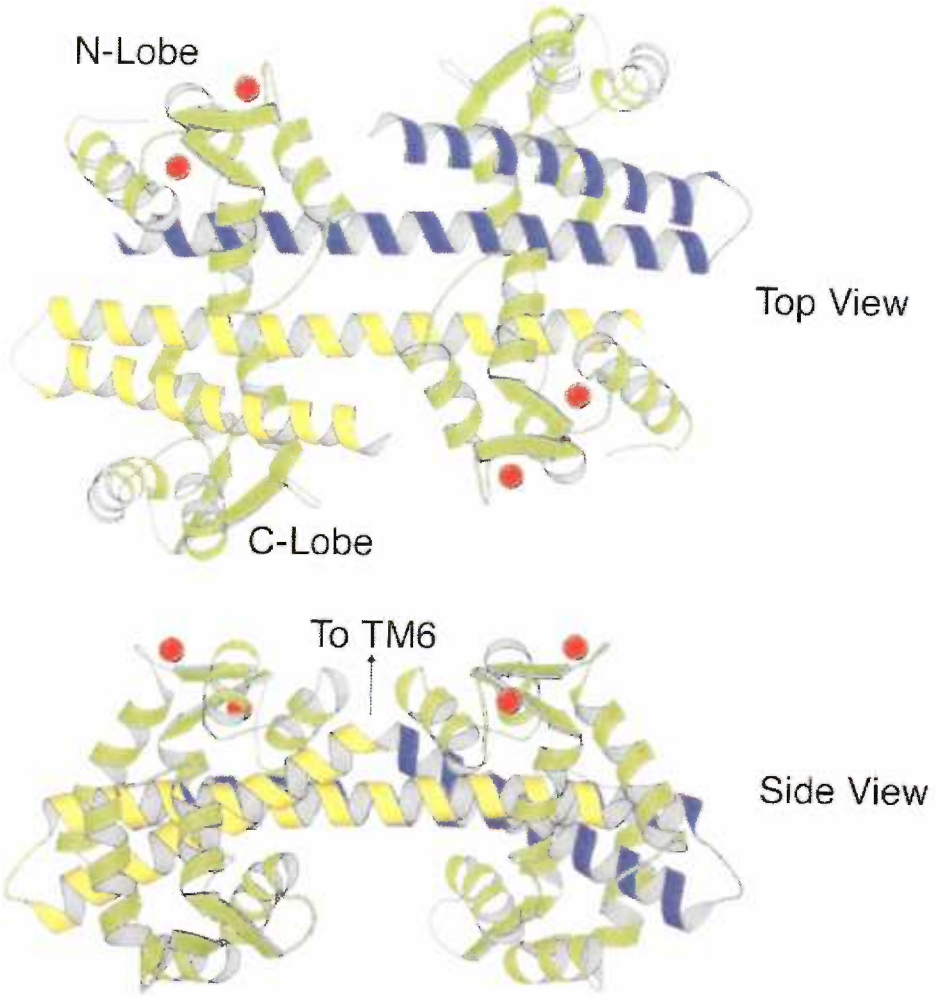

Figure i4. Top and side-views of the crystal structure of CaM complexed with the SK CaMBD in the presence of Ca^{2+}. CaM molecules are shown in green, Ca^{2+} as red spheres, and the two SK peptides are blue and yellow. The complex is a dimer-of-dimers and only two of four channel subunits are shown. Note that EF hands 1 and 2, but not 3 and 4, bind Ca^{2+}. Not resolved in the crystal are SK residues 396-412 that link this C-terminal domain to the TM6 helices. Adapted from Schumacher et al. [97].

iv. Missing pieces: coupling and location of the gate

Despite increasingly detailed work on the dynamic gating interactions between CaM and the SK C-terminus, little is known about the inner vestibule and gating movements of Ca^{2+}-gated SK channels. Indeed, all gating experiments on SK channels thus far have focused instead on elucidating the role of the C-terminal interaction with CaM. It is worth noting that the crystal structure of the CaM-CaMBD lacks structural information about the 18 residues that connect the cytoplasmic end of TM6 (395) to the first residue in the structure (413), despite the fact that these residues are present in the crystallized protein [97]. In addition, a nuclear magnetic resonance (NMR) study of the CaMBD failed to resolve residues 396-413 even in the absence of Ca^{2+} [101]. These residues lack an ordered structure despite the fact that they must be important for gating since they are the link between the Ca^{2+}-sensing domain and the pore of the channel. Whether the lack of structure is inherent to the protein, a complication of isolating the C-terminus from the rest of the channel, or experimental artifact remains to be resolved. The work presented in this thesis does not seek to resolve how CaM-CaMBD re-arrangements are coupled to the channel gate, but rather attempts to locate the physical gate itself, and to gain some understanding of how the pore, inner vestibule, and activation gate of SK channels correlate with other well-studied ion channels.

II. CHAPTER 2

Localization of the Activation Gate for Small Conductance Ca^{2+}-activated K^+ Channels

Andrew Bruening-Wright*, Maria A. Schumacher#, John P. Adelman*, James Maylie^

*Vollum Institute, #Department of Biochemistry and Molecular Biology, and

^Department of Obstetrics and Gynecology, Oregon Health and Sciences University,

Portland, Oregon

Abbreviated title: The SK channel gate

Please send correspondences to:

Dr. James Maylie, Ph.D.

Department of Obstetrics and Gynecology

Oregon Health Sciences University; L-458

3181 S.W. Sam Jackson Park Road

Portland, OR 97201

(503)-494-2106

(503)-494-5296 (fax)

mayliej@ohsu.edu (email)

Acknowledgments. This work was supported by National Institutes of Health grants to JPA and JM. The authors wish to acknowledge Chris Bond, Dr. Paco Herson, and Dr. Aaron Gerlach for stimulating discussions.

A. ABSTRACT

Small conductance Ca^{2+}-activated K^+ (SK) channels open in response to increased cytosolic Ca^{2+} and contribute to the AHP in many excitable cell types. Opening of SK channels is initiated by Ca^{2+} binding to CaM that is bound to the C-terminus of the channel. Based upon structural information, a chemo-mechanical gating model has been proposed in which the chemical energy derived from Ca^{2+}-binding is transduced into mechanical force that restructures the protein to allow K^+ ion conduction through the pore. However, the residues that comprise the physical gate of the SK channels have not been identified. In K_v channels access to the inner vestibule is controlled by a bundle crossing formed by the intracellular end of TM6 of each of the four channel subunits. Probing SK channels with internally applied quaternary amines suggests that the inner vestibules of K_v and SK channels share structural similarity. Using substituted cysteine accessibility mutagenesis, the relatively large molecule [2-(trimethylammonium)] methanethiosulfonate (MTSET) accessed positions near the putative bundle crossing more rapidly in the open than the closed state, but did not modify TM6 positions closer to the selectivity filter. In contrast, the smaller compound, MTSEA, modified a position predicted to lie in the lumen immediately intracellular to the selectivity filter equivalently in the open and closed states. The pore blocker TBuA impeded MTSEA access to this position in both open and closed channels. The results suggest that the SK channel gate is not formed by the cytoplasmic end of TM6, but resides deep in the channel pore in or near the selectivity filter.

B. INTRODUCTION

Three highly homologous SK channel subunits have been cloned (SK1, SK2 and SK3), each containing 6 putative TM segments with predicted topologies similar to K_v channels [102]. The fourth TM domain, TM4, contains positively charged residues but SK channels are not gated by voltage. Rather, they are gated solely by intracellular Ca^{2+} ions. SK channels function as heteromeric complexes with CaM that is constitutively attached to a binding domain, the CaMBD, in the membrane-proximal region of the intracellular C-terminus of the channel. CaM functions as the Ca^{2+}-sensor for SK channels, transducing the Ca^{2+}-gating signal through the CaMBD to a yet unidentified activation gate [95-97].

Crystal structure and electron paramagnetic resonance (EPR) studies of the bacterial K^+ channel, KcsA, and structure-function studies of K_v and CNG cation channels, have given rise to mechanistic models for the coupling of the gating cue to channel opening [62, 63, 103]. Within the KcsA channel, the four M2 segments form a vestibule in the shape of an inverted teepee [41]. The bundle crossing near the membrane interface with the cytoplasm forms a structure like the "smokehole" of a teepee that constitutes the physical gate of the channel. Rearrangement of the helices in response to the gating cue opens or closes the "smokehole". This model is supported by EPR measurements that detected relatively large movements near this region of KcsA during gating, and smaller movements on the intracellular side of the selectivity filter [63]. Further investigation of KcsA has led to the hypothesis that selectivity filter conformational changes during gating are coupled to the rearrangement of the channel activation gate [48, 63, 104].

For *Shaker* K_v channels, experiments using SCAM [60-62] and cross-linking methodologies [105] strongly suggest that the TM6 bundle crossing forms the activation gate. Thus, for both KcsA and K_v channels, the residues that form the activation gate are believed to reside at the cytoplasmic end of the inner vestibule. In contrast, studies of the CNG channel suggest that the selectivity filter of the CNG1 channel functions as the channel gate [66, 67, 103]. This is particularly relevant to SK channels since both CNG and SK channels are voltage-independent, relying on the binding of an intracellular ligand to a C-terminal domain for channel gating [68, 95, 96].

In this report, block by intracellular quaternary amines and SCAM were used to probe the topology of the SK2 channel inner vestibule, examine conformational changes during SK channel gating, and to test if the distal domain of TM6 forms an SK activation gate.

C. MATERIALS AND METHODS

a. Molecular Biology

Constructs were subcloned either into pJPA5 for expression in COSm6 cells, or into the oocyte expression vector, pBF. *In vitro* mRNA was synthesized from pBF constructs using SP6 polymerase (Life Technologies, Inc.). Site-directed mutagenesis was performed using PFU polymerase (Stratagene) and the overlap PCR technique [106]. The complete nucleotide sequences of the coding regions were verified prior to expression studies.

b. Electrophysiology

For COSm6 experiments, cells were transfected using Polyfect reagent (Qiagen, USA) as per manufacturer's instructions, plated on Fisherbrand Growth coverslips (Fisher Scientific, USA) and currents were recorded 24-48 hours post-transfection. For oocyte experiments, 50 nl mRNA (20-50 ng) per oocyte was micro-injected as previously described and currents were recorded 2-7 days after injection. Bath solution contained either 150 mM (COSm6) or 120 mM (oocyte) K^+ methanesulfonate, 10mM HEPES, 1mM EGTA, and CaOH to yield the desired free Ca^{2+} concentration, and adjusted to pH 7.2 with methanesulfonic acid [107]. Free Ca^{2+} for all open state experiments was adjusted to 1 μM to maximally activate the channels, except for A392C that was adjusted to 10 μM. For closed state experiments, no Ca^{2+} was added (0 Ca^{2+}) yielding a free Ca^{2+} level < 2 nM. Inside-out patches were pulled using borosilicate glass patch electrodes filled with 10 μM Ca^{2+} solution and pulled to resistances between 1.0 and 3.0 MΩ. Leak and background currents were measured by changing the bath solution on the inside face of the patch to 0 Ca^{2+} to close SK2 channels. Rapid solution changes were performed

using an RSC-200 (Molecular Kinetics, USA). Currents were measured and digitized with an EPC9 (Heka, Germany), currents sampled and filtered at 1 kHz, and analysis performed using Pulse (Heka, Germany) and Igor (Wavemetrics, USA) software. No differences in Ca^{2+} sensitivity, gating kinetics, or MTS reactivity were observed between patches from oocytes or COSm6 cells, and in some cases results obtained from both expression systems were combined. All reagents were diluted from concentrated stocks prepared the day of the experiment, and MTS compounds were used within 30 minutes of mixing into solution.

c. Data Analysis

All values are reported as the mean ± standard error of mean (SEM) of n experiments. Statistical significance was evaluated using a Students t test, and a p value ≤ 0.05 considered significant. Modification rates were related to the time constant (t) of single exponential fits to plots of current amplitude versus MTS exposure duration by the reciprocal of t*[MTS] where [MTS] was the concentration of MTSET or MTSEA used in the experiment. Dose response relationships for TEA, triethylhexylammonium (C6-TEA), TBuA, and tetrahexylammonium (THexA), were fit with a single binding isotherm; Icontrol*[X]/([X] + IC_{50}) where [X] is the concentration of blocker, Icontrol is the current amplitude before application of blocker, and IC_{50} represents the concentration at which macroscopic current is half-blocked.

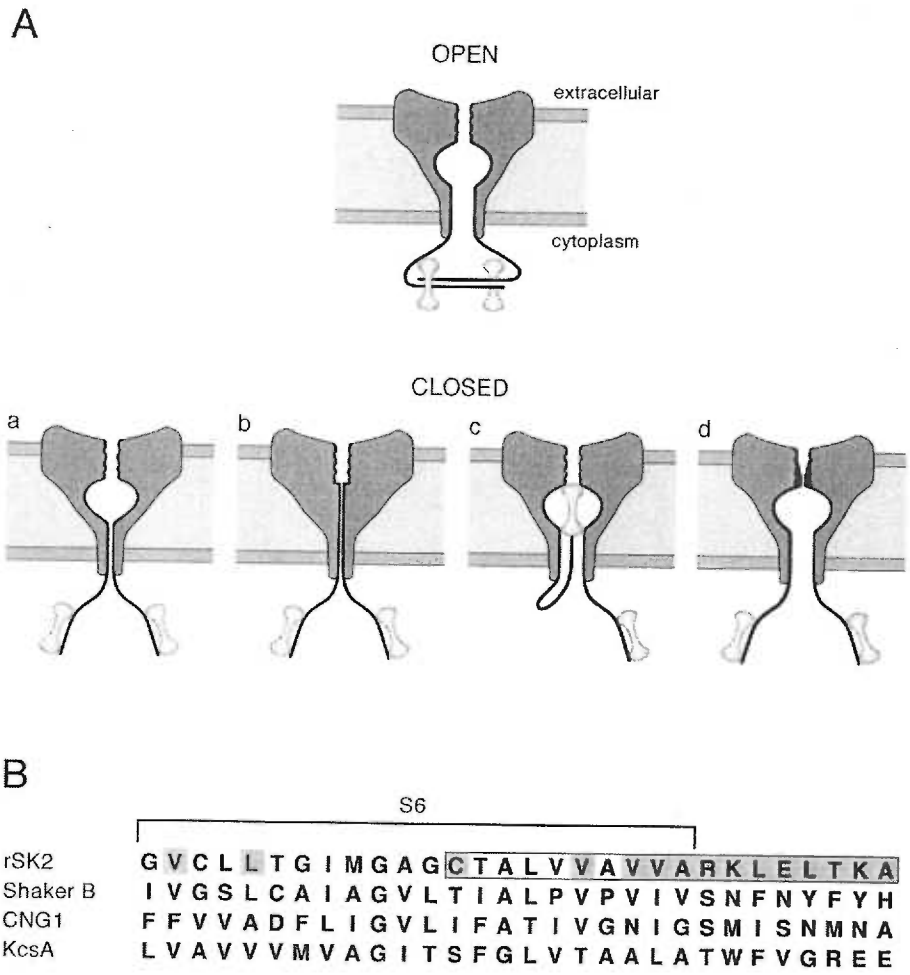

Figure 1. Possible SK channel gating mechanisms. *A,* SK channel gating models. In each model, two of four subunits are depicted in cross-section embedded in the membrane with CaM (dumbbells) associated with the intracellular C-terminal domain. For the open state, the SK-CaM complex is modeled as a dimer-of-dimers, as indicated by the CaMBD/Ca^2-CaM crystal structure. In the four closed state models (a-d), the CaMBD/CaM complex is monomeric [97]. (a) The TM6 bundle crossing acts as the gate preventing access to the lumen and selectivity filter, as suggested for K_v and KcsA channels. (b) Collapse of the inner vestibule, including the aqueous lumen, closes SK channels. (c) CaM may act as a blocking particle in a "ball-and-chain" type mechanism. (d) Selectivity filter rearrangement prevents ion permeation in closed SK channels, as suggested for ligand-gated CNG channels. *B*, Sequence alignments of TM6 and proximal cytoplasmic residues of *Shaker* B, a cyclic-nucleotide gated channel (CNG1), and the proton-gated bacterial K^+ channel, KcsA. The boxed region highlights the amino acids (386-403) examined with the SCAM technique in this study, numbered arrows indicate residues of particular importance (see results), and shaded residues are conserved in all SK family members.

D. RESULTS

At least four gating models may be postulated for SK channels (Fig. 1A). Channel opening and closing could occur, 1) by a "smokehole" at the TM6 bundle crossing similar to the KcsA and K_v channel gating models (model a); 2) by an expansion or collapse of the inner vestibule (model b); 3) by a "ball-and-chain" mechanism analogous to that which underlies N-type inactivation of K_v channels, perhaps with CaM as the blocking particle (model c); 4) by a rearrangement of the selectivity filter (model d). The different models were tested by examining the topology and gating-dependent conformational changes in the inner vestibule using excised membrane patches containing heterologously expressed SK2 channels.

a. A Conserved Inner Vestibule Topology Between SK and K_v Channels

Small quaternary amines such as TEA have been used to probe the architecture of the inner pore region of K_v channels, providing evidence for an inner vestibule within the membrane field that is accessed only in the open state [21, 55, 58, 60]. Further, these experiments showed that increasing the length of one or more of the four hydrophobic side-chains of TEA increases the potency of block, suggesting that a hydrophobic pocket stabilizes the interaction between channel and pore blocker [55, 81]. Despite limited primary sequence homology between SK and K_v channels in the inner vestibule region, both channel types have highly hydrophobic TM6 domains (Fig. 1B).

Dose-response relationships for block of SK2 by TEA and three of its derivatives, TBuA, THexA, and C6-TEA, were obtained by applying compounds to the intracellular face of

inside-out patches (Figure Aa-1). TEA only weakly blocked SK2 (IC_{50} = 46.8 ± 2.2 mM; n=8). However increasing one of the four side-chains from 2 carbons to 6 carbons (C6-TEA) decreased the IC_{50} more than 5-fold (8.6 ± 0.4 mM; n=3). When all four side-chains were increased from 2 to 4 carbons (TBuA), the IC_{50} decreased ~26-fold (1.8 ± 0.2 mM; n=6). Increasing all of the side chains to 6-carbons (THexA) increased blocking potency more than 3,000-fold (0.014 ± 0.002 mM; n=5). Therefore, the rank order of potency for block of SK2 channels by these compounds, THexA>TBuA>C6-TEA>TEA, is similar to that determined for K_v channels, although in general the IC_{50} was lower for SK2 than for *Shaker* channels (eg. ~ 120x lower for TEA and 86x lower for C6-TEA) [55]. For both channel types, the potency of block increased with increased side-chain length. Moreover, as for K_v channels, SK channel block by all of the compounds was voltage-dependent. Ratios of mean IC_{50} at 80mV to mean IC_{50} at –80 mV were 0.16, 0.04, 0.08, 0.17 for TEA, C6-TEA, TBuA and THexA, respectively. The results suggest open state access by TEA derivatives to an inner vestibule within the SK2 membrane field.

b. State-Dependent Conformational Changes in the TM6 Helix

State-dependent accessibility to the inner vestibule of SK2 channels was explored using SCAM and cysteine-reactive reagents. Each of 9 residues in TM6 and 8 residues C-terminal to TM6 were individually mutated to cysteine (Fig. 1B) and assayed for reactivity with MTS compounds when the channels were either open or closed. If the side chain of the introduced cysteine residue resides in the conduction pathway and is available to MTS compounds, then disulfide bond formation may irreversibly reduce K^+

permeation either through electrostatic or steric hindrance [59]. If the cysteine residue points away from the pore, buried in the lipid bilayer or surrounding protein, or if MTS reagents do not attach or attach only very slowly, little if any current reduction will be observed. Thus, the availability and orientation of specific residues can be tested in the open and closed state.

Inside-out patches containing heterologously expressed wild type (WT) or cysteine-substituted SK2 channels were exposed to 1mM MTSET for 8 s either in the open or closed state. This concentration and duration of exposure were sufficient to reveal sites that reacted quickly with MTSET and to reveal strong state-dependence while avoiding the complications of channel rundown observed in some of the mutant channels. Representative traces showing the effects of MTSET exposure in the open state and closed state are presented in Fig. 2 for WT and two different cysteine-substituted sites in SK2, A392C and R396C. For open state experiments, channels were first closed and opened confirming rapid solution exchange (typical time constants of 20 ms and 50 ms for activation and deactivation using 1 μM and 0 Ca^{2+} solutions, respectively). Channels were then exposed to 1mM MTSET for 8 s, and the fraction of irreversibly blocked current was measured after MTSET washout (Fig. 2A, left). WT SK2 contains 9 native cysteine residues, including one at position 386 in TM6 (Fig. 1B). As shown in figure 2A (left), WT SK2 channels were rapidly and reversibly blocked by ~14% in the open state, as current recovered to ~97% of the control level following MTSET washout. This suggests that MTSET does not react with endogenous cysteines to block ion permeation, but rather behaves as a reversible pore blocker. To evaluate reactivity in the closed state, channels were closed and then exposed to MTSET for 8 s, washed in 0 Ca^{2+} solution for

2 s, and re-opened to determine the amount of irreversible block. Figure 2A (right) shows that for WT channels, the current following closed state MTSET exposure was ~96% of the control current.

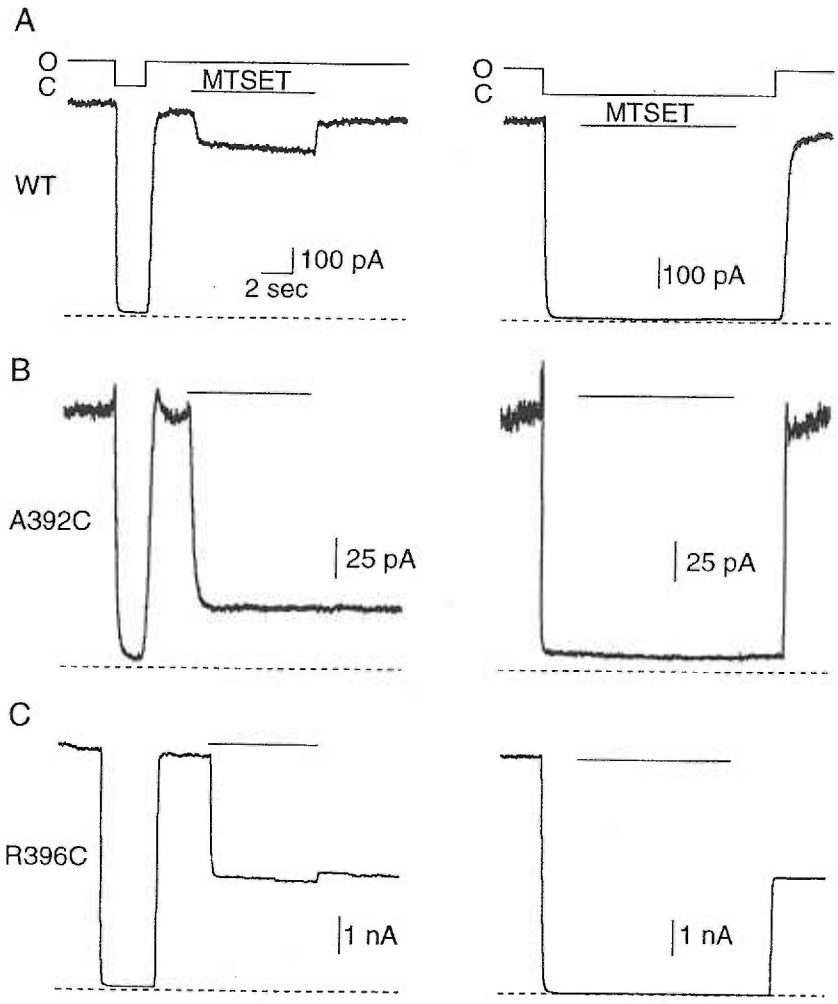

Figure 2. MTSET reactivity in WT and cysteine substituted SK2 channels. *A,B,C,* Representative traces showing open and closed state MTSET reactivity for WT, A392C, and R396C, respectively. For open state experiments (left), channels were first closed then re-opened using saturating Ca^{2+} solutions to verify adequate exchange rates. Then MTSET (1 mM) was applied to open channels for 8 s, MTSET was washed out, and current amplitudes before and after MTSET application were compared. For closed state experiments (right), MTSET (1 mM) was applied to closed channels (0 Ca^{2+}) for 8s, washed out with 0 Ca^{2+} solution for 2 s, channels re-opened and current amplitudes compared before and after closed state application. Bars above the traces indicate when MTSET was applied, the dashed line indicates 0 current level, and the solid line above the trace indicates Ca^{2+} steps from saturating (1 μM, "O" for open state) to "0 Ca^{2+}" (< 2nM, "C" for closed state) solution.

These results demonstrate that MTSET did not irreversibly react with WT SK2 in either the open or closed states (open state current reduced by 3.6 ± 1.1% n=8, closed state current reduced by 3.8 ± 1.3% n=6). In contrast, R396C, which is located just inside the cytoplasm beneath TM6, demonstrated irreversible reactivity with MTSET in both states (open state current reduced by 44.8 ± 3.7% n=5, closed state current reduced by 49.7 ± 4.5% n=3, Fig. 2C), suggesting that this site is available to MTSET whether channels are open or closed. A392C, which is located between the selectivity filter and the putative bundle crossing, showed state-dependent modification by MTSET, reacting rapidly and irreversibly in the open state and not in the closed state (Fig. 2B). The current was reduced by 69.4 ± 5.4% (n=8) and 1.6 ± 6.6% (n=9) in the open and closed states, respectively, suggesting that conformational changes occur at or near position 392 during gating.

To obtain more information about accessibility of introduced cysteines, the modification rates by MTSET were determined for both open and closed states. The open state modification rate was defined by the inverse exponential constant of a single exponential fit to the decay of the current amplitude plotted as a function of the product of cumulative exposure time and MTSET concentration (units of mMs; Fig. 3B, D). For the representative traces shown in Fig. 3B and D, open state exponential constants were 0.2 and 0.1 mMs and rates were 4.2×10^3 and 1.1×10^4 $M^{-1}s^{-1}$ for A392C and R396C, respectively. Closed state modification rates were determined by repeating the closed state protocol (Fig. 2, right panels) several times. Current amplitudes after MTSET washout and channel re-opening were measured after each 8 s exposure (Fig. 3A, C) and plotted as a function of the product of cumulative exposure time and MTSET

concentration (closed circles, Fig. 3B, D). The data points were fitted by a single exponential and the inverse of the exponential constant defined the closed state modification rate. For these A392C and R396C examples, closed state exponential constants were 65.9 and 0.2 mMs and rates were 15 and 5944 $M^{-1}s^{-1}$, respectively. For comparison, the open and closed state modification time courses were overlaid for A392C in Fig. 3B and for R396C in Fig. 3D.

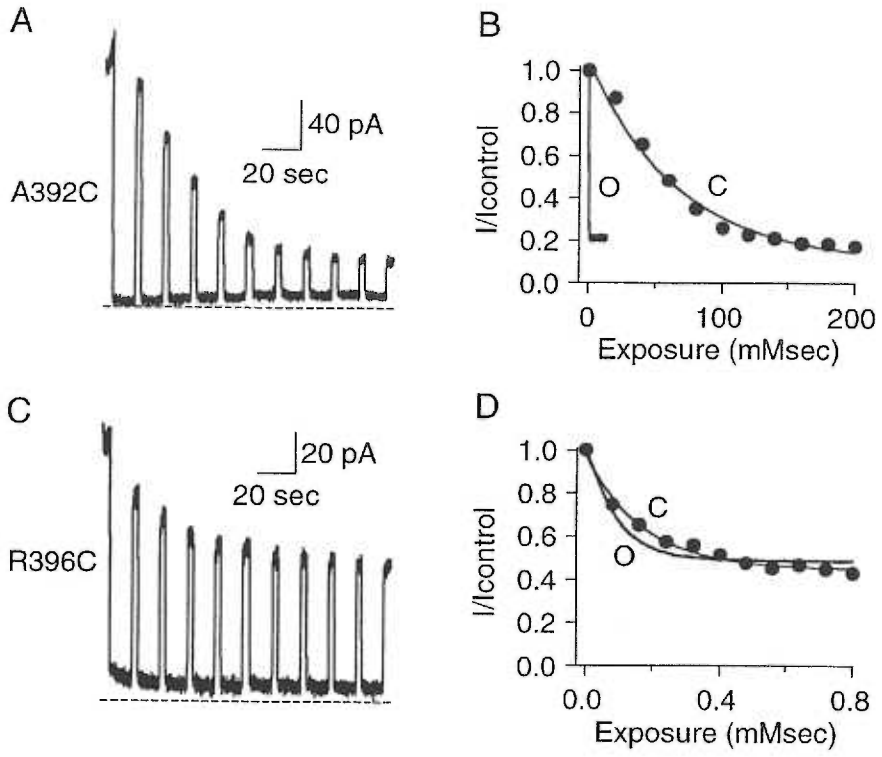

Figure 3. Determination of MTSET modification rates. *A*, Repeated closed state 1mM MTSET application to A392C channels using the protocol of Fig. 2. *B*, Open (O, black trace) and closed (C, closed circles) state decay time courses for A392C normalized to control current and plotted versus the product of cumulative MTSET exposure and MTSET concentration. The open state trace is taken from Fig. 2B, and the closed state decay determined by measuring current amplitude after each of the 10 applications of MTSET shown in A. A single exponential was fit to the data yielding an exponential constant of 0.2 and 65.9 mMs for the open and closed state, respectively. *C*, Closed state modification at position R396C. Channels were repeatedly exposed to 10 μM MTSET according to the closed state protocol shown in Fig. 2. *D*, Open (O, solid trace) and closed (C, closed circles) state decay time courses of R396C normalized as in B. The open state trace is taken from Fig. 2C, and the closed state rate was determined by measuring the current amplitude after each of the 10 applications of MTSET shown in A. A single exponential was fit to the data yielding an exponential constant of 0.09 and 0.17 mMs for open and closed states, respectively.

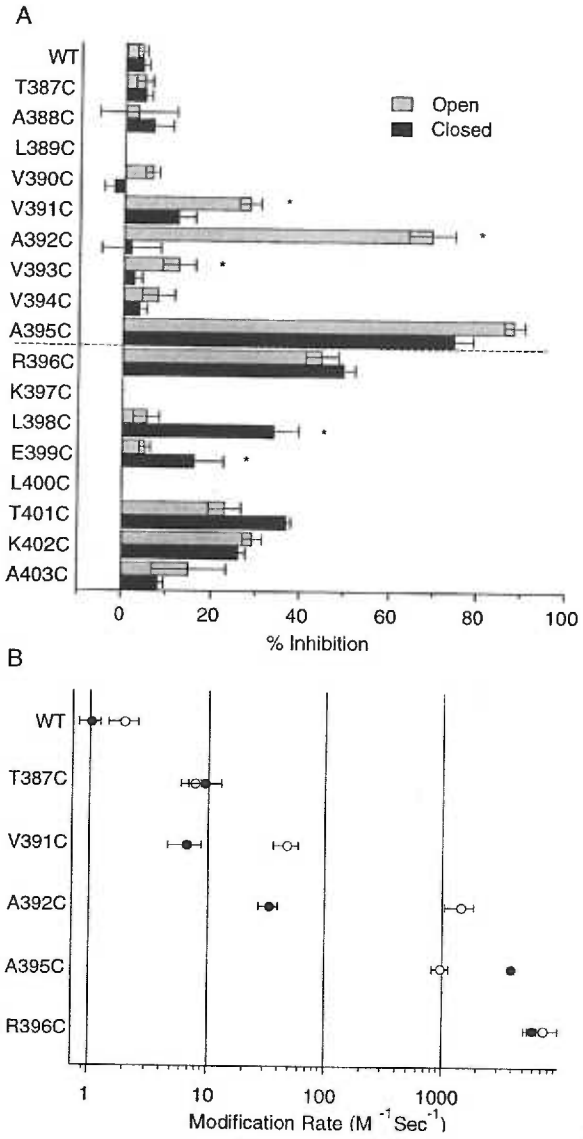

Figure 4. Summary of MTSET reactivity for WT and cysteine-substituted channels. *A*, Reactivity was measured for open (gray bars) or closed (black bars) channels and the dashed line indicates the predicted boundary between the cytoplasm and the membrane. Data from n≥3 patches was normalized and averaged, and plotted as the percent inhibition ± SEM after an 8 s exposure to 1mM MTSET. Note that positions 391, 392 and 393 show stronger open than closed state reactivity, while positions at the predicted membrane/cytoplasm boundary (395 and 396) show equal open and closed state reactivity. Cytoplasmic positions (398 and 399) show stronger closed than open state reactivity. Asterisks depict statistically significant differences between open and closed state reactivity ($p < 0.05$). Reactivity at position 390 could not be reliably measured (< 10% current reduction). *B*, Open and closed state modification rates for WT, T387C and 4 residues in the putative bundle crossing region. Rates were determined from single exponential fits to current decay (see results) and are presented as mean ± SEM from n≥3 patches.

A summary of the MTSET results for the different cysteine substituted channels is presented in Fig. 4 showing the percent inhibition following a single 8 s exposure to MTSET for each position in the open and closed states (Fig. 4A) and the modification rate for open and closed channels (Fig. 4B). Positions without bars either did not yield current, or current amplitudes were too small for reliable measurements (panel A). MTSET modification rates were determined as shown in Fig. 3 for two positions deep in the inner vestibule (386C and T387C) and four positions in the putative bundle crossing region (391, 392, 395 and 396). Current through WT or T387C channels was not affected by MTSET exposure in either the open or the closed state (modification rates less than 2 $M^{-1}s^{-1}$). Positions V391C, A392C, and V393C within TM6 showed significant state-dependence following a single MTSET exposure, and V391C and A392C were modified significantly faster in open than in closed channels (V391C: 47.9 ± 11.4 $M^{-1}s^{-1}$ n=4, 6.7 ± 2.1 $M^{-1}s^{-1}$ n=5, $p< 0.05$; A392C: 1.5 ± 0.4 x 10^3 $M^{-1}s^{-1}$ n=8, 33.6 ± 6.3 $M^{-1}s^{-1}$, n=6, $p<0.05$ for open and closed states, respectively). Modification of position 395 resulted in significant block in either state with channels in the closed state being more rapidly modified than those in the open state (open state: 9.7 ± 1.6 x 10^2 $M^{-1}s^{-1}$, n=4; closed state: 3.9 ± 2.4 x 10^3 $M^{-1}s^{-1}$, n=5, $p<0.0001$). State-independent modification was clearly observed for position 396 that resides on the TM6-cytoplasm interface (open state: 7.4 ± 2.4 x 10^3 $M^{-1}s^{-1}$, n=3, closed state: 5.9 ± 0.6 x 10^3 $M^{-1}s^{-1}$, n=6, $p>0.5$). Further into the cytoplasmic domain, at positions 398 and 399, the percentage of closed state inhibition was greater than open state inhibition (Fig. 4A). Significant MTSET reactivity was not detected at positions N-terminal to 391 in the open or closed states. It is important to note the differences between the percent inhibition following an 8 s exposure to MTSET and the modification rate. For example, Fig. 4A shows a much higher percent block for

A392C in the open than in the closed state after an 8 s exposure. However, the steady state percent block by MTSET during repeated application to closed A392C channels was similar to that in the open state (Fig. 3A). This is because access to position 392 is strongly state-dependent and therefore the modification rate is considerably slower in the closed state than in the open state, even though the block eventually reaches the same level. In contrast, an 8 s MTSET application to R396C channels produced equivalent current reductions, and the rates of modification in the open or closed state were similar (Fig. 3D, 4B). Taken together, the results suggest that the TM6 region of SK2 channels undergoes conformational changes during gating that alter MTS access to several positions.

c. Localization of the SK2 Activation Gate

The open state-dependent access to positions 391-393 can be interpreted in three ways: 1) these residues rotate away from the pore lumen during channel closing; 2) a gate C-terminal to 393 occludes MTSET access when channels are closed; 3) the inner vestibule narrows when channels close and this constriction restricts access to these positions.

Compared to a K^+ ion (Pauling radius 1.33 Å), MTSET is a relatively large molecule that may be modeled to fit in a cylinder ~5.8 Å in diameter and 10 Å long [59, 64], and so may be sterically hindered from reporting the availability of residues that K^+ ions might access, such as those N-terminal to position 391. MTSEA is a smaller, positively charged compound (head group diameter ~3.6 Å) that has been used to reveal state-dependent access to sites in the inner vestibule of *Shaker* channels and in the pore of CNG channels [60, 65]. Modification by MTSEA of residues examined in Fig. 4 yielded results similar

to those for MTSET. One important difference was that MTSEA could additionally access T387C, a site deeper in the SK2 inner vestibule that was not modified by MTSET (Fig. 5). Application of MTSEA (2.5 mM) to open or closed T387C channels resulted in complete block within 8 s (open state inhibition 99.9 ± 1.2%, n=4; closed state inhibition 94.2 ± 7.2%, n=6). WT channels containing 386C were not significantly altered by MTSEA in either the open (inhibition of 2.5 ± 3.3%, n=7) or closed state (increase of 1.3 ± 2.1%, n=3) and the double mutation C386S and T387C was completely blocked by MTSEA in both the open (99.6 ± 6.0%, n=5) and closed (97.9 ± 4.0%, n=3) states, demonstrating that MTSEA reacts specifically at position T387C. The rate of modification of T387C by MTSEA was determined following the protocol used for MTSET except that the exposure time during repeated MTSEA application in the closed state was decreased from 8 s to 1 s to accurately record channel modification (Fig. 5B). The open state and closed state modification rates of T387C by MTSEA were not significantly different (open state 379 ± 109 $M^{-1}s^{-1}$ n=6, closed state 286 ± 26 $M^{-1}s^{-1}$, n=3 $p>0.4$). Modification rates for WT channels were less than 1 $M^{-1}s^{-1}$ in either the open or closed states.

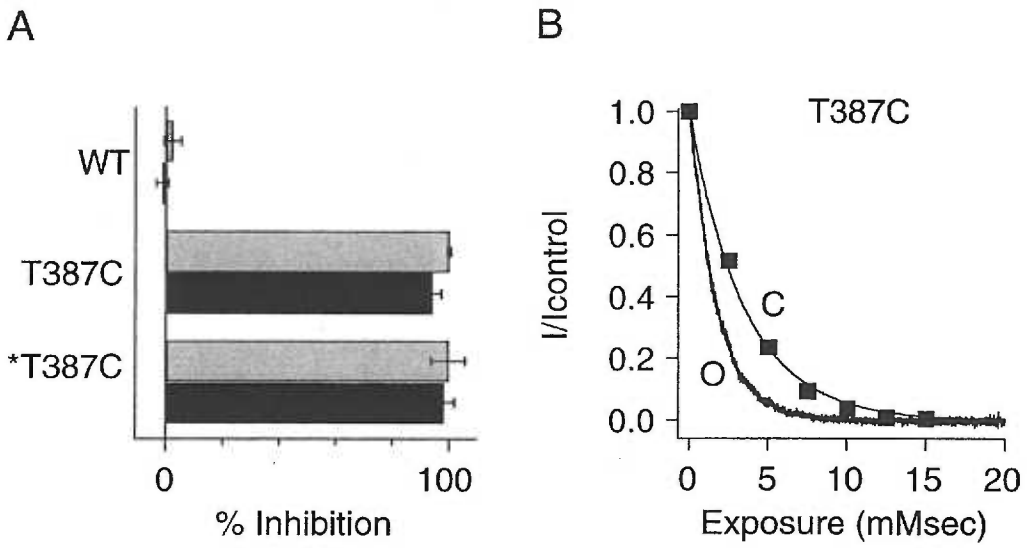

Figure 5. MTSEA reactivity for WT, T387C, and T387C/C386S channels. *A*, Current reduction was determined for the three channels using 8 s applications of 2.5mM MTSEA, as described for MTSET in Fig. 2. *T387C indicates T387C in the C386S background. *B*, Open (O, black trace) and closed (C, solid squares) state modification of T387C by MTSEA. Data are plotted and fitted as for MTSET in Fig. 3. Single exponential fits to the data yielded exponential constants of 1.7 and 3.5 mMs for open and closed states, respectively.

One concern when using MTSEA is that it may cross the membrane, in this case accessing T387C from the external vestibule and causing *trans* modification. This possibility was addressed by including 10 mM cysteine in the external patch pipette solution [108], which had no effect on the extent or rate of modification (not shown). It is also possible that MTSEA in an uncharged form might access position 387 by partitioning into the membrane or hydrophobic portions of the protein. If MTSEA accessed T387C only through the pore, then preapplication of TBuA, a pore blocker, should restrict MTSEA access to the site. Therefore, open or closed T387C channels were first exposed to 10 mM TBuA (~97% block of open state current). Then, in the continued presence of TBuA, 2.5 mM MTSEA was applied for 8 s. Following washout of both compounds, current amplitudes before and after exposure were compared (Fig. 6A, inset). The protocol was repeated several times, and the data plotted and fitted as described for Fig. 3A. As shown in Fig. 6, TBuA protected T387C from MTSEA modification in the open and the closed states. Rates were ~10-fold slower in the open state when channels were pre-blocked with TBuA (36.7 ± 7.5 $M^{-1}s^{-1}$, n=5) and ~18-fold slower in the closed state when TBuA was present (16.2 ± 3.6 $M^{-1}s^{-1}$, n=4). Taken together, the data suggest that MTSEA gains access to T387C by fitting into the pore in either the open or closed states.

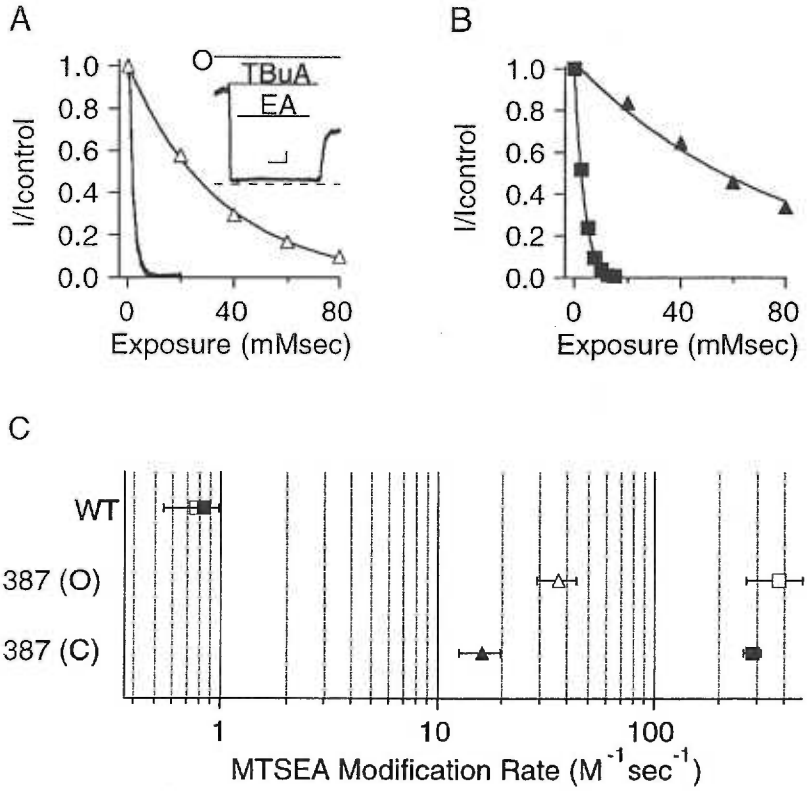

Figure 6. TBuA protects T387C from MTSEA modification. *A*, TBuA protects T387C from modification by MTSEA in the open state. The open state modification time course without TBuA (black trace) is the same as in Fig. 5B. Open state modification time course in the presence of 10mM TBuA (~97% block, open triangle) was determined by repeatedly applying 2.5 mM MTSEA for 8 s to blocked channels (inset) and measuring the fractional current remaining after each exposure (inset shows an example of a single exposure). Scale bars in inset are 50 pA and 2 s, and bars indicate when TBuA and MTSEA were applied to open (O) channels. Single exponential fits to the data yielded exponential constants of 1.7 and 34.9 mMs in the absence and presence of blocker, respectively. *B*, TBuA protects T387C from modification by MTSEA in the closed state. Closed state modification time course with no blocker present (closed squares) is taken from Fig. 5B. Closed state modification time course in the presence of TBuA (closed triangles) was determined by repeatedly applying 2.5 mM MTSEA for 8 s to closed channels in the presence of TBuA and measuring fractional current remaining after each exposure. Single exponential fits to the data yielded exponential constants of 3.7 and 77.5 mMs in the absence and presence of blocker, respectively. *C*, WT channel MTSEA modification rate in the open state (open squares) and closed state (closed squares) was less than 1 $M^{-1}s^{-1}$. Open state MTSEA modification rate of T387C without (open square) and with (open triangle) 10mM TBuA present and closed state MTSEA modification of T387C without (closed square) and with (closed triangle) 10mM TBuA. Data are presented as mean ± SEM from n≥3 patches.

E. DISCUSSION

The molecular details of Ca^{2+}-gating of SK channels have begun to emerge from biochemical, electrophysiological, and crystallographic studies [95, 97]. The results suggest that SK channel opening may involve a large-scale reorganization in which four monomeric CaMBD/CaM complexes transition into two dimers of CaMBD/Ca^{2+}-CaM. This rearrangement of the proximal C-terminus may impose a conformational alteration on the associated TM6 helices that opens the SK channel gate [97]. The structural identity of the gate, the positions that occlude ion permeation in the closed state, and the mechanism by which the conformational change is transduced from the CaMBD-CaM complex to the channel gate are not known.

SK2 channel block by TEA and longer side chain derivatives suggests that the inner vestibules of SK and K_v channels are conserved. SCAM results with the largest cysteine-specific probe used in this study, MTSET, revealed open state-dependent access to three positions just internal to the putative TM6 bundle crossing (391-393, Fig. 3, 4). This was in contrast to more distal positions such as A395C and R396C that rapidly reacted with MTSET in both the open and closed states of the channel, and to positions closer to the selectivity filter (386-390) that were not affected by MTSET exposure in either the open or closed state of the channel. These data are similar to the reactivity profile observed at analogous positions in *Shaker* K_v channels [60], and are consistent with a SK channel gate formed at the TM6 bundle crossing between positions 392 and 395 (Fig. 1A, model a).

The KcsA crystal structure reveals a wide aqueous lumen immediately cytoplasmic to the selectivity filter that is believed to be essential for rapid K^+ conduction [41, 48, 109]. This lumen is ~10 Å wide and accommodates a fully hydrated K^+ ion, thereby maintaining K^+ in a low energy state near the middle of the cell membrane [41]. Functional data from K_v channels and EPR data from KcsA support the maintenance of the lumen even in closed channels. For KcsA, the width of the lumen as measured by EPR does not markedly change when pH favors channel opening versus channel closing [63, 104]. For K_v channels, a long-chain TEA derivative can be trapped between the selectivity filter and the gate formed by TM6, presumably in an analogous aqueous lumen [58]. Thus, in K_v and KcsA channels, access to the lumen is regulated by an intracellular gate that prevents ion exchange with cytoplasmic K^+ in the closed state.

Two experiments presented here are consistent with the existence of a lumen, but not an intracellular gate, in closed SK channels. First, position 387 was rapidly modified by MTSEA even in closed channels, suggesting that there must be a lumen large enough to accommodate MTSEA even in closed channels (Fig. 5, 6). Second, a pore blocker with a fixed charge, TBuA, protected closed T387C channels from modification by MTSEA. The protection afforded was even greater in the closed than the open state, suggesting that the TBuA binding site is preserved in closed SK channels (Fig. 6). These data are not consistent with a gate formed by the TM6 bundle crossing between positions 392 and 395.

State-independent access to residue T387C deep in the vestibule raises the question of why MTSET access to the more distal position 392 is state-dependent (Fig. 4A, B). The

simplest interpretation of this result is that during channel closing, position 392 rotates away from the conduction pathway, perhaps into the channel protein surrounding the TM6 helices. In this way, an unobstructed path to position 387 is maintained in the closed channel, and state-dependent modification of position 392 is achieved. It is also possible that 392 does not move, but that surrounding protein moves to protect the site in the closed state. While this possibility cannot be ruled out, state-dependent MTSET access to V391C and V393C, immediately adjacent to A392C, and to the more distal L398C and E399C, is also consistent with a rotation of the TM6 helix during Ca^{2+} gating (Fig. 4).

To model the position of 387 and the other sites examined, SK2 residues were substituted for their counterparts in the KcsA crystal structure (Fig. 7). Despite the sequence divergence between KcsA and SK2, the orientations predicted from the substituted structure are consistent with results from the SCAM experiments in the inner vestibule. Residues that are predicted to reside in the inner vestibule, facing the permeation pathway (387, 391, 392) reacted with MTS compounds in open SK channels to reduce current amplitude, and residues that point away from the permeation pathway (386, 390), buried in surrounding protein or membrane, were not affected by MTS exposure. Although this model adequately predicts the reactivity of residues relatively deep in the inner vestibule (~386-392), more cytoplasmic residues are less well depicted. For example, position 396 appears to point away from the permeation pathway, but MTSET reactivity at this site significantly decreases current amplitude, and state-dependent access to positions 398 and 399 would not necessarily be predicted based on the model. This divergence from the data at the cytoplasmic end of the model is not surprising; not only is the gating mechanism fundamentally different between SK and KcsA channels, but MTSEA access

to T387C suggests that, at least in the closed state, the bundle crossing region of SK is wider than in KcsA.

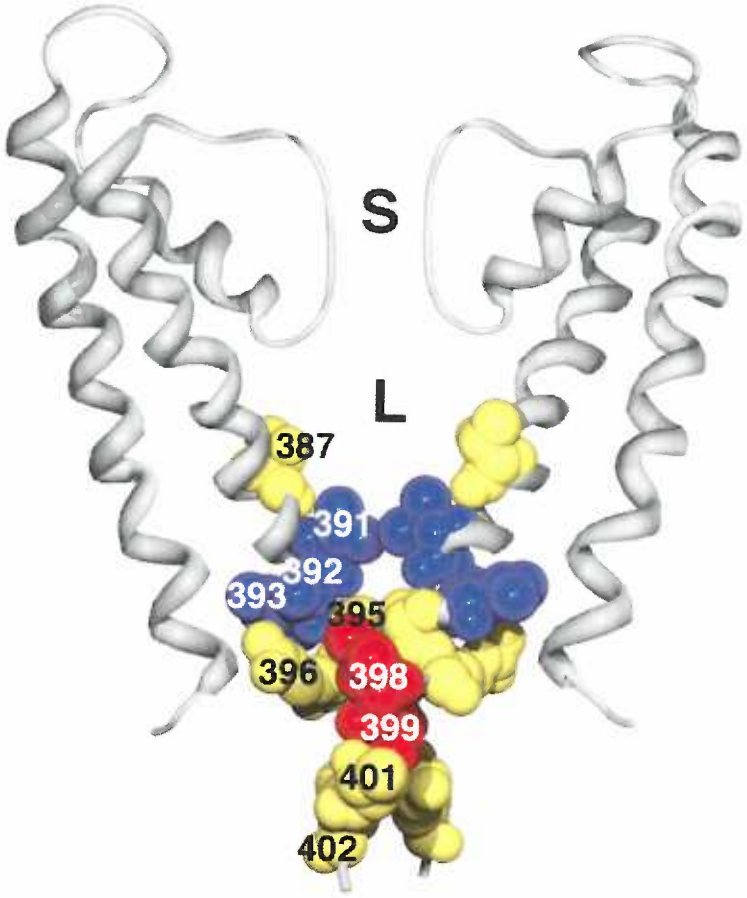

Figure 7. Model of SK2 residues substituted into the KcsA crystal structure. Two of four subunits are shown (gray ribbon). For each subunit, S5, the pore region, TM6, and the TM6 extension into the cytoplasm are shown. For reference, the selectivity filter at the top (S) is ~3.3 angstroms wide. L indicates the lumen immediately internal to the selectivity filter. Amino acids in yellow (387, 395, 396, 401, 402) show approximately equal open and closed state reactivity, blue residues (391, 392, 393) show open>closed state reactivity, and red (398, 399) show closed>open state reactivity. Reactivity to MTSET is shown for all residues except T387C, which depicts MTSEA reactivity.

Using the model of the deep inner vestibule and pore region as an approximation of the SK structure, position 387 projects into the lumen, residing ~8 Å from the selectivity filter (Fig. 7). Since MTSEA would fit in a cylinder ~6 Å wide by 10 Å long, with a head group ~3.6 Å in diameter [59, 64], a vestibule of at least these dimensions is predicted near position 387 even in closed SK channels. The closed state vestibule may be even larger than this, particularly if TBuA protects T387C from MTSEA by binding to its site close to the selectivity filter, as demonstrated for *Shaker* and KcsA channels [55, 57], and suggested by the voltage-dependence of the open state block in SK channels. If the "smokehole" (Fig. 1A, model a), the collapsing vestibule (Fig. 1A, model b) or the "ball-and-chain" (Fig. 1A, model c) mechanism accounts for SK2 channel gating, MTSEA access to T387C should be occluded in the closed state. Since open and closed state modification rates do not differ (Fig. 5B, 6C), these models cannot accurately describe SK2 channel gating. Rather, rapid access by MTSEA to the region immediately cytoplasmic to the selectivity filter even in the closed state suggests that the SK channel activation gate lies at or external to the selectivity filter (Fig. 1A, model d). The difference between K_v and SK channels is clearly reflected by the residue analogous to 387 in the *Shaker* K_v channel (I470C) that is rapidly modified by MTSEA in the open but not the closed state [60].

Recent evidence in other K^+ channels suggests structural changes may occur not only in the inner vestibule, but also in the selectivity filter during gating. When pH is altered to favor gating of KcsA, EPR measurements detected small movements at the intracellular end of the selectivity filter [63]. Further, KcsA crystal structures solved in high and low concentrations of K^+ show two distinct selectivity filter conformations, one presumably

conductive and the other non-conductive [48]. In an inward rectifier type K^+ channel, altering the electronegativity of the pore alters gating at hyperpolarized potentials [74]. Finally, in *Shaker* K_v channels, some mutations in the selectivity filter lead to subconductance states with ion selectivities that differ from the selectivity profile of fully open channels [75, 76].

The data presented here support a model for SK channel gating in which Ca^{2+}-induced rearrangements of the CaMBD/CaM complex are transduced through TM6 to the channel activation gate, which lies in or near the channel selectivity filter. This is similar to the gating model for CNG channels in which cyclic nucleotide binding to the channel C-terminus is transduced to a gate that presumably resides in the channel selectivity filter [67, 103]. Together these studies suggest that there may be a conserved selectivity-filter based gating mechanism for many channels gated by intracellular ligands, distinctly different from the activation gating mechanism proposed for voltage-gated channels.

III. CHAPTER 3

Evidence For a Deep Pore Activation Gate in Small Conductance Ca^{2+}-Activated K^+ Channels

Andrew Bruening-Wright*, James Maylie^ and John P. Adelman*

*Vollum Institute, and ^Department of Obstetrics and Gynecology, Oregon Health and Science University, Portland, Oregon

Abbreviated title: The SK channel gate

Please send correspondences to:

Dr. John P. Adelman, Ph.D.

Vollum Institute

Oregon Health and Science University, L-474

3181 S.W. Sam Jackson Park Road

Portland, OR 97239-3098

(503)-494-5450

(503)-494-4353 (fax)

adelmanj@ohsu.edu (email)

Acknowledgments. This work was supported by National Institutes of Health grants to JPA and JM, and a pre-doctoral NRSA award to AB-W.

Keywords: SK channel, pore, activation gate, barium, gating, inner vestibule

A. ABSTRACT

SK channels are heteromultimers, comprised of four membrane-embedded SK subunits complexed with four cytosolic CaM molecules. The SK subunits form a K^+ selective pore in the cell membrane; CaM acts as an intracellular Ca^{2+} sensor. The Ca^{2+}-triggered conformational changes in CaM are relayed to a channel gate that serves the critical function of regulating ion flux through the pore. The physical location of the gate was recently probed in SK channels. State-independent accessibility of a binding site internal to the region that forms a gate in other K^+ channels (the TM6 bundle crossing) suggested that the lower TM6 does not form an effective gate in SK channels, at least not to TBuA and the chemical modifying reagent MTSEA [110]. In the present study, Ba^{2+} is used to probe deep into the SK channel pore from the intracellular side. Ba^{2+}, which is smaller and less hydrophobic than TBuA or MTSEA, binds SK channels near the selectivity filter with strong voltage-dependence. It is demonstrated that Ba^{2+} can be "trapped" in the channel when applied in the open state and the gate subsequently closed. Ba^{2+} is not trapped when it is applied exclusively to closed channels and it cannot access its binding site from the closed state. Thus Ba^{2+} acts as a pure open channel blocker. Consistent with this, the Kd and on-rate of Ba^{2+} block are directly related to channel open probability (Po). Sequence alignment with other K^+ channels shows that T387 lies one helical turn below the "glycine hinge" (G383) that has been proposed as critical for K^+ channel gating. Taken together, the data suggest a mechanistic model in which the channel gate lies between the Ba^{2+} binding site at the selectivity filter and position 387. Additional flexibility in the inner vestibule could be provided by glycine residue 380, a

position that is conserved in all calmodulin-gated K^+ channels, but absent in every other type of K^+ channel.

B. INTRODUCTION

SK channels are important determinants of cell excitability. In certain neurons, blocking SK channels inhibits spike frequency adaptation, a phenomenon characterized by progressive slowing of action potential firing in the continued presence of stimulus [1, 9]. Thus, SK channels help determine the sensitivity of excitable cells to electrical stimuli.

The underlying mechanism of spike frequency modulation by SK channels becomes apparent if the action potential is examined. As the cell is depolarized during the upstroke of the action potential, voltage-gated Ca^{2+} channels open providing an influx of Ca^{2+}, and intracellular stores also release Ca^{2+} to the cytosol. SK channels sense this increase in intracellular Ca^{2+} (EC_{50} of approximately 600 nM), and open in response. The subsequent efflux of K^+ through SK channels serves to drive the membrane potential more negative as long as the Ca^{2+} stimulus is present. Thus SK channels create an afterhyperpolarization (AHP) that outlasts the action potential and dampens cell excitability. Both the amplitude and duration of the AHP depend on Ca^{2+} concentration, and thus increase with increases in action potential firing and release of Ca^{2+} from stores, leading to more pronounced spike frequency adaptation over time. In hippocampal neurons, blocking SK channels with the SK-specific toxin apamin lessens spike frequency adaptation by blocking an AHP of medium duration [9].

To play such a critical role in cell excitability, SK channels must be exquisitely tuned to detect fluctuations in intracellular Ca^{2+} levels. CaM, a ubiquitous Ca^{2+}-sensing molecule, provides this sensitivity to SK channels. Each SK channel consists of four subunits each containing six TM's. As for their voltage-gated cousins, the N- and C-termini of SK channels reside in the cytoplasm, and K^+ selectivity is conferred by a consensus "GYG" motif in the pore loop. CaM constitutively binds to a domain in the C-terminus, the CaMBD; Ca^{2+} is detected by two of the four "EF hand" motifs of CaM, EF 1 and 2. Ca^{2+} binding causes conformational changes in CaM that induce opening of the channel gate [95-97]. The mechanism of this coupling between CaM and the SK gate, and the location of the gate itself are not known.

Functional studies in K_v channels and crystallization studies of bacterial K^+ channels have suggested a gating mechanism for these channels. For *Shaker* K_v channels, systematic probing of the inner helix (TM6) with chemical modifying reagents has demonstrated strong state-dependent accessibility to positions internal to a region known as the "bundle crossing" [60-62]. These positions can be rapidly accessed in the open state of the channels, but not in the closed state. Positions cytoplasmic to the bundle crossing do not exhibit strong state-dependent accessibility, suggesting that the bundle crossing in lower TM6 forms an activation gate for the channels.

Data from the bacterial K^+ channels KcsA and MthK are consistent with this mechanism [40, 41]. The crystal structure of KcsA shows that the four inner helices (analogous to TM6 in *Shaker*) do indeed form a bundle crossing at their cytoplasmic end. In KcsA, this bundle crossing forms a constriction so tight it is speculated that K^+ could not permeate.

For this reason, it is believed KcsA is in the closed state. MthK, on the other hand, is in a dramatically different conformation. The lower inner helix is splayed open providing a wide unobstructed path to the selectivity filter; thus MthK is in the open state. The primary difference between the two structures is an approximately 30° bend in the inner helix of MthK at a residue termed "glycine hinge". This bend abolishes the bundle crossing in MthK. In contrast, the inner helix of KcsA is completely straight, allowing the formation of the bundle crossing gate at the cytoplasmic end of the helix.

The gating mechanism of Ca^{2+}-activated K^+ channels differs from *Shaker* and bacterial K^+ channels, and recent data suggests that the location of the gate may also be different [110]. Cysteine residues were introduced one-at-a time in lower TM6 and their accessibility to chemical modifying reagents probed in the open and closed states. A residue internal to the bundle crossing, T387C, was modified by MTSEA in the open and closed states of the channel with approximately equal rates. Further, pre-application of the pore blocking molecule TBuA protected this residue from MTSEA modification in both the closed and open states. This data was taken as evidence that the cytoplasmic end of the inner helix does not form an effective gate in SK channels, at least not to MTSEA or TBuA. Instead, it was proposed the gate resided in or near the selectivity filter. Interestingly, studies of cyclic-nucleotide gated channels, which like SK channels are gated by cytosolic signaling molecules, have suggested that these channels also do not have an activation gate in lower TM6 [64, 66, 67, 103].

In this study Ba^{2+}, an ion with physical and chemical properties very similar to K^+, is used to probe deeper into the pore of an SK channel to locate more precisely the

activation gate. Two lines of evidence suggest that Ba^{2+} binds at the internal end of the selectivity filter. First, mutant cycle analysis demonstrates strong Ba^{2+} interaction with rSK2 residue S359, two residues before the GYG motif of the selectivity filter [88, 89]. Consistent with this study, Ba^{2+} soaked into the KcsA crystal binds just below the selectivity filter, nearly overlaying with the internal K^+ binding site [90]. The data presented here show that Ba^{2+} can access this binding site only in the open state of the channel. Further, Ba^{2+} can be trapped in the pore of SK channels, and Ba^{2+} binding is strongly dependent on channel Po. Together with results showing state-independent MTSEA and TBuA accessibility to residue 387, it is proposed that the SK channel gate lies relatively high in the inner vestibule, between the selectivity filter and residue 387.

C. MATERIALS AND METHODS

a. Molecular Biology

Constructs were subcloned into the expression vector pJPA5 for expression in COSm6 cells. Site-directed mutagenesis was performed using PFU polymerase (Stratagene) and the overlap PCR technique [106]. The complete nucleotide sequence of the coding region of mutated molecules was verified by standard double stranded DNA sequencing technique prior to expression studies.

b. Electrophysiology

Cells were transiently transfected with 1 μg channel DNA, a ten-fold dilution (100 ng) of calmodulin (to increase channel expression), and CD-4 antigen using Polyfect reagent (Qiagen, USA). Cells were plated on Fisherbrand Growth coverslips (Fisher Scientific, USA), labeled with CD-4 antibody-coated polystyrene beads (Dynabeads M-450, Dynal,

Norway) and currents were recorded 24-48 hours post-transfection. Bath solution contained 150 mM K^+ hydroxide titrated with methanesulfonic acid to pH 7.2 to form K^+ methanesulfonate (KMES), 10mM HEPES, 1mM EGTA, and CaOH and BaOH to yield the desired free Ca^{2+} and Ba^{2+} concentrations [107]. The pipette solution contained either 2 mM KMES and 148 mM NaMES or 150 mM KMES, 10 mM HEPES, and approximately 100 μM free Ca^{2+}. All solutions were adjusted to pH 7.2 with methanesulfonic acid and all recordings were performed at room temperature (22-25° C). Free Ca^{2+} for open state experiments was adjusted to 2 μM to maximally activate the channels. For closed state experiments, no Ca^{2+} was added (0 Ca^{2+}) yielding a free Ca^{2+} level < 2 nM. Inside-out patches were pulled using borosilicate glass patch electrodes (TW150 F-4, Warner Instrument Corp, USA) pulled to resistances between 1.0 and 3.0 MΩ. Leak and background currents were measured by changing the bath solution on the inside face of the patch to 0 Ca^{2+} to close SK2 channels. Rapid solution changes were performed using an RSC-200 (Molecular Kinetics, USA). Currents were measured and digitized with an EPC9 (Heka, Germany), currents sampled and filtered at 1 kHz, and analysis performed using Pulse (Heka, Germany) and Igor (Wavemetrics, USA) software.

c. Data Analysis

All values are reported as the mean ± standard error of mean (SEM) of n experiments. Statistical significance was evaluated using a Students t test, and a p value ≤ 0.05 considered significant. Dose response relationships for Ba^{2+} were obtained by measuring current amplitudes in control solution and at the indicated concentration of Ba^{2+} across a range of voltages (ramp experiments) or by taking the average of the final 500 ms of a 5 s voltage step to 0 mV. Currents were normalized to the control amplitude and fit with a

single binding isotherm using a nonlinear least square procedure. The binding equation used was: Icontrol*[X]/([X] + IC_{50}) where [X] is the concentration of Ba^{2+}, Icontrol is the current amplitude before application of blocker, and IC_{50} represents the concentration at which macroscopic current is half-blocked. Salts were purchased from Sigma-Aldrich (USA), and Ca^{2+}, Ba^{2+} and EGTA were of the highest purity available from the Fluka division.

D. RESULTS

a. Ba^{2+} Block: Dependence on Voltage and External K^+

To qualitatively assess the voltage dependence of Ba^{2+} block, inside out patches were held in solution containing Ca^{2+} sufficient to maximally activate the channels (2 μM) and subjected to voltage ramps from –80 to 80 mV in the absence or presence of Ba^{2+} (0, 0.1, 0.3, 1, 3, 10 or 1000 μM). Figure 8A shows currents measured in a representative patch when internal and external solution contained symmetric 150 mM K^+. As previously reported [89], Ba^{2+} block was clearly voltage dependent under these conditions . Figure 8B shows traces from a patch in which the external K was lowered to 2 mM (with 150 mM internal K^+). As for the symmetrical K^+ experiment, Ba^{2+} block was again voltage-dependent. Figure 8C shows average apparent Kd's obtained across a range of voltages for both the symmetric and asymmetric K^+ conditions as estimated from the ramp protocols shown in panels A and B.

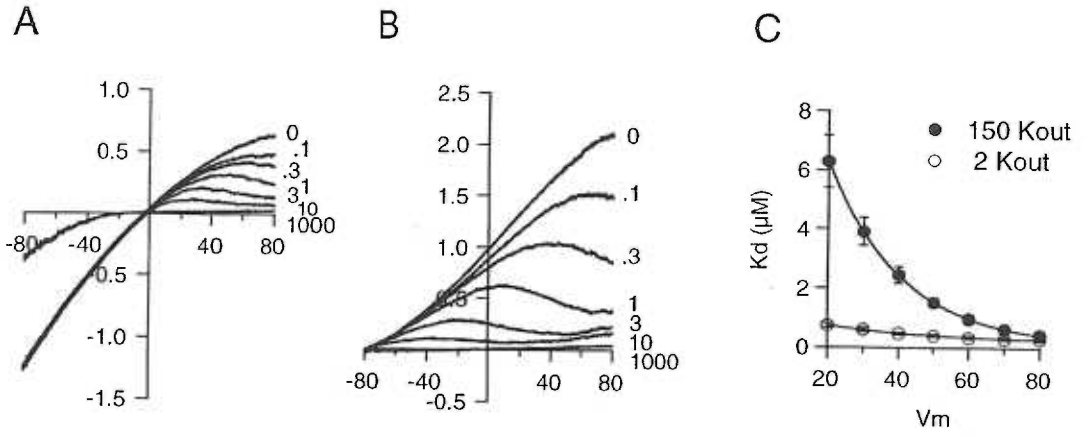

Figure 8. Ba^{2+} block of SK2, dependence on voltage and external K^+. A, Currents elicited by voltage ramps from –80 mV to 80 mV in the presence of indicated internal concentrations of Ba^{2+} (μM) (saturating 2 μM Ca^{2+}), and symmetrical 150 mM K^+. B, Protocol as for A, but 2 mM K^+ external. C, Average apparent dissociation constant (Kd) obtained at 10 mV intervals (from 20 mV to 80 mV) by estimating % block from ramps (n=6 $2K_{out}$, n=7 150 K_{out}).

b. Ba^{2+} Trap

The divalent ion Ba^{2+} blocks SK channels from the intracellular side with relatively high affinity, as demonstrated in Figures 8 and 12 (0mV Kd = 997 ± 177 nM) [88, 89]. The blocking site or barium is believed to lie just under the selectivity filter since it strongly interacts with filter residue S359 in rSK2 as assessed by mutant cycle analysis [89], and since it resides just below the filter when soaked into the crystallized KcsA channel [90]. Thus Ba^{2+} makes an ideal tool for probing the SK channel inner vestibule for three reasons: 1) the physical properties of Ba^{2+} closely approximate those of the permeant ion for the channel, K^+; 2) Ba^{2+} binds the channel with high affinity; 3) Ba^{2+} binds deep in the channel pore just below the selectivity filter.

Previous experiments using a SCAM approach together with pore blockers suggested that in SK channels, the activation gate was deep in the pore beyond residue T387 [110]. Based on analogy to CNG channels [64] and functional data suggesting a role for the selectivity filter in activation gating in *Shaker* K_v [75], bacterial K^+ [48, 63], and Kir [74] channels, it was proposed that the SK gate most likely resides in the selectivity filter of the channel, although the possibility of a TM6-formed gate could not be ruled out. To distinguish between these two possibilities, a Ba^{2+} "trap" experiment was performed with the reasoning that if there is a TM6 gate, Ba^{2+}, which binds deep in the pore beyond T387, should be trapped between the selectivity filter and the activation gate if applied in the open state and the gate subsequently closed. In contrast, a selectivity filter-based gate would not be expected to trap Ba^{2+} since the Ba^{2+} binding site is slightly internal to the selectivity filter.

Figure 9A shows the response of SK2 channels to rapid changes in intracellular Ca^{2+} and Ba^{2+} concentrations. An inside-out patch was excised and held in 2 μM free Ca^{2+} to fully activate the channels, Ca^{2+} was then removed to close the channels, and the channels were subsequently re-opened (trace 1). After a return to steady state, channels were exposed to 2 μM Ca^{2+} supplemented with 10 μM Ba^{2+} to block most of the channels. Ba^{2+} was then washed out and current recovery was recorded (trace 2). As expected based on Ba^{2+}'s low apparent Kd, Ba^{2+} washout was much slower than channel opening (average tau of Ba^{2+} washout 1160 ± 79 ms, average tau of channel opening 7.0 ± 1.8 ms). To assess if Ba^{2+} could be trapped in the closed channels, the channels were blocked with the 2 μM Ca^{2+}, 10 μM Ba^{2+} solution, closed with a nominally Ca^{2+} free solution ("0 Ca^{2+}") that also contained 10 μM Ba^{2+} and then the Ba^{2+} was washed out for 5s before re-opening the channels with the 2 μM Ca^{2+} solution without Ba^{2+} (trace 3o). During this re-opening (3o) the current recovered in two phases: a fast component corresponding to the small fraction of unblocked channels opening, and a slow component corresponding to Ba^{2+} washout from blocked channels. Figure 9B shows a time-expanded overlay of trace 1 and trace 3o from the patch shown in Figure 9A. Overlaid on the slow phase of the recovery is a single exponential fit to Ba^{2+} washout obtained from trace 2.

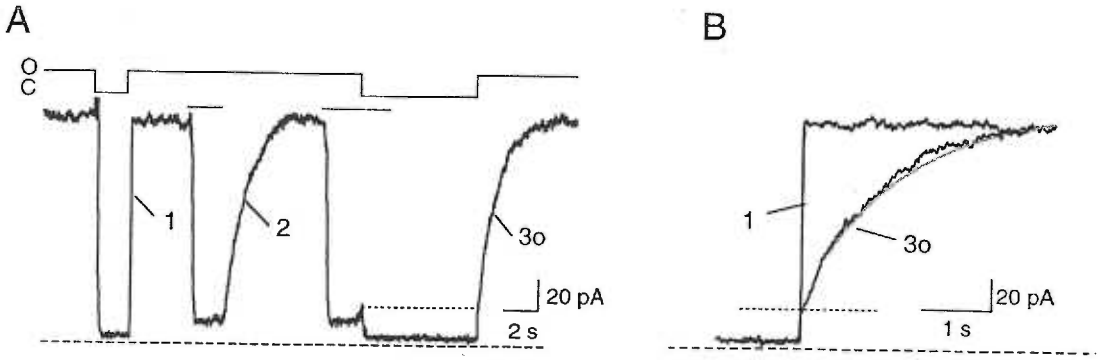

Figure 9. Ba^{2+} trap protocol, open state. A, An inside-out patch containing WT rSK2 channels was voltage clamped to 0 mV and the intracellular solution was altered to open or close the channels (2 μM or 0 μM free Ca^{2+}) and to expose the channels to 10 μM Ba^{2+}. Channels were first closed then re-opened using a rapid exchanger to measure the activation time course of channels in the absence of Ba^{2+} (trace 1). Ba^{2+} was then applied in the open state and washed off to approximate the Ba^{2+} off rate (trace 2). Finally, channels were blocked in the open state, closed in the continued presence of Ba^{2+}. The Ba^{2+} was subsequently washed off for 5s before re-opening the channels to measure the kinetics of current recovery (3o). B, Channel opening in the absence of Ba^{2+} (trace 1) is overlaid with channel opening after "trap" (trace 3o) for the patch shown in A. The fit overlaid on trace 3o is from the Ba^{2+} wash-out (A, trace 2).

c. State-Dependence of Ba^{2+} Binding in the Pore

To assay if Ba^{2+} could access the "trap" site from the closed state, a similar protocol was performed on the same patch (Figure 10A), but this time Ba^{2+} was not applied to open channels before closing. Instead, Ca^{2+} deactivation and activation (trace 1) and Ba^{2+} on and off kinetics (trace 2) were assessed as before, followed by channel closure for 2s before a 4s exposure to 10 μM Ba^{2+} in the absence of Ca^{2+}. Ba^{2+} was then washed for 5s before re-opening the channels in the absence of Ba^{2+} (trace 3c). In contrast to the experiment that showed trapping from the open state (Figure 9), channel re-opening could be well described by a single exponential. Figure 10B shows channel opening before (trace 1) and after (trace 3c) closed state Ba^{2+} exposure, and a single exponential fit to trace 1 (gray). A summary of the time constants derived from fits to the data in Figure 9 and Figure 10A and B is presented in figure 10C. Tau values were, in ms: channel opening 7.0 ± 1.8, Ba^{2+} off 1160 ± 79, open after trap (open state Ba^{2+} application, slow phase) 1126 ± 58, open after trap (closed state Ba^{2+} application) 8.4 ± 2.3.

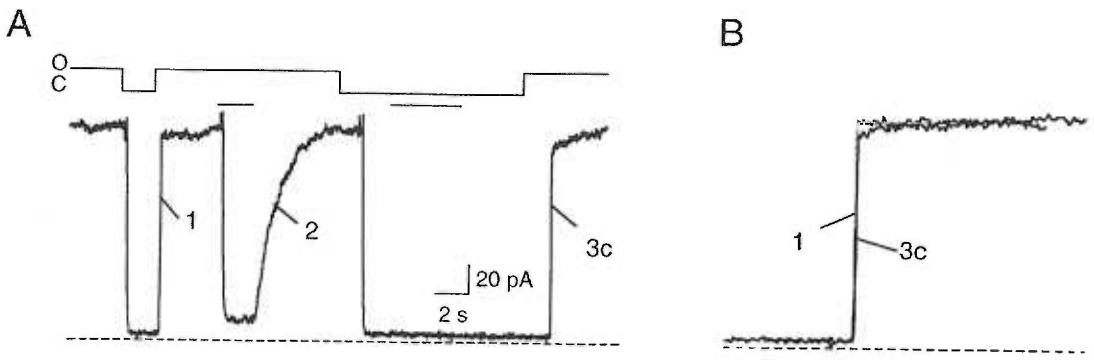

Figure 10. Ba^{2+} trap protocol, closed state. A, An inside-out patch containing WT rSK2 channels was voltage clamped to 0 mV and the intracellular solution was altered to open or close the channels (2 μM or 0 μM free Ca^{2+}) and to expose the channels to 10 μM Ba^{2+}. Channels were first closed then re-opened using a rapid exchanger to measure the activation time course of channels in the absence of Ba^{2+} (trace 1). Ba^{2+} was then applied in the open state and washed off to approximate the Ba^{2+} off rate (trace 2). Finally channels were closed and exposed to Ba^{2+} for 5 s in the closed state. The Ba^{2+} was then washed off for 5s before re-opening the channels to measure the kinetics of current recovery (trace 3c). B, Channel opening in the absence of Ba^{2+} (trace 1) and channel re-opening after Ba^{2+} exposure (trace 3c) are expanded and displayed for the patch shown in A. Traces 1 and 2 and 3c were all well fit by a single exponential function. C, Summary of trap protocol experiments. Bars indicate average time constants of single exponential fits to experiments described in Figures 9, and 10A and 10B.

If, as suggested by the trapping experiment, a gate exists between the Ba^{2+} binding site and the cytosol, closing the gate should prevent Ba^{2+} from accessing its' block site from the intracellular side. To test this hypothesis, an experiment was designed that utilized the greater than 10-fold difference between channel opening rate (tau 7.0 ± 1.8 ms, Figure 9) and 3 μM Ba^{2+} block rate (tau 140 ± 13 ms, Figure 13). Open channels were closed, exposed in the closed state to 3 μM Ba^{2+}, and re-opened in the presence of Ba^{2+}. If Ba^{2+} acts as a pure open channel blocker, the channels should first open and then be blocked by Ba^{2+}. Figure 11A shows the response of one patch to 3 μM Ba^{2+} exposure in the closed state for 1, 3, 10 or 100s, followed by channel opening in the presence of 3 μM Ba^{2+}. The individual traces are overlaid on a common time scale for representation. The inset shows opening in the presence of Ba^{2+} after 10s of closed state exposure on an expanded time scale. For all four durations of exposure, channels opened before onset of block. The duration of closed state exposure did not significantly affect the amount of current observed upon re-opening before onset of block (Figure 11B). In each case, approximately 20% of the initial current was not resolved before onset of block. Extrapolating a single exponential fit of the decay during block to estimate the actual percentage blocked suggests that a maximum of 5% of the current could be blocked by Ba^{2+} in the closed state.

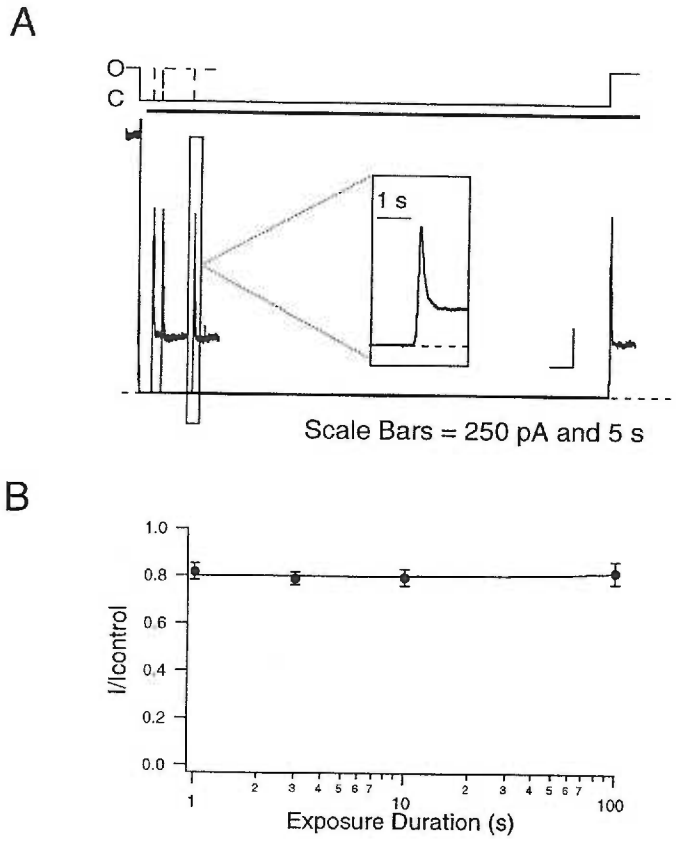

Figure 11. Ba^{2+} is an open state blocker. A, rSK2 channels in an inside-out patch were voltage clamped to 0 mV and the intracellular solution altered to open or close the channels (O or C, respectively) and apply 3 μM Ba^{2+} (thicker solid bar). Four traces from the same patch are overlaid. In each trace open channels were closed, exposed to Ba^{2+} for a given duration (1, 3, 10 or 100s) then re-opened in the presence of Ba^{2+}. For all four exposure durations, the channels opened before onset of Ba^{2+} block. *Inset*, the boxed area is expanded to demonstrate channel opening before onset of block for the 10s closed state Ba^{2+} exposure. B, Average peak current upon re-opening normalized to pre-exposure amplitude from four patches. Note that duration of closed state exposure does not affect peak current amplitude.

To further quantify the Po-dependence of Ba^{2+} block, Ba^{2+} dose responses were performed in concentrations of Ca^{2+} that either fully activate (2 μM) or activate approximately 20% (0.4 μM) of SK2 channels. Inside-out patches were stepped from −80 mV to 0 mV for 5 s to obtain steady state block at 0 mV for each concentration of Ba^{2+} (Figure 12A). Concentrations of Ba^{2+} assayed were 0.01, 0.1, 0.3, 1, 3, and 1000 μM (2 μM Ca^{2+}, left panel), or 0.01, 0.03, 0.1, and 0.3 μM (0.4 μM Ca^{2+}, right panel). Figure 12B shows the normalized current amplitudes for the two patches in Figure 12A plotted against concentration of Ba^{2+}. Data are fitted with the single binding isotherm (see methods) and apparent Kd's were 802 nM in 2 μM Ca^{2+}, and 44.6 nM in 0.4 μM Ca^{2+}. Average Kd's from four patches were 997 ± 177 nM, and 33.5 ± 8.8 nM, and average normalized Po's were 1 and 0.19 ± 0.03 for 2 μM and 0.4 μM Ca^{2+}, respectively.

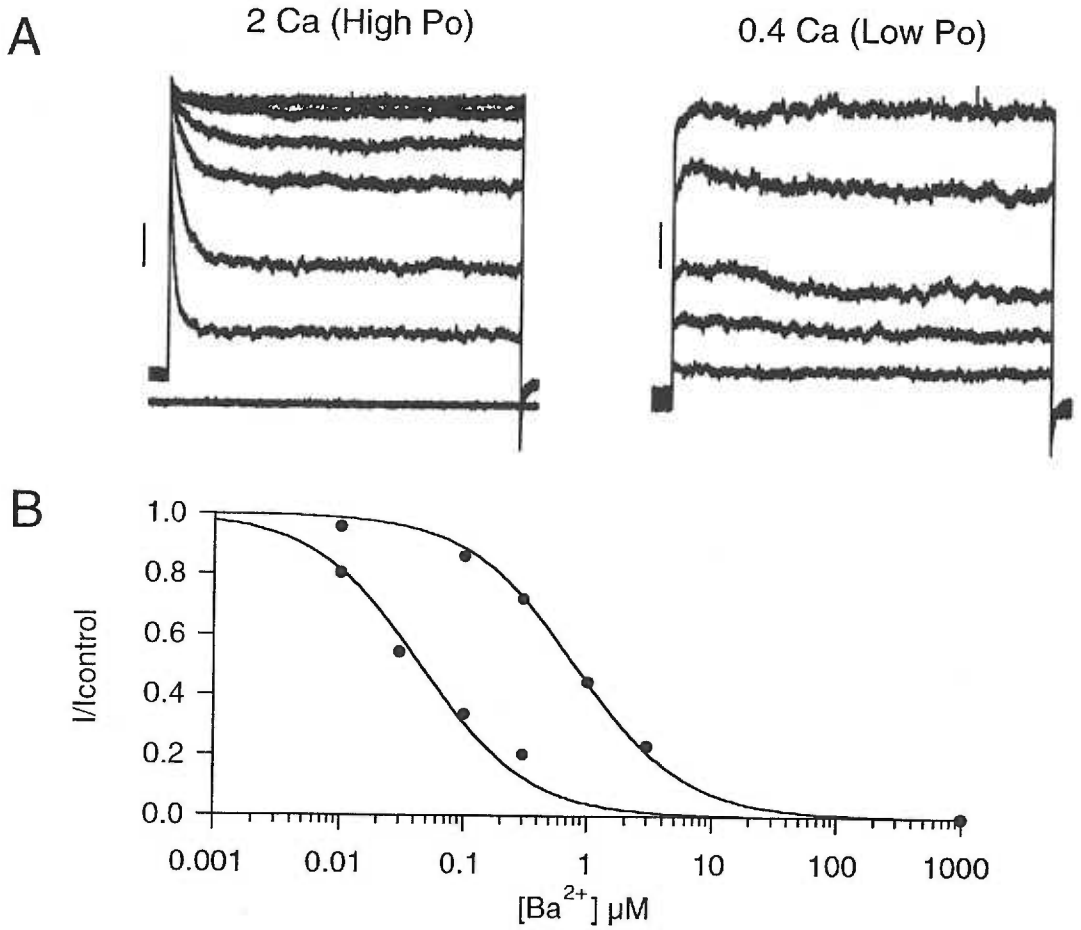

Figure 12. Po-dependence of Ba^{2+} inhibition of WT rSK2. A, Several concentrations of Ba^{2+} were applied to inside-out patches expressing WT rSK2 channels in Ca^{2+} sufficient to either saturate activation (2 µM Ca^{2+}) or activate approximately 20% of channels (0.4 µM Ca^{2+}). Responses were recorded during a 5 s voltage step from –80 mV to 0 mV in barium concentrations of 0.01, 0.1, 0.3, 1 or 3 µM (2 µM Ca^{2+}) or 0.01, 0.03, 0.1, 0.3 µM (0.4 µM Ca^{2+}). Scale bars depict 100 pA. B, Dose response curves from the traces shown in A fitted with a single binding isotherm. The Kd in saturating Ca^{2+} was 802 nM and 44.6 nM in 0.4 µM Ca^{2+}.

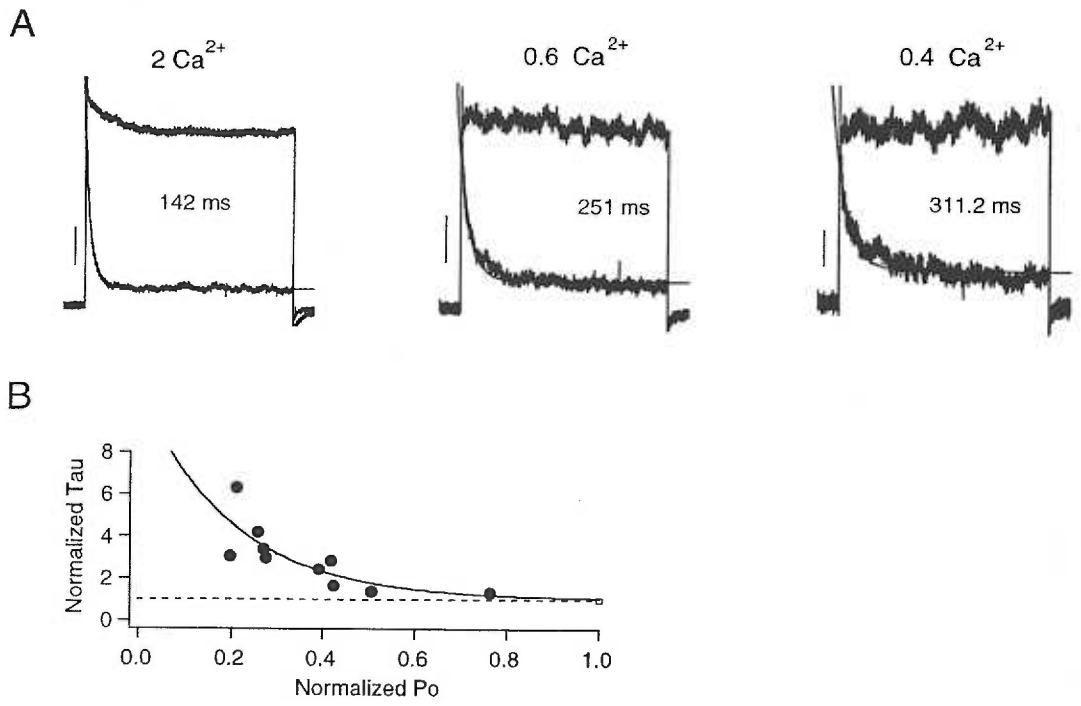

Figure 13. Po-dependence of kinetics of Ba^{2+} inhibition of WT rSK2. A, Voltage steps from -80 to 0 mV in the presence of, from left to right, 2 μM Ca^{2+}, 0.6 μM Ca^{2+}, or 0.4 μM Ca^{2+}, each with and without 3 μM Ba^{2+}. Time constant of Ba^{2+} block was estimated by fitting the decay with a single exponential function. The time constant increased as Po decreased (from left to right: 142 ms, 251 ms and 311 ms). Scale bars represent, from left to right, 100, 50 and 25 pA, respectively. B, Normalized time constant for 10 patches was plotted against the normalized Po for each patch and data were fit with a single exponential for display purposes. Note that the on rate of Ba^{2+} slows as the Po decreases.

The Po-dependence of block was further examined by determining the on rate of Ba^{2+} block at 0 mV across a range of open probabilities (Figure 13). The strong voltage-dependence of Ba^{2+} block (Figure 8) allowed determination of the on rate using voltage-steps, thereby eliminating possible underestimation of rates due to "hindered diffusion" in the inside-out patch [111]. Patches were held at –80 mV in solutions containing 2 μM, 0.6 μM, or 0.4 μM Ca^{2+} with or without 3 μM Ba^{2+} for greater than 5 s, and then stepped to 0 mV. Since more channels are blocked at 0 mV than at –80 mV, steps in the presence of Ba^{2+} demonstrated a time dependent decay as Ba^{2+} entered and blocked the pore. Figure 13A demonstrates the response of one patch held in the three different Ca^{2+} concentrations (from left to right: 2 μM, 0.6 μM, 0.4 μM). For each concentration of Ca^{2+} the top trace represents the response in the absence of Ba^{2+}, and the lower decaying trace represents the response to Ba^{2+}. Blocking time constants were derived from single exponential fits to the decay in the presence of Ba^{2+}. For the traces in Figure 13A, time constants of block were 142 ms, 251 ms and 311 ms for 2 μM, 0.6 μM, 0.4 μM, respectively. To assess Po-dependence of the blocking rate, Po was estimated in each patch by normalizing current amplitude in sub-saturating Ca^{2+} (0.4 or 0.6 μM) to current amplitude in saturating Ca^{2+} (2 μM). Figure 13B shows the normalized time constant of block versus normalized Po for 7 different patches (10 data points since in 3 of the patches, two different sub-saturating Ca^{2+} concentrations were used as shown in figure 13A). To illustrate the Po-dependence of the Ba^{2+} block rate, the data points are fit with a single exponential function.

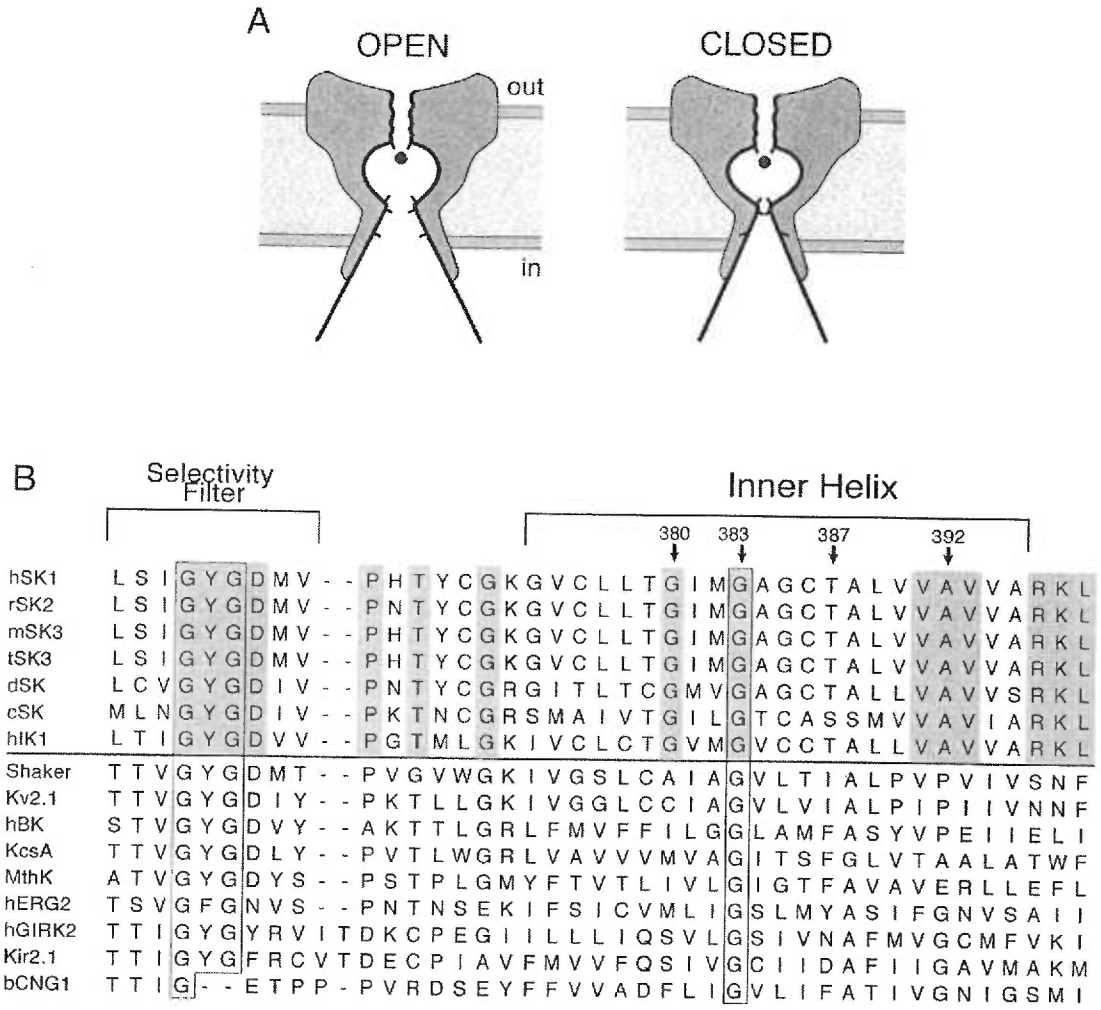

Figure 14. A, Cartoon representing a possible mechanism of SK channel gating. Two of four subunits are shown in cross-section in either in the open state (left) or closed state (right). Ba^{2+} is shown as a black ball and its position is estimated from its binding site in the crystal structure of the KcsA K^+ channel. S359, which is believed to form part of the Ba^{2+} binding site is indicated by the two uppermost dashes at the bottom of the selectivity filter. The other dashes represent, from top to bottom, residues G380, T383, and A392. In this model, a gate would be formed when the region between G380 and G383 collapses inwards. B, Sequence alignment of the selectivity filter through inner helix region of a variety of K^+ channels. Sequences were obtained from NIH databases and aligned by eye. The line separates Ca^{2+}-gated K channels from other channels. The boxed glycine represents the "glycine hinge" that is conserved across the ion channel superfamily and believed to be a critical point of flexibility for K^+ channel gating [40]. Note that all SK and IK channels have a second glycine (380) residue three amino acids N-terminal to the glycine hinge residue (383).

E. DISCUSSION

A central goal of ion channel research is to understand at the molecular level the mechanisms that underlie channel gating. To this end, much progress has been made, particularly for the K_v family of ion channel [112]. Complementing years of functional work on native and cloned K_v channels, a series of remarkable crystal structures of K channels have now been presented. Emerging from these crystallography and functional experiments is a growing consensus that many channels regulate ion flux at a gate formed by the intracellular end of the pore [22, 40, 41, 60, 100]. The gating hypothesis for these channels is that in the closed state the inner helices from each of the four channel subunits form a restrictive barrier to permeation by crossing very near the cytoplasmic interface. In the open state, the bundle crossing is removed by large-scale protein conformational changes.

For bacterial channels, the conformational change can occur at a "glycine hinge" approximately halfway between the bundle crossing and the selectivity filter [40]. Flexibility at the hinge allows the inner helices to bend approximately 30°, resulting in a complete abolishment of the bundle crossing. Instead of forming a gate, the intracellular end of the pore is splayed wide open, allowing unrestricted K^+ permeation through the pore. For K_v channels it has been proposed that in the open state a proline-X-proline motif, starting 7 amino acids cytoplamic to the glycine hinge, may introduce a kink in the otherwise rigid inner helices [62]. In the closed state, as has been proposed for the bacterial channels, the inner helices would straighten and form a gate near the cytoplasmic interface. Finally, a crystal structure and sequence alignment analysis of Kir channels suggests that this familly, too, has a cytoplasmic gate formed by the inner

helices, but again, the region of flexibility is proposed to differ from the other K channels [100].

In a recent paper, we probed the intracellular end of TM6 with MTS reagents to assess if a similar gate is formed in the closed state of SK channels [110]. In contrast to the functional data obtained on the *Shaker* channel, a position internal to the bundle crossing region (T387C) could be accessed whether the channel was open or closed. In addition, the pore blocker TBuA was shown to protect this position from MTSEA modification in both the closed and open states of the channel. Taken together, the data suggested that the activation gate for SK channels could reside in or near the selectivity filter.

While these data are reasonably compelling, they are unsatisfying in that the probes used are larger and more hydrophobic than a K^+ ion, and they do not react with positions above the glycine hinge, making it impossible to probe deep into the pore with them. Furthermore, the rate of reactivity at position T387C is relatively slow, raising the possibility that state-dependence could be difficult to detect if channels are not completely closed and reagents can be "trapped" in the channel as discussed by Phillips et al. [113].

To circumvent these limitations, we probed the SK pore with Ba^{2+}. Ba^{2+} is an ideal probe since it is nearly identical to K^+ in size (pauling radii 1.35 Å versus 1.33 Å for K^+). Moreover, the binding site for Ba^{2+} is located very deep in the SK channel pore immediately below the selectivity filter [89], and it blocks with high affinity. We reasoned that if Ba^{2+} binds internal to a gate, it should be trapped in the SK pore if the

gate is closed behind it, as has been shown for a BK channel [24] and for K_v channels [22, 58]. This is exactly what we observed; Ba^{2+} could be readily trapped at its binding site in closed SK channels (Figure 9). Consistent with this result, Ba^{2+} can't access this binding site from the closed state (Figure 10, Figure 11). If Ba^{2+} blocks the SK conduction pathway by binding at a single site that is stabilized as channel open probability is lowered (ie. as trapping is favored), the Ba^{2+} block rate should be slowed, and potency of block increased, as Po is lowered. Figure 12 and 13 show that experimental data match these predictions. The binding rate of Ba^{2+} block is significantly slowed as Po is lowered, and the Kd of block is lower at a lower Po.

The simplest interpretation of this data is that in SK channels, a gate exists between the Ba^{2+} binding site at the selectivity filter and the intracellular end of the protein. Taken together with the MTSEA data, the lower limit for the location of the gate is position G386, three residues below the glycine analogous to the glycine that forms the "hinge" in MthK channels. Thus the data is consistent with an activation gate that resides between the selectivity filter and the region near the glycine hinge. This model is appealingly simple; Ba^{2+} would bind at a single site just underneath the selectivity filter and a gate would be free to close behind it. The main difference between this and the gating models proposed for K_v and bacterial K channels is the location of the gate; in the SK channel model the gate lies relatively deep in the pore, whereas for other channels the gate is localized to the cytoplasmic end of the pore.

Nonetheless, it is important to consider an intriguing alternative interpretation of our data. It is possible that Ba^{2+} is trapped not between the selectivity filter and the glycine hinge,

but in the selectivity filter itself. Consistent with this idea, it is believed that Ba^{2+} can pass through the selectivity filter and that there are at least three Ba^{2+} binding sites in and near the selectivity filter, at least in BK and *Shaker* channels [25, 26, 94, 114]. Furthermore, crystal structures and functional data suggest that the selectivity filter re-orients during gating such that K^+ can no longer permeate [48, 63, 75, 76, 100]. Despite loss of K^+ conduction, crystal structures of presumably closed K^+ channels show K^+ remains in the selectivity filter. K^+ is, in effect, trapped in the closed filter. If Ba^{2+} acts like K^+, it is not unreasonable to imagine Ba^{2+} trapping by the selectivity filter. In this model, the selectivity filter would have to also act as the activation gate, and the binding site would necessarily change as the channel transitioned between open-blocked and closed-blocked states. If, for example, there was a gate at the intracellular end of the selectivity filter, it could be imagined that as the channel closed in the presence of blocker, the Ba^{2+} would be absorbed from the open-blocked site to a site deeper in the selectivity filter, and the channel would enter the closed-blocked state with Ba^{2+} trapped in the filter. Thus the allosteric transition from opened to closed would be accompanied by a shifting of the Ba^{2+} binding site from just underneath the selectivity filter to within the selectivity filter.

Differentiating between these two models is not possible given the current data. However, we favor the first model for three reasons. First, it is the simpler of the two. Second, when Ba^{2+} was added to the crystallized K channel that represents the closed state (KcsA), its electron density co-localized with rubidium (representing K^+) at the "inner ion" site just below the selectivity filter, not in the selectivity filter. Finally, the existence of multiple bacterial K channels that appear to share a common gating

mechanism utilizing an intracellular gate, taken together with solid functional data from the *Shaker* K_v channel suggesting that it possesses an intracellular gate, is compelling.

How could an intracellular gate be formed in SK channels? Aligning the amino acid sequence of the SK channel family against sequences from a wide variety of other channels may provide a clue (Figure 14). In addition to the consensus K filter sequence "GYG" (boxed), SK channels possess a glycine at the "hinge" location (boxed). Interestingly, all small and intermediate-conductance Ca^{2+}-activated K (SK and IK) channels have a second conserved glycine three amino acids internal to the glycine hinge. A search of all major K^+ channel families shows that this glycine is unique to calmodulin-gated K^+ channels. We propose that this double glycine could provide additional flexibility to the hinge region that is known to be important for gating. In one possible gating model, the flexible region would occlude the permeation pathway in the resting (closed) state, but be pulled apart in the open state. It could be imagined that this would occur if, upon binding Ca^{2+}, CaM exerted a "downward" force on the linker region between the CaMBD and the glycine gate. This movement would straighten the TM6 α-helices and pull them apart at the constriction formed by the glycine-rich region.

V. DISCUSSION

SK channels and their close relatives, IK channels, are unique in that their gating is entirely voltage-independent, responding instead to changes in intracellular Ca^{2+} levels. CaM acts as a constitutively bound Ca^{2+}-sensor for these channels, relaying the gating signal to a physical structure, the activation gate, that regulates ion flux through the pore. The central finding of this thesis is that, like the Ca^{2+} -sensing mechanism, the location of the SK channel activation gate appears to be unique.

A. SK CHANNELS SHARE FEATURES WITH OTHER K^+ CHANNELS

Despite these differences, SK channels share many general features with other ion channels, especially the well-studied K^+ channels. We now believe that the overall architecure of the inner vestibule resembles that of *Shaker* K_v and crystallized bacterial channels. For example, the inner helix of the SK channel pore is formed by TM6, just as it is in these other K^+ channels. Evidence for this is two-fold. First, individual TM6 residues that are mutated to cysteine are readily accessible to MTS reagents from the intracellular face of the channel (Figure 2, 3). These reagents covalently attach to the TM6 cysteines and block conduction through the pore in a voltage-dependent manner, suggesting they lie in the permeation pathway. Second, the voltage-dependent pore blocker TBuA (Figure Aa-2) can protect one of these cysteines (T387C) from modification by an MTS reagent, suggesting that the residue must reside near the TBuA binding site in the pore (Figure 6). Indeed, the T387C mutation confers increased sensitivity to TBuA block (Fig. Aa-3), suggesting it forms part of the TBuA binding site.

Another similarity to other K^+ channels is that the TM6 region appears to move during gating. In support of this, several residues in TM6 are available to MTS reagents in a state-dependent manner, suggesting that either these residues or surrounding protein move during gating (Figure 4). Further, channel block by Ba^{2+}, an ion that binds deep in the pore near the selectivity filter, is dependent on Po, suggesting that as the channel transitions between open and closed states, access to this binding site or the binding site itself changes conformation (Figures 11-13). Finally, Ba^{2+} can be "trapped" in the channel pore. If open channels are blocked with Ba^{2+} and then closed, the Ba^{2+} remains in the channel until it is opened again (Figure 9).

B. LOCATION OF THE SK CHANNEL ACTIVATION GATE

Where is the gate located in SK channels? Taking the Ba^{2+} data alone, one could presume that the gate resides at the intracellular end of the channel pore as it does in K_v and bacterial K^+ channels. However, the data presented in Chapter 2 are not consistent with this model. MTSEA can access position 387 deep in the pore in a state-independent manner, and this position can be protected in both the closed and open states by TBuA (Figure 5, 6). These data suggest that both MTSEA and TBuA can block deep in the pore, even in closed channels. Therefore, the activation gate of SK channels must reside deep in the pore, past position 387. The most likely position for this gate, based on analogy to CNG channels and some evidence from the KcsA and *Shaker* channels, was taken to be the selectivity filter (see Chapter 2), though a gate between the selectivity filter and position 387 could not be ruled out. To address this issue, the Ba^{2+} experiments of Chapter 3 were performed. Surprisingly, Ba^{2+} showed strong state-dependent access to its' binding site very near the selectivity filter, and could be trapped in closed channels.

This data suggested that the activation gate must lie between the Ba^{2+} binding site and the cytoplasm. Taken together with the MTS and TBuA data, it is concluded that the activation gate in SK channels is most likely located between position 387 and the selectivity filter.

Since the data suggested that the SK channel gate is located relatively deep in the pore (deeper than the *Shaker* or bacterial K^+ channel gates) sequence alignments of all cloned SK channels and a wide variety of other channels were compared in an attempt to gain clues about how SK channels could form a deep pore gate. Glycine or proline residues have been of particular interest in channel gating since they introduce flexibility to the otherwise rigid helices that line the inner vestibule [40, 62]. Whereas all other channels contain one or two glycines in the vestibule-lining TM6 region, sequence alignments reveal a group of three glycines in the SK channel pore in and near the suspected gate area. We speculate that the inner vestibule of SK channels may be more flexible than other channels, allowing a gate to be formed deep in the inner vestibule.

C. FUTURE EXPERIMENTS

a. Structure-Function Studies

Testing of this hypothesis will require a combination of electrophysiology and chemical modification of select mutant channels. For example, it will be interesting to see if intersubunit disulfide bonds can be formed between cysteines introduced at positions deep in the pore that are expected to form the gate in SK channels. If the model proposed in Figure 14 is correct, for example, one could imagine cross-linking residues around position G380 in the closed state of the channel, but not in the open state, since cross-

linking rate is dependent on distance (and orientation) between thiol groups. Such an approach has been useful for delineating gating movements near the bundle crossing region of CNG channels [64]. It will also be fruitful to identify residues deep in the pore (for example, near the selectivity filter) that rapidly and irreversibly interact with Cd^{2+} or Ag^{+} ions so that these can be used as probes for state-dependence. One Cd^{2+}-reactive residue (391C) that lies internal to the putative bundle crossing region has been identified in SK channels. 391C appears to be readily accessed by Cd^{2+} in both the open and closed states of the channel (Figure Aa-4) suggesting that the bundle crossing does not form an effective barrier to this position. This residue is analogous to the residue probed in CNG channels (391C, no state-dependence) [64], and *Shaker* channels (474C, strong state-dependence) [60]. One important caveat of all these experiments, however, is that this particular position is very close to the putative gate. Thus, rotational or translational flexibility of the region on a fast time-scale could influence the apparent block rate. For example, if closed SK or CNG channels have a high degree of freedom in the closed state around position 391C, the position could be modified in closed channels even though a gate to K^{+} still exists cytoplasmic to the residue.

b. Crystal Structures

Crystallization of an SK channel pore would provide much insight into the possible pore re-arrangements that accompany SK channel gating. To this end, great strides have been made by crystallizing pores, and in some cases the entire body, of bacterial ion channels [40-43, 100, 115, 116]. One common theme emerging from K^{+} pore crystals is the existence of a flexible region in the inner helix that allows bending and formation of a distal gate. In the MthK structure, this flexibility is centered at a "glycine hinge" residue.

By comparison with KcsA, for which the inner helices are essentially straight, it is inferred that this glycine hinge "straightens" during gating and the cytoplasmic end of the helices cross each other to form the bundle crossing activation gate (Figure i2). Interestingly, the recently crystallized 6 TM voltage-gated K^+ channel K_v AP [117] also bends near the conserved glycine hinge (though to a lesser extent than MthK) even though the channel is, based on the position of the voltage-sensing domain, in the closed state [43]. While this anomaly remains unresolved, it could be explained by the fact that the structure was solved with large Fab fragments of monoclonal antibodies attached to each TM4 domain. Fab attachment was shown to alter the conformation of the voltage sensing domain of the channel (TM1-TM4) since, when crystallized independent of the pore, it assumed a very different conformation [43]. It was subsequently demonstrated that by merging the full-length structure with the structure of the isolated voltage-sensing domain, a reasonable model could be obtained.

Functional accessibility assays on the voltage-sensing domain of heterologously expressed K_v AP channels are consistent with this modified model [49], but don't rule out traditional models of voltage-sensor position relative to other parts of K_v channels [1]. It is suggested that crystal-packing constraints imposed by the Fab attachments alter not only the structure of the voltage sensor, but also pull the channel open by bending the inner helix at the glycine hinge [43]. Thus, despite qualitative complications in interpreting the K_v AP structure, it is apparent from the crystal structure that TM6 can bend near the conserved glycine hinge. Resolution of a structure of the isolated K_v AP pore domain (TM5–TM6) could help resolve if the helices do straighten to a KcsA-like position to form a gate in closed K_v AP channels.

Another crystallized K channel, KirBac1.1, does in fact have straightened inner helices that form a gate in the closed state [100]. Interestingly, the helices do bend (approximately 12°) at a glycine residue (G134) analogous to the glycine hinge in MthK, but not enough to splay the channel open. Instead, the distal inner helix crosses near a phenylalanine residue (F146) that would form an activation gate. Based on sequence alignments with other Kir channels, it is proposed that the flexibility for channel opening is conferred not by G134 (which is absent in some K_{ir} channels), but by a glycine further down the inner helix, G143. Nonetheless, the authors propose that the basic gating mechanism in which the inner helices are bent apart in the presence of a gating signal, is conserved between a large range of channels. This idea is very similar to that proposed by Gary Yellen's group based on functional data before any "open" K^+ channel structures were solved. For K_v channels, they proposed, the primary bending during gating occurs at a proline-x-proline motif in the inner helix, that, like G143 in KirBac1.1, lies cytoplasmic to the glycine hinge residue of MthK [62].

Unfortunately, there is no crystal structure of the pore domain of an SK channel. Based on the emerging theme of gating by bending of inner helices across a wide range of K^+ channels, it is appealing to imagine that SK channels may also bend at some flexible region of TM6. It is striking that the SK family has a relatively high concentrations of glycine residues in TM6 that could provide the flexibility necessary to form a gate, and it is easy to imagine mechanisms consistent with the functional data obtained in this thesis (eg. Figure 14). Ultimately, though, a complete understanding of SK channel gating will require more than functional data. In addition to obtaining crystal structures of the SK

pore in both the open and closed conformations, it will be critical to understand the conformation of the CaM-CaMBD interaction in the absence of calcium, the role of the linker region between the CaMBD and TM6, and possible unidentified roles of other portions of the channel or β-subunits.

VI. SUMMARY AND CONCLUSIONS

In this thesis I have verified that, as for other 6 TM channels, TM6 lines the conduction pathway of SK channels and undergoes re-orientation during gating. Specific positions in TM6 were identified that, when mutated to cysteine, reacted with chemical modifying reagents in a state-dependent manner. Access to a position in the inner vestibule (T387C) was not state-dependent as assessed by MTSEA reaction rate and by the ability of TBuA to protect the position from MTSEA modification. In contrast, Ba^{2+} access to its binding site near the selectivity filter was strongly state-dependent, and Ba^{2+} could be trapped between the selectivity filter and an internal gate.

A model is proposed in which SK channels, like K_v and bacterial K channels, have an internal activation gate. Different from these channels, this gate likely lies deep in the pore, between the selectivity filter and T387. Unique to the Ca^{2+}-activated class of K^+ channels, the force necessary to open the gate is provided by a β-subunit, CaM. Increases in intracellular Ca^{2+} allow Ca^{2+} ions to bind CaM EF hands 1 and 2, triggering conformational changes in CaM. These structural changes are conferred to the C-terminus of the channel through the CaMBD, and are relayed to the activation gate deep in the inner vestibule. This thesis contributes to our knowledge of the SK channel gating mechanism by localizing the activation gate. A complete understanding of SK channel gating will require understanding how the three primary players - the activation gate, the gating domain (CaM-CaMBD), and the linker region – work in unison to open and close the conduction pore.

VII. REFERENCES

1. Hille, B., *Ion channels of excitable membranes.* 3rd ed. 2001, Sunderland, Mass.: Sinauer. xviii, 814.
2. Armstrong, C.M., *Ionic pores, gates, and gating currents.* Q Rev Biophys, 1974. **7**(2): p. 179-210.
3. Barrett, E.F. and J.N. Barret, *Separation of two voltage-sensitive potassium currents, and demonstration of a tetrodotoxin-resistant calcium current in frog motoneurones.* J Physiol, 1976. **255**(3): p. 737-74.
4. Yarom, Y., M. Sugimori, and R. Llinas, *Ionic currents and firing patterns of mammalian vagal motoneurons in vitro.* Neuroscience, 1985. **16**(4): p. 719-37.
5. Madison, D.V. and R.A. Nicoll, *Control of the repetitive discharge of rat CA 1 pyramidal neurones in vitro.* J Physiol, 1984. **354**: p. 319-31.
6. Lancaster, B., R.A. Nicoll, and D.J. Perkel, *Calcium activates two types of potassium channels in rat hippocampal neurons in culture.* J Neurosci, 1991. **11**(1): p. 23-30.
7. Sah, P., *Properties of channels mediating the apamin-insensitive afterhyperpolarization in vagal motoneurons.* J Neurophysiol, 1995. **74**(4): p. 1772-6.
8. Sah, P., *Ca2+-activated K+ currents in neurones: types, physiological roles and modulation.* Trends Neurosci., 1996. **19**(4): p. 150-4.
9. Stocker, M., M. Krause, and P. Pedarzani, *An apamin-sensitive Ca2+-activated K+ current in hippocampal pyramdial neurons.* Proc. Natl. Acad. Sci. USA, 1999. **96**: p. 4662-4667.

10. Hirschberg, B., et al., *Gating properties of single SK channels in hippocampal CA1 pyramidal neurons.* Biophys J, 1999. **77**(4): p. 1905-13.

11. Behnisch, T. and K.G. Reymann, *Inhibition of apamin-sensitive calcium dependent potassium channels facilitate the induction of long-term potentiation in the CA1 region of rat hippocampus in vitro.* Neurosci Lett, 1998. **253**(2): p. 91-4.

12. Stackman, R.W., et al., *Small conductance Ca2+-activated K+ channels modulate synaptic plasticity and memory encoding.* J Neurosci, 2002. **22**(23): p. 10163-71.

13. Ikonen, S., B. Schmidt, and P. Riekkinen, Jr., *Apamin improves spatial navigation in medial septal-lesioned mice.* Eur J Pharmacol, 1998. **347**(1): p. 13-21.

14. Fiorillo, C.D. and J.T. Williams, *Glutamate mediates an inhibitory postsynaptic potential in dopamine neurons.* Nature, 1998. **394**(6688): p. 78-82.

15. Bevan, M.D. and C.J. Wilson, *Mechanisms underlying spontaneous oscillation and rhythmic firing in rat subthalamic neurons.* J Neurosci, 1999. **19**(17): p. 7617-28.

16. Vergara, C., B. Ramirez, and M.I. Behrens, *Colchicine alters apamin receptors, electrical activity, and skeletal muscle relaxation.* Muscle Nerve, 1993. **16**(9): p. 935-40.

17. Neelands, T.R., et al., *Small-conductance calcium-activated potassium currents in mouse hyperexcitable denervated skeletal muscle.* J Physiol, 2001. **536**(Pt 2): p. 397-407.

18. Jacobson, D., et al., *SK channels are necessary but not sufficient for denervation-induced hyperexcitability.* Muscle Nerve, 2002. **26**(6): p. 817-22.

19. Behrens, M.I., et al., *Possible role of apamin-sensitive K+ channels in myotonic dystrophy.* Muscle Nerve, 1994. **17**(11): p. 1264-70.

20. Bond, C.T., et al., *Respiration and parturition affected by conditional overexpression of the Ca2+-activated K+ channel subunit, SK3.* Science, 2000. **289**(5486): p. 1942-6.

21. Armstrong, C.M. and B. Hille, *The inner quaternary ammonium ion receptor in potassium channels of the node of Ranvier.* J. Gen. Physiol., 1972. **59**(4): p. 388-400.

22. Armstrong, C.M., *Interaction of tetraethylammonium ion derivatives with the potassium channels of giant axons.* J Gen Physiol, 1971. **58**(4): p. 413-37.

23. Armstrong, C.M., *Inactivation of the potassium conductance and related phenomena caused by quaternary ammonium ion injection in squid axons.* J Gen Physiol, 1969. **54**(5): p. 553-75.

24. Miller, C., *Trapping single ions inside single ion channels.* Biophys J, 1987. **52**(1): p. 123-6.

25. Neyton, J. and C. Miller, *Potassium blocks barium permeation through a calcium-activated potassium channel.* J Gen Physiol, 1988. **92**(5): p. 549-67.

26. Neyton, J. and C. Miller, *Discrete Ba2+ block as a probe of ion occupancy and pore structure in the high-conductance Ca2+ -activated K+ channel.* J Gen Physiol, 1988. **92**(5): p. 569-86.

27. Salkoff, L. and R. Wyman, *Genetic modification of potassium channels in Drosophila Shaker mutants.* Nature, 1981. **293**(5829): p. 228-30.

28. Wu, C.F. and F.N. Haugland, *Voltage clamp analysis of membrane currents in larval muscle fibers of Drosophila: alteration of potassium currents in Shaker mutants.* J Neurosci, 1985. **5**(10): p. 2626-40.

29. Papazian, D.M., et al., *Cloning of genomic and complementary DNA from Shaker, a putative potassium channel gene from Drosophila.* Science, 1987. **237**(4816): p. 749-53.

30. Tempel, B.L., et al., *Sequence of a probable potassium channel component encoded at Shaker locus of Drosophila.* Science, 1987. **237**(4816): p. 770-5.

31. Timpe, L.C., et al., *Expression of functional potassium channels from Shaker cDNA in Xenopus oocytes.* Nature, 1988. **331**(6152): p. 143-5.

32. Hodgkin, A.L. and A.F. Huxley, *Currents carried by sodium and potassium ions through the membrane of the giant axon of Loligo.* J Physiol, 1952. **116**: p. 449-472.

33. Hodgkin, A.L. and A.F. Huxley, *The components of membrane conductance in the giant axon of Loligo.* J Physiol, 1952. **116**: p. 473-496.

34. Hodgkin, A.L. and A.F. Huxley, *A quantitative description of membrane current and its application to conduction and excitation in nerve.* J Physiol, 1952. **117**: p. 500-544.

35. Noda, M., et al., *Primary structure of Electrophorus electricus sodium channel deduced from cDNA sequence.* Nature, 1984. **312**(5990): p. 121-7.

36. Christie, M.J., et al., *Heteropolymeric potassium channels expressed in Xenopus oocytes from cloned subunits.* Neuron, 1990. **4**(3): p. 405-11.

37. Isacoff, E.Y., Y.N. Jan, and L.Y. Jan, *Evidence for the formation of heteromultimeric potassium channels in Xenopus oocytes.* Nature, 1990. **345**(6275): p. 530-4.

38. Ruppersberg, J.P., et al., *Heteromultimeric channels formed by rat brain potassium-channel proteins.* Nature, 1990. **345**(6275): p. 535-7.

39. MacKinnon, R., *Determination of the subunit stoichiometry of a voltage-activated potassium channel.* Nature, 1991. **350**(6315): p. 232-5.

40. Jiang, Y., et al., *The open pore conformation of potassium channels.* Nature, 2002. **417**(6888): p. 523-6.

41. Doyle, D.A., et al., *The structure of the potassium channel: molecular basis of K+ conduction and selectivity.* Science, 1998. **280**(5360): p. 69-77.

42. Jiang, Y., et al., *Crystal structure and mechanism of a calcium-gated potassium channel.* Nature, 2002. **417**(6888): p. 515-22.

43. Jiang, Y., et al., *X-ray structure of a voltage-dependent K(+) channel.* Nature, 2003. **423**(6935): p. 33-41.

44. Heginbotham, L., et al., *Mutations in the K+ channel signature sequence.* Biophys J, 1994. **66**(4): p. 1061-7.

45. Aiyar, J., et al., *The signature sequence of voltage-gated potassium channels projects into the external vestibule.* J Biol Chem, 1996. **271**(49): p. 31013-6.

46. Ranganathan, R., J.H. Lewis, and R. MacKinnon, *Spatial localization of the K+ channel selectivity filter by mutant cycle-based structure analysis.* Neuron, 1996. **16**(1): p. 131-9.

47. Bezanilla, F. and C.M. Armstrong, *Negative conductance caused by entry of sodium and cesium ions into the potassium channels of squid axons.* J Gen Physiol, 1972. **60**(5): p. 588-608.

48. Zhou, Y., et al., *Chemistry of ion coordination and hydration revealed by a K+ channel- Fab complex at 2.0 A resolution.* Nature, 2001. **414**(6859): p. 43-8.

49. Jiang, Y., et al., *The principle of gating charge movement in a voltage-dependent K(+) channel.* Nature, 2003. **423**(6935): p. 42-8.

50. Horn, R., *Coupled movements in voltage-gated ion channels.* J Gen Physiol, 2002. **120**(4): p. 449-53.

51. Gandhi, C.S. and E.Y. Isacoff, *Molecular models of voltage sensing.* J Gen Physiol, 2002. **120**(4): p. 455-63.

52. Bezanilla, F., *Voltage sensor movements.* J Gen Physiol, 2002. **120**(4): p. 465-73.

53. Larsson, H.P., *The search is on for the voltage sensor-to-gate coupling.* J Gen Physiol, 2002. **120**(4): p. 475-81.

54. Lopez, G.A., Y.N. Jan, and L.Y. Jan, *Evidence that the S6 segment of the Shaker voltage-gated K+ channel comprises part of the pore.* Nature, 1994. **367**(6459): p. 179-82.

55. Choi, K.L., et al., *The internal quaternary ammonium receptor site of Shaker potassium channels.* Neuron, 1993. **10**(3): p. 533-41.

56. Baukrowitz, T. and G. Yellen, *Two functionally distinct subsites for the binding of internal blockers to the pore of voltage-activated K+ channels.* Proc Natl Acad Sci U S A, 1996. **93**(23): p. 13357-61.

57. Zhou, M., et al., *Potassium channel receptor site for the inactivation gate and quaternary amine inhibitors.* Nature, 2001. **411**(6838): p. 657-61.

58. Holmgren, M., P.L. Smith, and G. Yellen, *Trapping of organic blockers by closing of voltage-dependent K+ channels: evidence for a trap door mechanism of activation gating.* J. Gen. Physiol., 1997. **109**(5): p. 527-35.

59. Karlin, A. and M.H. Akabas, *Substituted-cysteine accessibility method.* Methods. Enzymol., 1998. **293**: p. 123-45.

60. Liu, Y., et al., *Gated access to the pore of a voltage-dependent K+ channel.* Neuron, 1997. **19**(1): p. 175-84.

61. del Camino, D. and G. Yellen, *Tight steric closure at the intracellular activation gate of a voltage- gated K+ channel.* Neuron, 2001. **32**(4): p. 649-56.

62. del Camino, D., et al., *Blocker protection in the pore of a voltage-gated K+ channel and its structural implications.* Nature, 2000. **403**(6767): p. 321-5.

63. Perozo, E., D.M. Cortes, and L.G. Cuello, *Structural rearrangements underlying K+-channel activation gating.* Science, 1999. **285**(5424): p. 73-8.

64. Flynn, G.E. and W.N. Zagotta, *Conformational changes in S6 coupled to the opening of cyclic nucleotide-gated channels.* Neuron, 2001. **30**(3): p. 689-98.

65. Liu, J. and S.A. Siegelbaum, *Change of pore helix conformational state upon opening of cyclic nucleotide-gated channels.* Neuron, 2000. **28**(3): p. 899-909.

66. Becchetti, A., K. Gamel, and V. Torre, *Cyclic nucleotide-gated channels. Pore topology studied through the accessibility of reporter cysteines.* J. Gen. Physiol., 1999. **114**(3): p. 377-92.

67. Sun, Z.P., et al., *Exposure of residues in the cyclic nucleotide-gated channel pore: P region structure and function in gating.* Neuron, 1996. **16**(1): p. 141-9.

68. Zagotta, W.N. and S.A. Siegelbaum, *Structure and function of cyclic nucleotide-gated channels.* Annu. Rev. Neurosci., 1996. **19**: p. 235-63.

69. Trudeau, M.C. and W.N. Zagotta, *Mechanism of calcium/calmodulin inhibition of rod cyclic nucleotide-gated channels.* Proc Natl Acad Sci U S A, 2002. **99**(12): p. 8424-9.

70. Trudeau, M.C. and W.N. Zagotta, *Calcium/calmodulin modulation of olfactory and rod cyclic nucleotide-gated ion channels.* J Biol Chem, 2003.

71. Karpen, J.W., et al., *Interactions between divalent cations and the gating machinery of cyclic GMP-activated channels in salamander retinal rods.* J Gen Physiol, 1993. **101**(1): p. 1-25.

72. Fodor, A.A., K.D. Black, and W.N. Zagotta, *Tetracaine reports a conformational change in the pore of cyclic nucleotide-gated channels.* J Gen Physiol, 1997. **110**(5): p. 591-600.

73. Fodor, A.A., S.E. Gordon, and W.N. Zagotta, *Mechanism of tetracaine block of cyclic nucleotide-gated channels.* J Gen Physiol, 1997. **109**(1): p. 3-14.

74. Lu, T., et al., *Probing ion permeation and gating in a K+ channel with backbone mutations in the selectivity filter.* Nat. Neurosci., 2001. **4**(3): p. 239-46.

75. Zheng, J. and F.J. Sigworth, *Selectivity changes during activation of mutant Shaker potassium channels.* J. Gen. Physiol., 1997. **110**(2): p. 101-17.

76. Zheng, J. and F.J. Sigworth, *Intermediate conductances during deactivation of heteromultimeric Shaker potassium channels.* J. Gen. Physiol., 1998. **112**(4): p. 457-74.

77. Hoshi, T., W.N. Zagotta, and R.W. Aldrich, *Biophysical and molecular mechanisms of Shaker potassium channel inactivation.* Science, 1990. **250**(4980): p. 533-8.

78. Rettig, J., et al., *Inactivation properties of voltage-gated K+ channels altered by presence of beta-subunit.* Nature, 1994. **369**(6478): p. 289-94.

79. Hoshi, T., W.N. Zagotta, and R.W. Aldrich, *Two types of inactivation in Shaker K+ channels: effects of alterations in the carboxy-terminal region.* Neuron, 1991. 7(4): p. 547-56.

80. Lopez-Barneo, J., et al., *Effects of external cations and mutations in the pore region on C-type inactivation of Shaker potassium channels.* Receptors Channels, 1993. **1**(1): p. 61-71.

81. Choi, K.L., R.W. Aldrich, and G. Yellen, *Tetraethylammonium blockade distinguishes two inactivation mechanisms in voltage-activated K+ channels.* Proc. Natl. Acad. Sci. U S A, 1991. **88**(12): p. 5092-5.

82. Yellen, G., et al., *An engineered cysteine in the external mouth of a K+ channel allows inactivation to be modulated by metal binding.* Biophys J, 1994. **66**(4): p. 1068-75.

83. Liu, Y., M.E. Jurman, and G. Yellen, *Dynamic rearrangement of the outer mouth of a K+ channel during gating.* Neuron, 1996. **16**(4): p. 859-67.

84. Kiss, L., J. LoTurco, and S.J. Korn, *Contribution of the selectivity filter to inactivation in potassium channels.* Biophys J, 1999. **76**(1 Pt 1): p. 253-63.

85. Romey, G. and M. Lazdunski, *The coexistence in rat muscle cells of two distinct classes of Ca2+-dependent K+ channels with different pharmacological properties and different physiological functions.* Biochem Biophys Res Commun, 1984. **118**(2): p. 669-74.

86. Kohler, M., et al., *Small-conductance, calcium-activated potassium channels from mammalian brain.* Science, 1996. **273**(5282): p. 1709-14.

87. Ishii, T.M., J. Maylie, and J.P. Adelman, *Determinants of apamin and d-tubocurarine block in SK potassium channels.* J Biol Chem, 1997. **272**(37): p. 23195-200.

88. Soh, H. and C.S. Park, *Inwardly rectifying current-voltage relationship of small-conductance Ca2+-activated K+ channels rendered by intracellular divalent cation blockade.* Biophys J, 2001. **80**(5): p. 2207-15.

89. Soh, H. and C.S. Park, *Localization of divalent cation-binding site in the pore of a small conductance Ca(2+)-activated K(+) channel and its role in determining current-voltage relationship.* Biophys J, 2002. **83**(5): p. 2528-38.

90. Jiang, Y. and R. MacKinnon, *The barium site in a potassium channel by x-ray crystallography.* J. Gen. Physiol., 2000. **115**(3): p. 269-72.

91. Diaz, F., et al., *Interaction of internal Ba2+ with a cloned Ca(2+)-dependent K+ (hslo) channel from smooth muscle.* J Gen Physiol, 1996. **107**(3): p. 399-407.

92. Miller, C., R. Latorre, and I. Reisin, *Coupling of voltage-dependent gating and Ba++ block in the high-conductance, Ca++-activated K+ channel.* J Gen Physiol, 1987. **90**(3): p. 427-49.

93. Ogielska, E.M. and R.W. Aldrich, *A mutation in S6 of Shaker potassium channels decreases the K+ affinity of an ion binding site revealing ion-ion interactions in the pore.* J Gen Physiol, 1998. **112**(2): p. 243-57.

94. Harris, R.E., H.P. Larsson, and E.Y. Isacoff, *A permanent ion binding site located between two gates of the Shaker K+ channel.* Biophys J, 1998. **74**(4): p. 1808-20.

95. Xia, X.M., et al., *Mechanism of calcium gating in small-conductance calcium-activated potassium channels.* Nature, 1998. **395**(6701): p. 503-7.

96. Keen, J.E., et al., *Domains responsible for constitutive and Ca2+-dependent interactions between calmodulin and small conductance Ca2+-activated potassium channels.* J. Neurosci., 1999. **19**(20): p. 8830-8.

97. Schumacher, M.A., et al., *Structure of the gating domain of a Ca2+-activated K+ channel complexed with Ca2+/calmodulin.* Nature, 2001. **410**(6832): p. 1120-4.

98. Lee, W.S., et al., *Small conductance Ca2+-activated K+ channels and calmodulin: Cell surface expression and gating.* J Biol Chem, 2003.

99. Sun, Y., et al., *Mechanism of glutamate receptor desensitization.* Nature, 2002. **417**(6886): p. 245-53.

100. Kuo, A., et al., *Crystal Structure of the Potassium Channel KirBac1.1 in the Closed State.* Science, 2003.

101. Wissmann, R., et al., *A helical region in the C terminus of small-conductance Ca2+-activated K+ channels controls assembly with apo-calmodulin.* J Biol Chem, 2002. **277**(6): p. 4558-64.

102. Kohler, M., et al., *Small-conductance, calcium-activated potassium channels from mammalian brain.* Science, 1996. **273**(5282): p. 1709-14.

103. Flynn, G.E., J.P. Johnson, Jr., and W.N. Zagotta, *Cyclic nucleotide-gated channels: shedding light on the opening of a channel pore.* Nat. Rev. Neurosci., 2001. **2**(9): p. 643-51.

104. Liu, Y.S., P. Sompornpisut, and E. Perozo, *Structure of the KcsA channel intracellular gate in the open state.* Nat. Struct. Biol., 2001. **8**(10): p. 883-7.

105. Holmgren, M., K.S. Shin, and G. Yellen, *The activation gate of a voltage-gated K+ channel can be trapped in the open state by an intersubunit metal bridge.* Neuron, 1998. **21**(3): p. 617-21.

106. Ho, S.N., et al., *Site-directed mutagenesis by overlap extension using the polymerase chain reaction.* Gene, 1989. **77**(1): p. 51-9.

107. Fabiato, A. and F. Fabiato, *Calculator programs for computing the composition of the solutions containing multiple metals and ligands used for experiments in skinned muscle cells.* J. Physiol., 1979. **75**(5): p. 463-505.

108. Holmgren, M., et al., *On the use of thiol-modifying agents to determine channel topology.* Neuropharmacology, 1996. **35**(7): p. 797-804.

109. Roux, B. and R. MacKinnon, *The cavity and pore helices in the KcsA K+ channel: electrostatic stabilization of monovalent cations.* Science, 1999. **285**(5424): p. 100-2.

110. Bruening-Wright, A., et al., *Localization of the activation gate for small conductance Ca2+-activated K+ channels.* J Neurosci, 2002. **22**(15): p. 6499-506.

111. Zimmerman, A.L., J.W. Karpen, and D.A. Baylor, *Hindered diffusion in excised membrane patches from retinal rod outer segments.* Biophys J, 1988. **54**(2): p. 351-5.

112. Yellen, G., *The voltage-gated potassium channels and their relatives.* Nature, 2002. **419**(6902): p. 35-42.

113. Phillips, L.R., D. Enkvetchakul, and C.G. Nichols, *Gating dependence of inner pore access in inward rectifier K(+) channels.* Neuron, 2003. **37**(6): p. 953-62.

114. Vergara, C., O. Alvarez, and R. Latorre, *Localization of the K+ lock-In and the Ba2+ binding sites in a voltage-gated calcium-modulated channel. Implications for survival of K+ permeability.* J Gen Physiol, 1999. **114**(3): p. 365-76.

115. Dutzler, R., et al., *X-ray structure of a ClC chloride channel at 3.0 A reveals the molecular basis of anion selectivity.* Nature, 2002. **415**(6869): p. 287-94.

116. Dutzler, R., E.B. Campbell, and R. MacKinnon, *Gating the selectivity filter in ClC chloride channels.* Science, 2003. **300**(5616): p. 108-12.

117. Ruta, V., et al., *Functional analysis of an archaebacterial voltage-dependent K+ channel.* Nature, 2003. **422**(6928): p. 180-5.

VIII. APPENDIX A
Supplementary Data

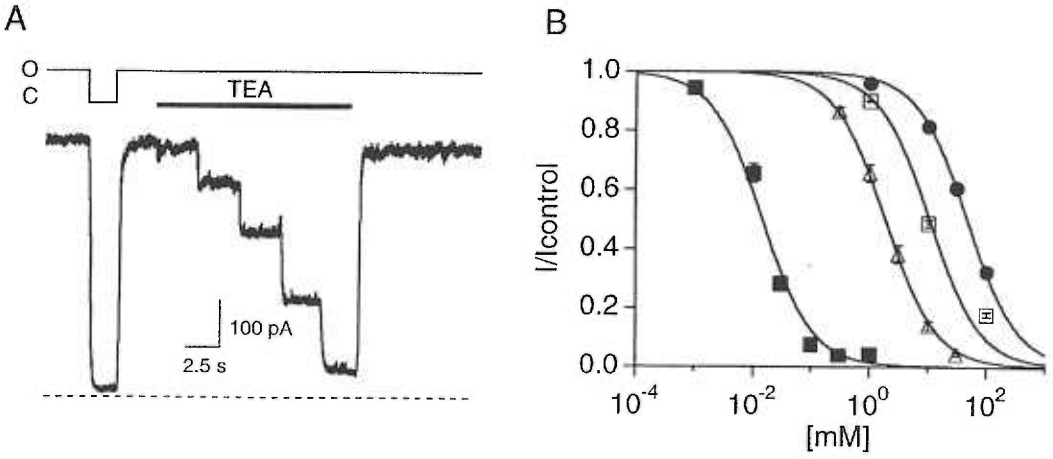

Figure Aa-1. TEA derivative block of SK2. A, Inside-out patches were held at 60 mV and exposed to increasing concentrations of TEA (2s each application, 1, 10, 30, 100, 300 mM) to obtain steady-state block. Bars indicate when channels were open (2 μM Ca^{2+}, O), or closed (zero Ca^{2+}, C), and when TEA was applied. The dashed line indicates zero current level and patches were not background-subtracted. B, Averages (n > 5) of normalized current plotted against concentration for 4 different compounds (circles TEA, open squares C6-TEA, open triangles TBuA, closed squares THexA). Note that block potency increases with increased hydrophobicity, consistent with a binding site in the hydrophobic pocket of the channel inner vestibule.

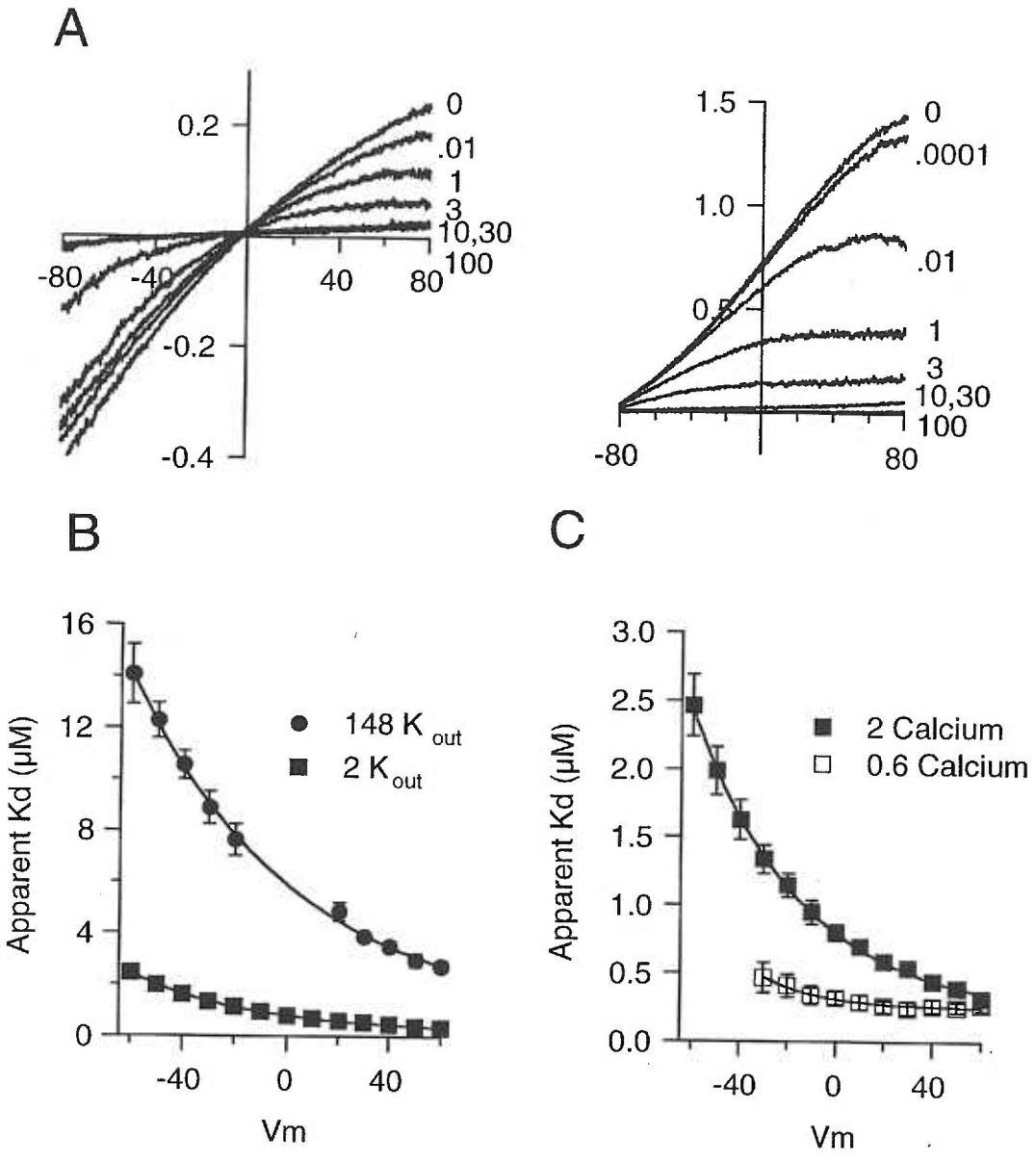

Figure Aa-2. TBuA block of SK2, voltage and Po-dependence. A, Current (nA) elicited in inside-out patches by ramps from –80 to 80 mV in the presence of 2 μM Ca^{2+}, indicated concentrations of Ba^{2+}, 150 K_{in}, and 148 K_{out} (left panel) or 2 K_{out} (right panel). B, Apparent Kd values from –60 mV to 60 mV estimated from ramps such as those in A from patches containing 148 K_{out} or 2K_{out} (n > 4). C, Apparent Kd values in the presence of saturating (2 μM) Ca^{2+} and Ca^{2+} sufficient to approximately half-activate channels (0.6 μM), 2 K_{out} (n > 4). Apparent Kd values at voltages below –30 mV in 0.6 μM Ca^{2+} could not be resolved due to limited current amplitudes.

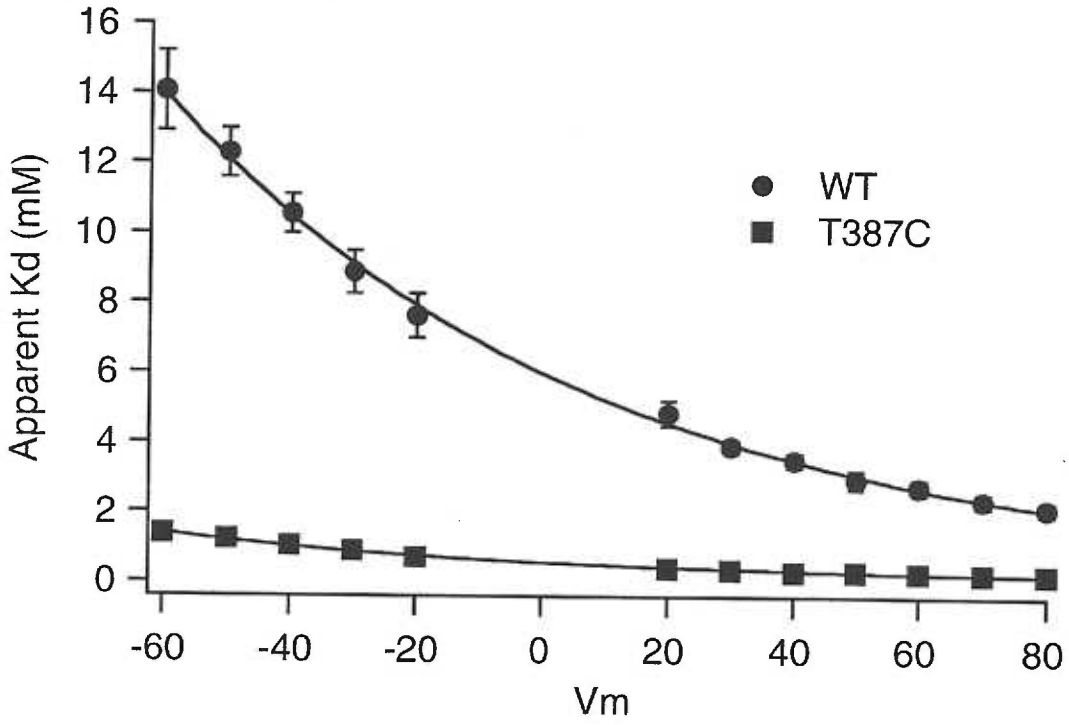

Figure Aa-3. Mutation T387C in the inner vestibule increases potency of TBuA block. Apparent Kd values are plotted against a range of voltages as in figure Aa-1 for WT SK2 channels and T387C channels in symmetrical 150 mM K^+.

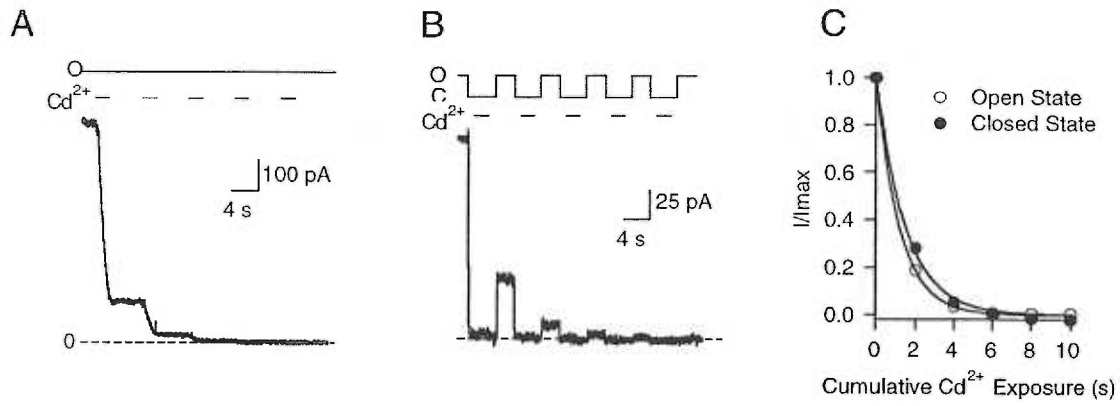

Figure Aa-4. Cd^{2+} reactivity of 391C channels in the open and closed states. A,B 5 μM Cd^{2+} was applied five times (dashes, 2s duration each application) to the inside face of inside-out patches excised from CosM6 cells transiently transfected with V391C channels. Patches were voltage clamped to 0 mV in asymmetrical K^+ (2 Kout, 150 Kin) and outward current was monitored. Application was either to open (A, 2 μM Ca^{2+} solution) or closed (B, nominally Ca^{2+} free solution) channels. Lines above the traces indicate when channels were open (O) or closed (C) and the dashed lines below the traces indicate the zero current level. C, Current amplitude after each 2s application was measured, normalized to the maximum current before application, and plotted versus time to determine the modification time course of the representative traces shown in A and B for open (open circles, tau = 1.2 s) or closed (closed circles, tau = 1.5 s) channels, respectively.

IX. APPENDIX B

Bicuculline Block of Small Conductance Calcium-Activated Potassium Channels

Radwan Khawaled*, Andrew Bruening-Wright*, John P. Adelman*, James Maylie#

*Vollum Institute, # Department of Obstetrics and Gynecology

Oregon Health and Science University, Portland, OR

Please send correspondences to:

Dr. James Maylie, Ph.D.

Department of Obstetrics and Gynecology

Oregon Health and Science University; L-458

3181 S.W. Sam Jackson Park Road

Portland, OR 97201

(503)-494-2106

(503)-494-5296 (fax)

mayliej@ohsu.edu (email)

Acknowledgments: This work was supported by National Institutes of Health grants to JPA and JM, and a grant from ICAgen, Inc.

Keywords: SK channels; bicuculline block; slow AHP; $GABA_A$ receptors

A. ABSTRACT

Small conductance calcium-activated potassium channels (SK channels) are gated solely by intracellular calcium ions and their activity is responsible for the slow afterhyperpolarization (AHP) which follows an action potential in many excitable cells. Brain slice studies commonly employ a methyl derivative of bicuculline (bicuculline-m), a $GABA_A$ (γ-aminobutyric acid) receptor antagonist, to diminish the tonic inhibitory influences of GABAergic synapses, or to investigate the role of these synapses in specialized neural networks. However, recent evidence suggests that bicuculline-m may not be specific for $GABA_A$ receptors and may also block the slow afterhyperpolarization. Therefore, the effects of bicuculline-m on cloned apamin-sensitive SK2 and apamin-insensitive SK1 channels were examined following expression in *Xenopus* oocytes. The results show that at concentrations employed for slice recordings, bicuculline-m potently blocks both apamin-sensitive SK2 currents and apamin-insensitive SK1 currents when applied to outside-out patches. Apamin-insensitive SK1 currents run down in excised patches. The potency of bicuculline-m block also decreases with time after patch excision. Site-directed mutagenesis which changes two residues in the outer vestibule of the SK1 pore that confers apamin sensitivity also reduces rundown of the current in patches, and endows stable sensitivity to bicuculline-m indistinguishable from SK2. Therefore, the use of bicuculline-m in slice recordings may mask apamin-sensitive slow AHPs that are important determinants of neuronal excitability. In addition, bicuculline-m-insensitive slow AHPs may indicate that the underlying channels have undergone rundown.

B. INTRODUCTION

In many neurons, the action potential is followed by a slow afterhyperpolarization (slow AHP), which is due to the activation of small conductance calcium-activated potassium channels (SK channels). SK channels are not gated by voltage and are activated by submicromolar concentrations of intracellular calcium. In the sustained presence of excitatory neurotransmitter, the slow AHP becomes increasingly prominent, reflecting the continued increase of intracellular calcium levels, until the cell is no longer able to reach threshold for a subsequent action potential, a phenomenon termed spike-frequency adaptation, an important regulator of excitability [4, 11, 24, 27]. Two types of slow AHPs may be distinguished. In many neurons, such as hippocampal interneurons [40], the slow AHP is sensitive to the bee venom toxin, apamin, has relatively faster kinetics and is not regulated by neurotransmitters. In hippocampal pyramidal neurons, the slow AHP is insensitive to apamin, exhibits very slow kinetics, and is modulated by neurotransmitter-induced second messengers such as protein kinase A (PKA) [17, 20, 23]. These two types of slow AHPs are not mutually exclusive, as apamin-sensitive and apamin-insensitive transmitter-regulated components are present in many neurons such as vagal motoneurons [29], neocortical neurons [19], and pyramidal neurons of the sensorimotor cortex [30].

Brain slice preparations are commonly used for studies of synaptic transmission. An attractive feature of the slice preparation is that much of the intrinsic neuronal circuitry remains functionally intact, including inhibitory, GABAergic synapses. In brain slice and other tissue preparations, many investigators have included bicuculline, an antagonist of $GABA_A$ receptor-channels, in the solution bathing the slice to improve stimulus-evoked

responses, or to probe the role of $GABA_A$ receptor-channels in synaptic responses [5, 15, 22, 26, 32, 34-37]. Bicuculline is supplied as either the free base or a methyl derivative (herein referred to bicuculline-m) which uses either chloride, bromide, or iodide, as the counter-ion; the salts are water-soluble and are the most widely employed.

It has been assumed that bicuculline is a specific $GABA_A$ antagonist, however several reports have suggested that in addition to the antagonism of $GABA_A$ receptor channels, bicuculline-m also blocks the slow AHP. Recordings from dopamine neurons in the ventral tegmental area and the substantia nigra pars compacta showed that bicuculline-m, but not picrotoxin, another $GABA_A$ antagonist, blocked the apamin-sensitive slow AHP. This effect persisted in the presence of tetrodotoxin (TTX), suggesting that it was not due to reduced calcium entry but rather a direct effect on the SK channels [31]. Bicuculline-m also potentiated the NMDA-dependent burst firing in these neurons by reducing the slow AHP, similar to the effects of apamin [14]. In thalamic reticular neurons, where the role of GABAergic inhibitory synapses in thalamocortical synchronization has been examined using bicuculline-m [15, 36], the methiodide, methbromide, and methylchloride salts produced a an enhancement of the low threshold calcium spike, not seen with picrotoxin, and which persisted in the presence of TTX; this effect was due to block of the current underlying the slow AHP, IsAHP [9].

These results suggest that bicuculline-m may directly block the channels underlying the slow AHP. Three SK channels have been cloned and reflect the different pharmacologies of the slow AHP in neurons; SK2 and SK3 channels are apamin-sensitive, while SK1

channels are apamin-insensitive [13, 16]. Therefore, we examined the effects of bicuculline methylchloride and the bicuculline free base on the cloned SK channels.

C. MATERIALS AND METHODS

Xenopus care and handling were in accordance with the highest standards of institutional guidelines. Frogs underwent no more than two surgeries, separated by at least three weeks, and surgeries were performed using well established techniques. Frogs were anesthetized with an aerated solution of 3-aminobenzoic acid ethyl ester. Oocytes were studied 2-8 days after injection with 0.2-2 ng of mRNA. *In vitro* mRNA synthesis and oocyte injections were performed as previously described [1]. Outside-out macropatch recordings were made at room temperature (approximately 23° C) with electrodes pulled from thin-walled, filamented borosilicate glass (World Precision Instruments) and filled with 120 K-gluconate, 5 HEPES, (pH 7.2, adjusted with KOH) supplemented with $CaCl_2$ to give free calcium concentration of 10 μM; the proportion of calcium binding to gluconate was determined assuming a stability constant for Ca^{2+} gluconate of $15.9M^{-1}$ [8]. To obtain Ca^{2+} concentrations below 1 μM, 1 mM EGTA was added to the internal solution and $CaCl_2$ was added as calculated using published stability constants [21]. Electrode resistance was typically 1-3 MΩ. Excised patches were superfused with a solution containing 120 mM K-gluconate, 5 mM HEPES (pH 7.2, adjusted with KOH). Patch formation and excision were performed within ~30 s and drugs were applied by positioning the patch in front of a series of flow pipes allowing for a solution exchange in approximately 1 second. Voltage-clamp recordings were performed with an Axopatch 1B-100/1 headstage (Axon Instruments) or an EPC9 patch clamp amplifier (HEKA electronics). The data were low-pass Bessel filtered at 2 kHz and acquired using Pulse

software (HEKA Electronik). Currents elicited by 2 second voltage ramps between the potentials indicated in the text were acquired at a sampling frequency of 1 kHz. Data analysis was performed using Pulse (HEKA) and IGOR (Wavemetrics). Concentration response curves were obtained as follows: current amplitudes were measured at the indicated voltage and corrected for rundown as indicated in the text, data were normalized to the average of the control values obtained immediately before and after each concentration response, and a single binding isotherm was fit to the normalized data. The equation used was $(f_c-f_f)*I.C._{50}/(x+I.C._{50})+f_f$, where x is concentration of drug, f_c is normalized control value in the absence of drug, f_f is the fraction of current not blocked by the drug, and $I.C._{50}$ is concentration at half maximum response; a nonlinear least square procedure was used to determine f_c, f_f, and $I.C._{50}$. All data points are presented as mean ± SD of n experiments as indicated. Statistical differences were determined using an unpaired t-test; p values <0.05 were considered significant. Bicuculline free base and methylchloride (bicuculline-m), and picrotoxin were purchased from RBI (Natick, MA).

D. RESULTS

a. Bicuculline Blocks SK channels

SK channels were expressed in *Xenopus* oocytes and outside-out patches were examined using symmetrical 120 mM K^+ solutions and a saturating concentration of Ca^{2+} (10 μM) in the patch pipette internal solution; currents were evoked by voltage ramp commands. Application of bicuculline-m in the solution bathing outside-out patches from oocytes expressing apamin-sensitive SK2 channels resulted in a concentration dependent inhibition of the current measured at –60 mV, with an $I.C._{50}$ = 1.1 ± 0.1 μM; n=3;

representative current traces and concentration response are shown in Figure 1 A, B. SK currents in excised patches demonstrate rundown as a function of time after patch excision which varied with oocyte batch and was different among the cloned SK channels; in general the extent of rundown of SK2 is only modest (closed circles, Figure 1C) [13]. Initial experiments suggested that bicuculline-m block changed with time after patch excision. Indeed, when current amplitude and block were examined at different time points after patch excision (open circles, Figure 1C), the data showed that blocking potency decreased slightly in parallel with rundown (Figure 1B, C). For the representative patch shown in Figure 1, SK2 currents diminished 11% over 21 minutes and the $I.C._{50}$ increased from 1.1 to 1.8 μM. On average the $I.C._{50}$ increased from 1.1 ± 0.1 μM to 1.7 ± 0.3 μM over 21-31 min (n=3) and the rundown was 9 ± 5%. Experiments performed using physiological ionic conditions (5 mM K^+ in the extracellular solution and 120 mM K^+ in the intracellular solution) yielded similar results ($I.C._{50}$ at 0 mV = 1.3 ± 0.2 μM; n=3). These data show that bicuculline-m blocks SK2 channels at concentrations which are routinely used in brain slice experiments to block $GABA_A$ receptor channels (10-30 μM).

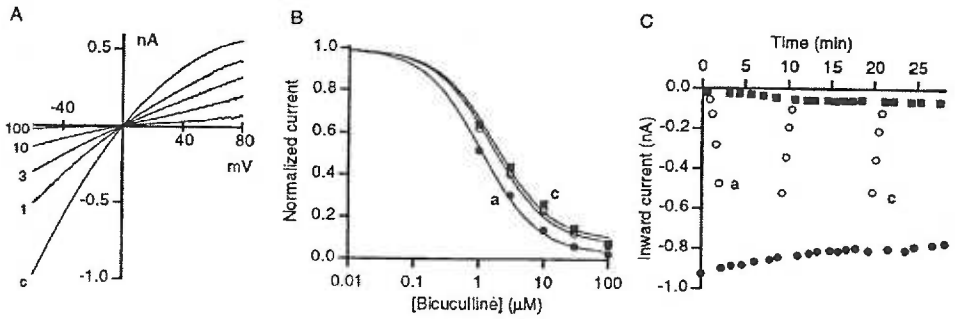

Figure Ab-1. Concentration response of bicuculline-m block of SK2. A. Current traces elicited by 2 s voltage ramp from –60 to 80 mV from an out-side out macropatch excised from an oocyte expressing SK2. The traces were obtained in control solution (c) and in the presence of 1, 3, 10, 100 μM bicuculline-m (labeled accordingly) within the first 2 min following patch excision. B. Bicuculline-m concentration-response curves measured at 3 times following patch excision (response curves labeled a and c correspond to time points in panel C). The current measured at -60 mV was normalized by the response in the control solution prior to each series and plotted as a function bicuculline-m concentration. Nonlinear least squares fit to a Langmuir isotherm (continuous line) yielded an $I.C._{50}$ of 1.1, 1.6 and 1.8 μM for a-c, respectively. An offset was included to account for residual, unblocked current which increased during the time course of recording (panel C) from 0.03 in series a to 0.09 in series c. Series a is measured from the current traces in panel A. C. Time dependence of inward current recorded at –60 mV as a function of time following patch excision. Plotted are current values in control solution (closed circles), 100 μM bicuculline-m (closed squares) and 3 concentrations response curves to 1, 3, 10, and 30 μM bicuculline-m (open circles). The first and last series are indicated by a and c.

Apamin-insensitive SK1 currents were also blocked by bicuculline-m when applied to outside-out patches immediately after excision, and concentration response experiments measured at -60 mV yielded an $I.C._{50}$ of 1.4 ± 0.4 μM, n = 4; not markedly different than for SK2 (p=0.4). SK1 currents undergo a greater degree of rundown than SK2 currents ([13]; Figure 2C). As shown in the example in Figure 2C, the current measured at –60 mV (closed circles) initially increased immediately following patch excision and was then followed by rundown; the time course could be described by a sum of two exponentials (solid line), one for the increasing and one for the decreasing phase. Currents within a concentration response obtained early after patch excision were subject to rundown which would bias the $I.C._{50}$. Therefore, current amplitudes were corrected for rundown by normalizing to the control current predicted from the time course of rundown.

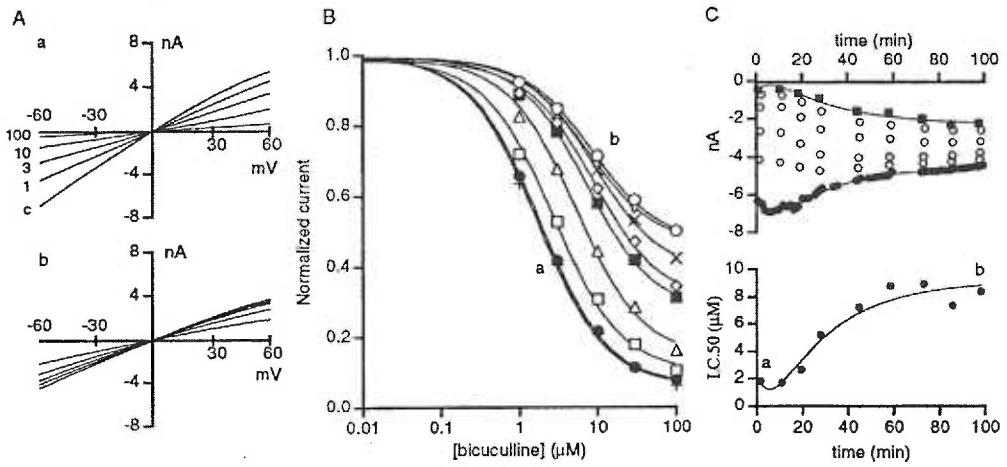

Figure Ab-2. Bicuculline-m block of SK1 decreases with time following patch excision. A. Current traces elicited by 2 s voltage ramp from –60 to 60 mV from an outside out macropatch excised from an oocyte expressing SK1. The traces were obtained in control solution (c) and in the presence of 1, 3, 10, 100 μM bicuculline-m (labeled accordingly) within the first 2 min (a) and 100 min (b) following patch excision. B. Bicuculline-m concentration-response curves at –60 mV measured at increasing times following patch excision (response curves labeled a and b correspond to first and last series illustrated in panel A and to the time points labeled a and b in panel C). The shift in the concentration response curve corresponds to increasing time following patch excision. Nonlinear least squares fit to a Langmuir isotherm (continuous line) yielded an increase in $I.C._{50}$ from 1.7 to 8.4 μM measured 2 min and 98 min following patch excision (a and b, respectively). The fraction of SK1 not blocked by bicuculline-m increased from 0.06 to 0.44 between a and b. C. Time dependence of inward current recorded at –60 mV (upper panel) and $I.C._{50}$ from concentration response curves in panel B (lower panel) as a function of time following patch excision. Plotted in the upper panel are current values in control solution (closed circles), 100 μM bicuculline-m (closed squares) and 9 concentrations response curves to 1,3,10,30 μM bicuculline-m (open circles). The first and last series are indicated by a and b in the upper and lower panel. The time course of rundown of the control data was described by a sum of two exponentials (continuous line through closed circles, upper panel) which was used to correct for rundown as described in the text. The same exponential function was applied to the time course of the current measured in 100 μM bicuculline-m and the $I.C._{50}$ allowing only the amplitude to change by fixing the exponential time constants to that determined for control values (continuous lines through closed squares in upper panel and closed circles in lower panel, respectively).

Figure 2B shows concentration responses to bicuculline-m measured at different times following patch excision. Initially, SK1 currents were as sensitive to bicuculline-m as SK2 currents, but the $I.C._{50}$ increased over time and by the end of the experiment (98 min after patch excision) the $I.C._{50}$ was 8.4 μM (Figure 2B,C). Associated with the decreased affinity between bicuculline-m and SK1, the fraction of current not blocked by 100 μM bicuculline-m increased (Figure 2C, closed squares). Concentrations greater than 100 μM have not be evaluated but based on the fits of a single binding isotherm to the concentration response, the fraction of SK1 current not blocked by bicuculline-m (100 μM) increased from 0.06 to 0.44. The increase in the $I.C._{50}$ for bicuculline-m appeared to parallel the time course of rundown. On average the increase in $I.C._{50}$ from 1.4 ± 0.4 μM to 24.4 ± 19.8 μM was associated with a rundown of 66 ± 22% over 32-98 min (n=4) while the fraction of current not blocked by bicuculline-m increased from 0.11±0.05 to 0.48 ± 0.21. The bicuculline-m resistant current reflects a fraction of SK channels not blocked by bicuculline-m because substitution of external K^+ for Na^+ eliminated the residual inward current in the presence of 100 μM bicuculline-m and removal of Ca^{2+} in inside-out patches eliminated the current. These data show that SK1 and SK2 are equally sensitive to bicuculline-m but that over time SK1 currents rundown and the block by bicuculline-m decreases.

The rate of current rundown of SK1 is strikingly similar to the time course of increase of the $I.C._{50}$ suggesting that these processes are linked (Figure 2C). Although the molecular mechanisms responsible for SK channel rundown are not known, the decrease in the current with time might result from a shift in the calcium sensitivity of the channels

and a reduction in open probability. Therefore, the Ca^{2+} sensitivity of the channels was examined immediately and 20 minutes after excision of inside-out patches, however, no shift in the Ca^{2+} concentration response was observed for SK1 and SK2 (data not shown).

To determine whether bicuculline-m is an open channel blocker, bicuculline block was examined using 0.3 μM Ca^{2+} in the patch pipette (internal solution), a concentration close to the $I.C._{50}$ [16, 39] where the open probability of the channels will be reduced compared to the saturating concentrations used in the previous experiments. Under these conditions, bicuculline-m concentration response measurements showed that the $I.C._{50}$ was not different than when 10 μM Ca^{2+} was present in the patch pipette (1.5 ± 0.1 μM; n = 2, p=0.8).

b. Residues Influencing Rundown and Reduced Bicuculline Sensitivity

Two amino acids residing on opposite sides of the deep pore are responsible for apamin-block in SK2 channels, and substitution of these residues into SK1 endows apamin sensitivity [13]. In the course of those previous studies it was noticed that the doubly mutated, apamin-sensitive SK1 channels (E330D, H357N) also showed reduced rundown (unpublished observation). Therefore, the bicuculline-m sensitivity of SK1 (E330D, H357N) currents was examined. Bicuculline-m blocked SK1 (E330D, H357N) currents with an $I.C._{50}$ not different from SK2 or SK1 currents immediately after patch excision (Figure 3A,B). The average $I.C._{50}$ was 0.9 ± 0.2 μM (n=3). However, similar to SK2 currents, SK1 (E330D, H357N) currents showed reduced rundown (30 ± 6%)

compared to SK1 and stable bicuculline-m sensitivity; the $I.C._{50}$ increased to 1.3 ± 0.5 μM over 27-56 min (Figure 3B, C).

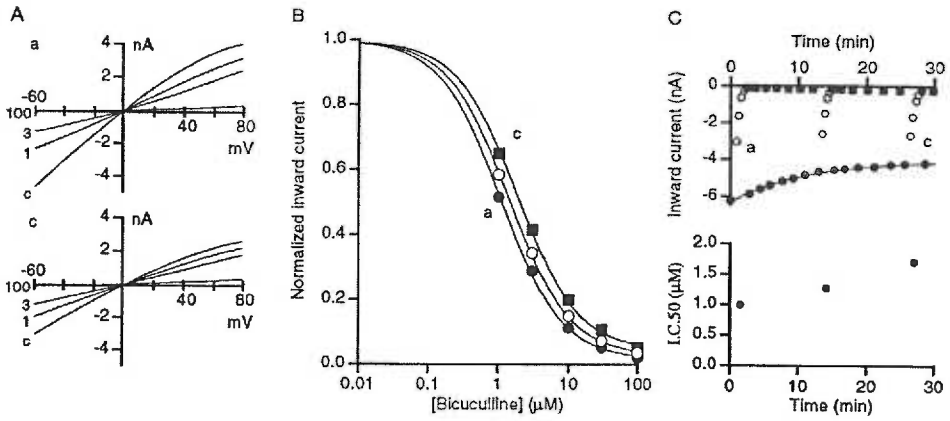

Figure Ab-3. Mutations E330D, H357N in the outer vestibule of SK1 reduce the time dependent shift of bicuculline-m block of SK1. A. Current traces elicited by 2 s voltage ramp from –60 to 80 mV from an out-side out macropatch excised from an oocyte expressing SK1 (E330D,H357N). The traces were obtained in control solution (c) and in the presence of 1, 3, and 100 μM bicuculline-m (labeled accordingly) within the first 2 min (a) and 28 min (c) following patch excision. B. Bicuculline-m concentration response curves measured at 3 times following patch excision (response curves labeled a and c correspond to concentration response traces in panel Aa and Ac, respectively and to time points labeled a and c in panel C). The I.C.$_{50}$ for the three series were 1.1, 1.4 and 1.8 μM for a-c, respectively and the fraction of current not blocked by bicuculline-m increased from 0.02 to 0.05. C. Inward current recorded at –60 mV (upper panel) and I.C.$_{50}$ (lower panel) as a function of time following patch excision. Plotted are current values in control solution (closed circles), 100 μM bicuculline-m (closed squares) and 3 concentrations response curves to 1, 3, 10, and 30 μM bicuculline-m (open circles). The first and last series are indicated by a and c.

c. Voltage-Dependence of Bicuculline-m Block

Bicuculline-m affected inward currents more than outward currents for both SK1 and SK2 channels (see Figures 1A, 2A). Therefore, the $I.C._{50}$ for bicuculline-m was examined as a function of voltage for SK1 and SK2 (Figure 4). The concentration response was determined from a series of voltage ramps for the different concentrations of bicuculline-m by measuring the current at 10 mV increments between –60 and 80 mV (Figure 4A, B lower panel, respectively; the closed symbols represent inward current and the open symbols represent outward current). The concentration response at each voltage was fit with a single binding isotherm (see methods) and the derived $I.C._{50}$ was plotted as a function of voltage (Figure 4C). The results show that for inward currents, at voltages less than 0 mV in symmetrical K^+, the bicuculline-m $I.C._{50}$ changed little as a function of voltage but significantly increased for outward current as the voltage became positive. The mean data from 3 patches were fit with a single exponential plus an offset, yielding a voltage dependence of 37.9 mV/e-fold change in the concentration of bicuculline-m for SK2 (Figure 4C, closed circles), and was 30.7 mV (n=4, Figure 4C, open circles) for SK1. Application of the Woodhull equation [38] suggests that the fraction of the membrane electric field influencing bicuculline-m block (δ) assuming a single charge on bicuculline-m was 0.83 and 0.67 for SK1 and SK2 channels, respectively.

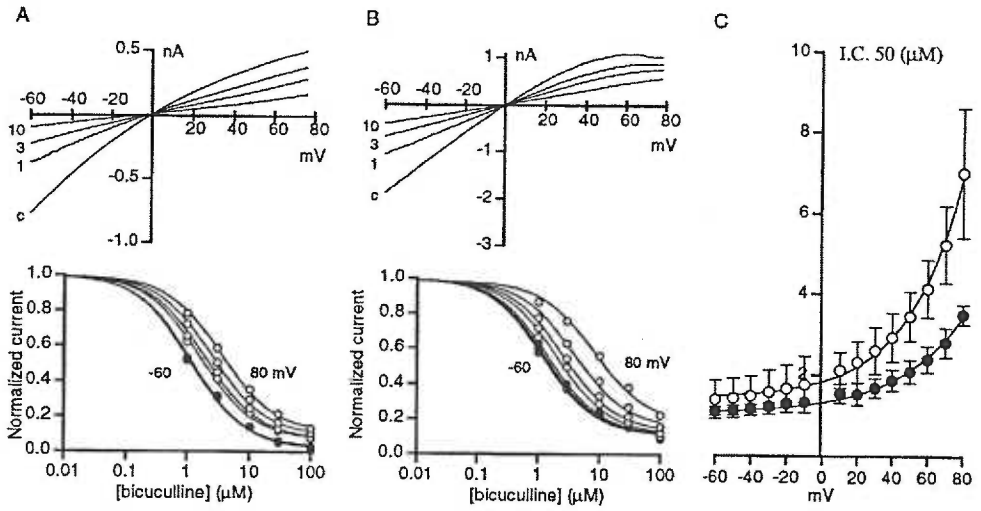

Figure Ab-4. Voltage-dependence of bicuculline-m block of SK2 and SK1. A. Bicuculline-m concentration response of SK2. (Upper panel), Current traces elicited by 2 s voltage ramp from –60 to 80 mV from an out-side out macropatch excised from an oocyte expressing SK2. The traces were obtained in control solution (c) and in the presence of 1, 3 and 10 μM bicuculline-m (labeled accordingly) within the first 2 min following patch excision. (Lower panel), concentration response curves measured at 20 mV increments from –60 to 80 mV; concentration response curves measured for inward and outward currents are displayed with closed and open circle, respectively (the concentration response curve was not measured at the reversal potential of 0 mV). Nonlinear least squares fit to a Langmuir isotherm (continuous lines) yielded an increase in $I.C._{50}$ from 1.0 at –60 mV to 2.8 μM 80 mV. The fraction of SK2 not blocked by bicuculline-m increased from 0.05 at –60 mV to 0.1 at 80 mV. B. Bicuculline-m concentration response of SK1, protocol as described in panel A. The $I.C._{50}$ increased from 1.2 at –60 mV to 8.2 μM at 80 mV and the fraction of SK1 not blocked by bicuculline-m increased from 0.11 at –60 mV to 0.18 at 80 mV. C. $I.C._{50}$ for SK2 (closed circles, n=3) and SK1 (open circles, n=4) plotted versus patch potential. The data were fit with a single exponential plus a constant (continuous curve) yielding $1.05+0.29*e^{V/37.9}$ and $1.43+0.4*e^{V/30.7}$ for SK2 and SK1, respectively.

The apparent voltage dependence of bicuculline-m block may result either from an intrinsic voltage-dependence or to a 'knock-off' effect by K^+ ions passing through the pore [2]. To distinguish these possibilities, the $I.C._{50}$ for bicuculline was determined as a function of voltage when the concentration of K^+ in the internal pipette solution was lowered to 20 mM while the external K^+ concentration was maintained at 120 mM (Figure 5). Figure 5A shows a series of current traces in response to voltage ramps from –60 to 100 mV in different bicuculline-m concentrations with 20 mM K^+ in the patch pipette. Decreasing internal K^+ shifted the reversal potential ~30 mV in the positive direction and decreased the outward current. Concentration response curves measured at 10 mV increments are shown in Figure 5B; the increase in unblocked current with increasing voltage probably reflects a greater contribution from leak current at more positive voltages under these conditions in which the outward current is dramatically reduced. The mean $I.C._{50}$ for bicuculline-m block of SK2 at –60 mV was 1.7 ± 0.1 μM (n=2). To compare the voltage dependence to that in symmetrical K^+, the $I.C._{50}$ was displayed relative to the baseline value (Figure 5C) and shows that the voltage dependence in low internal K^+ was shifted by ~30 mV compared to that in symmetrical 120 mM K^+. This result indicates that at least part of the apparent voltage-dependence of bicuculline-m block is due to destabilization of binding by K^+ ions passing through the pore, a 'knock-off' effect, and that bicuculline-m blocks SK channels by a direct occlusion of the pore.

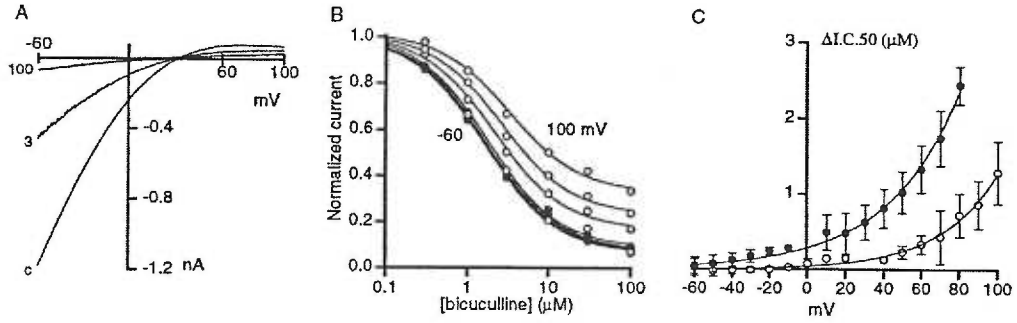

Figure Ab-5. Voltage dependence of bicuculline-m block of SK2 in asymmetrical K^+. A. Current traces elicited by 2 s voltage ramp from –60 to 100 mV from an out-side out macropatch containing 20 mM internal K^+ (20 mM Kgluconate, 100 mM Nagluconate, 5 Hepes, pH 7.2 with NaOH) excised from an oocyte expressing SK2. The traces were obtained in control solution (c) and in the presence of 3, and 100 μM bicuculline-m (labeled accordingly) within 2 min following patch excision. B. Concentration response curves measured at 20 mV increments from –60 to 100 mV; concentration response curves measured for inward and outward currents are displayed with closed and open circle, respectively. The $I.C._{50}$ increased from 1.7 at –60 mV to 3.3 μM 100 mV and the fraction of SK2 not blocked by bicuculline-m increased from 0.07 at –60 mV to 0.3 at 100 mV. C. The change in $I.C._{50}$ relative to baseline determined from the exponential fits ($\Delta I.C._{50}$) for SK2 in symmetrical 120 mM K^+ (closed circles) and asymmetrical K^+ (open circles) plotted versus patch potential. The data represent the mean±SD for 3 patches (symmetrical K^+) and 2 patches (asymmetrical K^+). The absolute values of the $I.C._{50}$ were fit with a single exponential plus a constant (continuous curve) yielding $1.05+0.29*e^{V/37.9}$ and $1.72+0.04*e^{V/30.0}$ for symmetrical and asymmetrical K^+, respectively.

Bicuculline-m block from the inside of the membrane was also examined. Although some sensitivity was observed, it was markedly less than that seen for external bicuculline-m application, with 100 μM blocking 10.08 ± 9.34 % (n = 8) of the inward current at -80 mV and 30.31 ± 11.01 % (n = 8) of the outward current at 80 mV.

The effects of bicuculline free base were also examined. The free base of bicuculline blocked SK1 and SK2 channels but with lower affinity than the methylchloride salt; concentration response curves measured at –60 mV yielded an average $I.C._{50}$ of 46.3 ± 9.9 μM for SK1 (n=5) and 63.3 ± 23.9 μM for SK2 (n=3) when examined immediately after patch excision. The block by the free base was voltage dependent with the $I.C._{50}$ increasing between –60 and 80 mV from 34.4 μM to 76.5 μM for SK2 and 38.9 μM to 123.4 μM for SK1 (Figure 6A, B). When plotted versus patch potential (Figure 6C, D) the $I.C._{50}$ versus voltage was well described by an exponential function yielding an average voltage dependence of 47.0 ± 8.3 mV (n=3) and 41.6 ± 5.9 mV (n=5) for SK2 and SK1, respectively. Similar to that observed for the methylchloride salt the $I.C._{50}$ of the free base block of SK1 increased with time following patch excision (data not shown). Thus, at concentrations which effectively block $GABA_A$ receptor-channels (10 μM), the free base form of bicuculline will have little effect on SK channels.

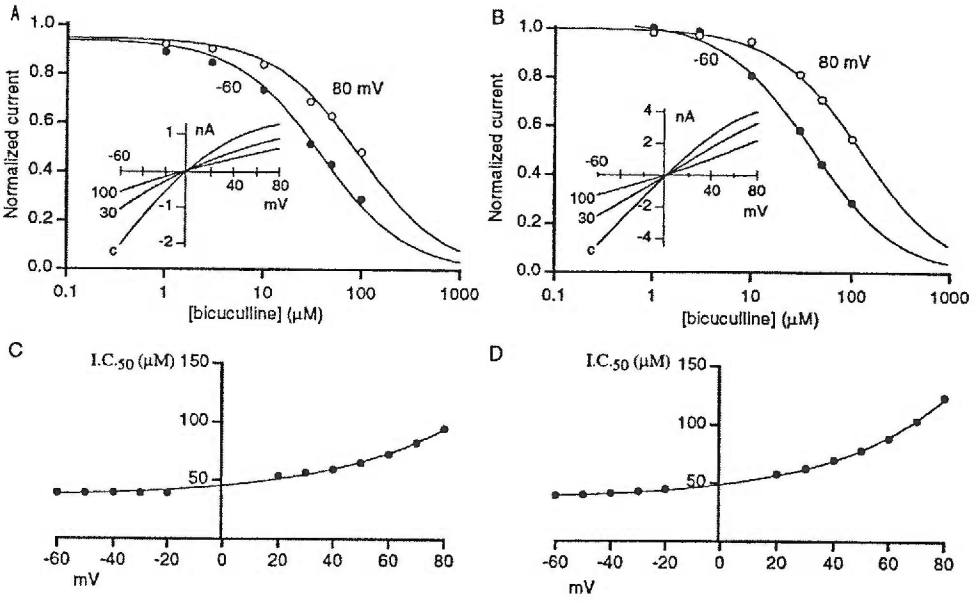

Figure Ab-6. Concentration response of block of SK2 and SK1 by the free base of bicuculline. A. Concentration response curves measured at –60 and 80 mV of SK2. The free base was added from a stock solution of 100 mM in DMSO. Concentrations greater than 100 μM did not readily dissolve in the recording solution and were not tested. Hence the data were fit with a single Langmuir isotherm with the offset forced to zero. The $I.C._{50}$ of block by bicuculline free base increased from 34.4 μM at –60 mV to 76.5 μM at 80 mV. *inset* , current traces elicited by voltage ramps from –60 to 80 mV in control solution (c) and in the presence of 30, and 100 μM bicuculline (labeled accordingly). B. Concentration response curves measured at –60 and 80 mV of SK1. The $I.C._{50}$ increased from 38.9 μM at –60 mV to 123.4 μM at 80 mV. *inset* , current traces elicited by voltage ramps from –60 to 80 mV in control solution (c) and in the presence of 30, and 100 μM bicuculline (labeled accordingly). C. Voltage dependence of block of SK2 by bicuculline free base. The data were fit with a single exponential function yielding $35.7+10.1*e^{V/45.5}$. D. Voltage dependence of block of SK1 by bicuculline free base. The data were fit with a single exponential function yielding $36.3+12.5*e^{V/41.4}$.

Picrotoxin is another widely used compound for inhibition of $GABA_A$-mediated responses. However, the concentration of picrotoxin generally employed in brain slice experiments (100 μM) did not significantly reduce either SK1 or SK2 currents. At 10-fold higher concentrations (1 mM) picrotoxin produced a variable but significant reduction of outward (32 ± 13%, n = 4; p = 0.03) and inward (36 ± 15%, n = 4; p = 0.02) currents (data not shown).

E. DISCUSSION

The results presented here demonstrate that bicuculline-m potently blocks cloned SK channels at concentrations routinely employed in brain slice experiments. Therefore, the methyl derivative of bicuculline can no longer be regarded as a selective antagonist of $GABA_A$ receptor-channels. As the cloned SK channels likely represent the channels which are responsible for the slow AHP and spike-frequency adaptation in native neurons, the use of bicuculline-m in brain slice experiments may have profound effects on excitability parameters such as firing frequencies and accommodation, compromising interpretations of the role of $GABA_A$ synapses. Similarly, experiments designed to evaluate the AHP in a GABAergic-free background using bicuculline will also be compromised. In contrast, picrotoxin, another commonly employed $GABA_A$ antagonist, has no effect on cloned SK channels at a concentration routinely used for brain slice studies.

Like many channels, cloned SK channels undergo rundown following patch excision. The molecular basis for channel rundown is not understood but may be due to the loss of

associated intracellular second messenger proteins such as protein kinases [6, 18], protein phosphatases [25], or inositol phosphates [3, 12, 33]. Consistent with this hypothesis, the extent of SK current rundown shows considerable variability among different batches of oocytes. There is also an intrinsic distinction between SK1 and SK2 channels as rundown is much more pronounced for SK1 channels. Interestingly, for both channels, block by bicuculline-m and bicuculline free base is also altered with time after patch excision, and although there is no clear evidence that rundown and altered sensitivity are functionally coupled, in all experiments they correlated well; the extent of current decrease was proportional to the increase of the $I.C._{50}$ for both forms of bicuculline. This suggests that in addition to a decrease in channel activity, rundown, presumably initiated by an intracellular process, imposes a slow conformational change on the outer vestibule of the SK channel pore which reduces the affinity for external bicuculline. This process is affected by residues in the outer vestibule of the pore, as substitution of two amino acids from SK2 into SK1 reduced the extent of rundown and the shift in the $I.C._{50}$ to that seen for SK2. Immediately after patch excision, SK1 and SK2 channels show similar block by bicuculline-m or free base, suggesting that the molecular determinants for binding are found in both channel types. There are only three amino acid differences in the pore region between SK1 and SK2 [16] and two of these are important for the altered topography of the outer vestibule with time after excision. These results suggest that the pore region is not maintained in a rigid conformation. This is consistent with the observations presented by Guillemare and coworkers who showed that the biophysical properties and sensitivity to neurotoxins of the brain delayed-rectifier K^+ channels Kv1.2 were affected by the levels of channel expression in *Xenopus* oocytes [10].

Several recent reports have shown that in brain slice experiments bicuculline-m blocks the IsAHP [9, 14, 31]. However, in some preparations this is clearly not the case. For instance, in whole cell recordings from hippocampal pyramidal neurons, a prominent apamin-insensitive IsAHP remains in the presence of bicuculline-m at concentrations which block the IsAHP in other brain regions, and effectively block the cloned channels [25]. Hippocampal pyramidal neurons are one of the few cell types in which only an apamin-insensitive slow AHP has been reported. If SK1 channels underlie the slow AHP in hippocampal pyramidal neurons, then the lack of bicuculline-m sensitivity may indicate that the channels have undergone rundown. Further, bicuculline-m application may have obscured an apamin-sensitive slow AHP, similar to other cell types which demonstrate both components [7, 19, 28, 30].

F. REFERENCES

1. Adelman JP, Shen KZ, Kavanaugh MP, Warren RA, Wu YN, Lagrutta A, Bond CT and North RA (1992). Calcium-activated potassium channels expressed from cloned complementary DNAs. Neuron 9: 209-216

2. Armstrong CM (1971). Interaction of tetraethylammonium ion derivatives with the potassium channels of giant axons. J. Gen. Physiol. 58: 413-437

3. Baukrowitz T, Schulte U, Oliver D, Herlitze S, Krauter T, Tucker SJ, Ruppersberg JP and Fakler B (1998). PIP2 and PIP as determinants for ATP inhibition of K_{ATP} channels. Science 282: 1141-1144

4. Blatz AL and Magleby KL (1986). Single apamin-blocked Ca-activated K+ channels of small conductance in cultured rat skeletal muscle. Nature 323: 718-720

5. Chu Z and Hablitz JJ (1998). Activation of group I mGluRs increases spontaneous IPSC frequency in rat frontal cortex. J. Neurophysiol. 80: 621-627

6. Chung SK, Reinhart PH, Martin BL, Brautigan D and Levitan IB (1991). Protein kinase activity closely associated with a reconstituted calcium-activated potassium channel. Science 253: 560-562

7. Constanti A and Sim JA (1987). Calcium-dependent potassium conductance in guinea-pig olfactory cortex neurones in vitro. J. Physiol. 387: 173-194

8. Dawson RMC, Elliot DC, Elliot WH and Jones UM. (1969). Data for biochemical research (New York: Oxford University Press).

9. Debarbieux F, Brunton J and Charpak S (1998). Effect of bicuculline on thalamic activity: a direct blockade of I_{AHP} in reticularis neurons. J. Neurophysiol. 79: 2911-2918

10. Guillemare E, Honore E, Pradier L, Lesage F, Schweitz H, Attali B, Barhanin J and Lazdunski M (1992). Effects of the level of mRNA expression on biophysical properties, sensitivity to neurotoxins, and regulation of the brain delayed-rectifier K+ channels Kv1.2. Biochemistry 31: 12463-12468

11. Hille B. (1992). Ionic Channels of Excitable Membranes (Sunderland: Sinauer Associates Inc.).

12. Huang C, Feng S and Hilgemann DW (1998). Direct activation of inward rectifier potasssium channels by PIP2 and its stabilization by Gßγ. Nature 391: 803-806

13. Ishii TM, Maylie J and Adelman JP (1997). Determinants of apamin and d-tubocurarine block in SK potassium channels. J. Biol. Chem. 272: 23195-23200

14. Johnson SW and Seutin V (1997). Bicuculline methiodide potentiates NMDA-dependent burst firing in rat dopamine neurons by blocking apamin-sensitive Ca^{2+} - activated K^+ currents. Neurosci. Lett. 231: 13-16

15. Kim U, Sanchez-Vives MV and McCormick DA (1997). Functional dynamics of GABAergic inhibition in the thalamus. Science 278: 130-133

16. Köhler M, Hirschberg B, Bond CT, Kinzie JM, Marrion NV, Maylie J and Adelman JP (1996). Small-conductance, calcium-activated potassium channels from mammalian brain. Science 273: 1709-1714

17. Lancaster B and Adams PR (1986). Calcium-dependent current generating the afterhyperpolarization of hippocampal neurons. J. Neurophys. 55: 1268-1282

18. Levitan IB (1985). Phosphorylation of ion channels. J. Memb. Biol. 87: 177-90

19. Lorenzon NM and Foehring RC (1992). Relationship between repetitive firing and afterhyperpolarizations in human neocortical neurons. J. Neurophysiol. 67: 350-363

20. Madison DV and Nicoll RA (1986). Actions of noradrenaline recorded intracellularly in rat hippocampal CA1 pyramidal neurons *in vitro*. J. Physiol. 372: 221-244

21. Martell AE and Smith RM. (1974). Critical Stability Constants, Volume Vol 1 Amino Acids (New York: Plenum Press).

22. Muramatsu M, Lapiz MDS, Tanaka E and Grenhoff J (1998). Serotonin inhibits synaptic glutamate currents in rat nucleus accumbens neurons via presynaptic $5HT_{1B}$ receptors. Euro. J. Neurosci. 10: 2371-2379

23. Nicoll RA (1988). The coupling of neurotransmitter receptors to ion channels in the brain. Science 241: 545-551

24. Park YB (1994). Ion selectivity and gating of small conductance Ca^{2+}-activated K^+ channels in cultured rat adrenal chromaffin cells. J. Physiol. 481: 555-570

25. Pedarzani P, Krause M, Haug T and Storm JF (1998). Modulation of the Ca^{2+}-activated K^+ current sI_{AHP} by a phosphatase-kinase balance under basal conditions in rat CA1 pyramidal neurons. J. Neurophysiol. 79: 3252-3256

26. Pedarzani P and Storm J (1996). Interactions between α– and ß-Adrenergic receptor antagonists modulating the slow Ca^{2+} -activated K^+ current IAHP in hippocampal neurons. Eur. J. Neurosci. 8: 2098-2110

27. Sah P (1996). Ca^{2+}-activated K^+ currents in neurons: types, physiological roles and modulation. TINS 4: 150-154

28. Sah P and Mclachlan EM (1991). Ca^{2+}-activated K^{+} currents underlying the afterhyperpolarization in guinea pig vagal neurons: a role for Ca^{2+}-activated Ca^{2+} release. Neuron 7: 257-264

29. Sah P and McLachlan EM (1992). Potassium currents contributing to action potential repolarization and the afterhyperpolarization in rat vagal motoneurons. J. Neurophysiol. 68: 1834-1841

30. Schwindt PC, Spain WJ and Crill WE (1992). Calcium-dependent potassium currents in neurons from cat sensorimotor cortex. J. Neurophysiol. 67: 216-226

31. Seutin V, Scuvee-Moreau J and Dresse A (1997). Evidence for a non-GABAergic action of quaternary salts of bicuculline on dopaminergic neurones. Neuropharmacol. 36: 1653-1657

32. Shinohara S and Kawasaki K (1997). Electorophysiological changes in rat hippocampal pyramidal neurons produced by cholecystokinin octapeptide. Neurosci. 78: 1005-1016

33. Shyng S-Y and Nicols CG (1998). Membrane phospholipid control of nucleotide sensitivity of K_{ATP} channels. Science 282: 1138-1141

34. Tanabe M, Gähwiler BH and Gerber U (1998). L-type calcium channels mediate the slow Ca^{2+}-dependent afterhyperpolarization current in rat CA3 pyramidal cells in vitro. J. Neurophysiol. 80: 2268-2273

35. Tempie F, Miniaci MC, Anchisi D and Strata P (1998). Postsynaptic current mediated by metabotropic glutamate receptors in cerebellar purkinje cells. J. Neurophysiol. 80: 520-528

36. Ulrich D and Hugenard JR (1997). Nucleus-specific chloride homeostasis in rat thalamus. J. Neurosci. 17: 2348-2354

37. Wong WT, Sanes JR and Wong ROL (1998). Developmentally regulated spontaneous activity in the embryonic chick retina. J. Neurosci. 18: 8839-8852

38. Woodhull AM (1973). Ionic blockage of sodium channels in nerve. J. Gen. Physiol. 61: 687-708

39. Xia X-M, Fakler B, Rivard A, Wayman G, Johnson-Pais T, Keen JE, Ishii T, Hirschberg B, Bond CT, Lutsenko S, Maylie J and Adelman JP (1998). Mechanism of calcium gating in small-conductance calcium-activated potassium channels. Nature 395: 503-507

40. Zhang L and McBain CJ (1995). Potassium conductances underlying repolarization and afterhyperpolarization in rat CA1 hippocampal interneurones. J. Physiol. 488: 661-672